RADAR BACKSCATTERING DATA FOR SURFACES OF GEOLOGICAL INTEREST

C.H. Shultz, T.L. Oliver and W.H. Peake

The Ohio State University

ElectroScience Laboratory

(formerly Antenna Laboratory)
Department of Electrical Engineering
Columbus, Ohio 43212

TECHNICAL REPORT 1903-7
2 December 1969

Contract Number NSR-36-008-027

National Aeronautics and Space Administration
Office of Grants and Research Contracts
Washington, D.C. 20546

NOTICES

When Government drawings, specifications, or other data are used for any purpose other than in connection with a definitely related Government procurement operation, the United States Government thereby incurs no responsibility nor any obligation whatsoever, and the fact that the Government may have formulated, furnished, or in any way supplied the said drawings, specifications, or other data, is not to be regarded by implication or otherwise as in any manner licensing the holder or any other person or corporation, or conveying any rights or permission to manufacture, use, or sell any patented invention that may in any way be related thereto.

REPORT 1903-7

REPORT
by
THE OHIO STATE UNIVERSITY ELECTROSCIENCE LABORATORY
COLUMBUS, OHIO 43212

Sponsor	National Aeronautics and Space Administration Office of Grants and Research Contracts Washington, D.C. 20546
Contract Number	NSR-36-008-027
Investigation of	Radar and Microwave Radiometric Techniques for Geoscience Experiments
Subject of Report	Radar Backscattering Data for Surfaces of Geological Interest
Submitted by	C.H. Shultz, Department of Geology T.L. Oliver and W.H. Peake, ElectroScience Laboratory Department of Electrical Engineering
Date	2 December 1969

CONTENTS

RADAR BACKSCATTERING DATA FOR SURFACES OF GEOLOGICAL INTEREST

I. INTRODUCTION

Future use of microwave radar for remote sensing over areas of agricultural and geological interest (for example, see Reference 1) requires basic information about the return characteristics of such surfaces. This report presents measurements of the normalized backscattering cross section (per unit "projected" area), $\gamma(\theta_i)$, which have been made over the past few years on a number of surfaces of geological interest. Corresponding data for agricultural surfaces are given in Reference 2.

The significance of these ground-based radar measurements is twofold: first, they serve as a calibration for airborne radars and provide estimates of radar return for system designers; secondly, they provide measurements over well-defined, homogeneous surfaces which are accompanied by rather detailed surface descriptions. Thus they can serve as basic data for the interpretation of surface response in terms of surface parameters. However, no specific interpretations are offered in this report, although a number of interesting conclusions have already been drawn[3] from the data presented here.

In many cases, brightness temperature data were taken for the same surface or site as the radar measurements on the same day or (occasionally) within one or two days. These data may be found in Reference 4, and may be identified on the basis of the date and surface descriptions.

Definition of the Radar Cross Section Parameters

The objective of the radar measurements is to determine the noralized backscattering parameters of the terrain, $\sigma^o{}_{jk}(\theta_i)$ or $\gamma_{jk}(\theta_i)$, where θ_i is the angle with respect to the surface normal. The parameter governing surface response at microwave frequencies is actually the normalized bistatic scattering cross section (per unit surface area),[3] $\sigma^o{}_{jk}(i,s)$, where (see Fig. 1) the subscript j refers to the polarization of the radiation incident on the surface of area A, and the subscript k designates that polarization component of the scattered signal which is accepted by the receiving antenna; i, s refer to the angles (θ_i,ϕ_i) and (θ_s,ϕ_s) respectively, defining the propagation directions of the incident and scattered radiation.

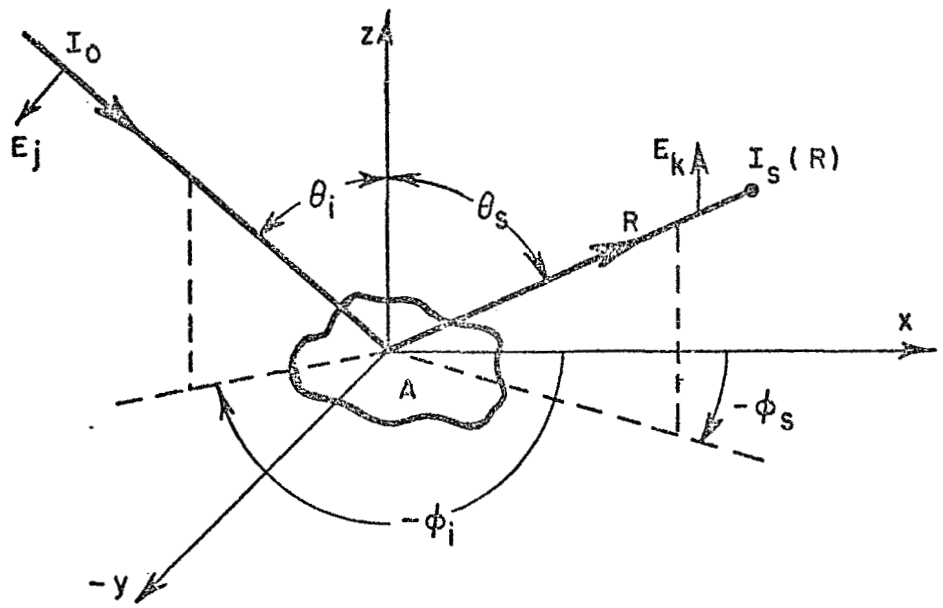

Fig. 1. Geometry of the scattering problem.

Operationally, the bistatic cross section is defined by considering an area A which is illuminated by a plane wave of power density I_o (watts/m^2), and which produces a scattered intensity I_s at a distance R. The normalized bistatic scattering cross section $\sigma^o_{jk}(i,s)$ is then defined by the equation[5]

$$(1) \qquad \sigma^o_{jk}(i,s) = \frac{4\pi R^2 \, I_s}{A \, I_o} = \sigma^o_{kj}(s,i) \qquad \text{(reciprocity theorem)},$$

where this normalized bistatic cross section, σ^o, is related to the conventional radar cross section, σ, by $\sigma^o = \sigma/A$. In terms of this parameter, the normalized radar backscattering cross section is $\sigma^o_{jk}(i,i)$ or just $\sigma^o_{jk}(\theta_i)$. The particular polarization states used in this report are designated by the following notation:

	Transmitted wave	Received scattered wave
$\sigma^{o}VV$	vertically polarized	vertically polarized
$\sigma^{o}VH$	vertically polarized	horizontally polarized
$\sigma^{o}HH$	horizontally polarized	horizontally polarized
$\sigma^{o}HV$	horizontally polarized	vertically polarized

The words "vertically polarized" refer to a wave with its electric vector in the plane of incidence; the words "horizontally polarized" refer to a wave with its electric vector in the plane of the surface.

To work with a parameter which is independent of the illuminated area of the terrain, the bistatic radar return parameter per unit "projected" area, γ, is introduced by the relation

$$\gamma_{jk}(i,s) = \frac{\sigma^{\circ}_{jk}(i,s)}{\cos\theta_i} = \frac{4\pi R^2 I_s}{I_o(A\cos\theta_i)} \quad . \tag{2}$$

Once again, the parameter of concern here is the backscattering component $\gamma_{jk}(i,i)$ or $\gamma_{jk}(\theta_i) = \sigma^{\circ}(\theta_i)/\cos\theta_i$. It is this parameter $\gamma(\theta_i)$ which is plotted in Section IV.

II. INSTRUMENTATION

The Ohio State University multi-frequency terrain-return facility has been described in detail elsewhere[6]. Briefly, however, it consists of four truck mounted radar systems of the high-gain, narrow beam, c-w doppler type, operated at 1.8, 10, 15, and 35 GHz. The block diagram of a typical system is shown in Fig. 2. The microwave systems are attached at the end of a hydraulic boom which is located at the center of the truck (see Fig. 3). The doppler signal is generated by driving the truck alongside the surface to be measured. The angle of incidence, θ_i, is controlled from within a van mounted on the rear of the truck, by rotating the enclosure containing the microwave system. Any linear polarization may be obtained by rotating the antenna.

Since two signal processing channels are available, any two of the four radars may be operated simultaneously. The instantaneous return power is integrated over a strip of terrain, typically 100 feet long, in order to reduce statistical fluctuations in the return parameters. The instantaneous return power is monitored on an analog strip-chart recorder, while the integrated power is recorded in digital form, at a rate of one sample per second.

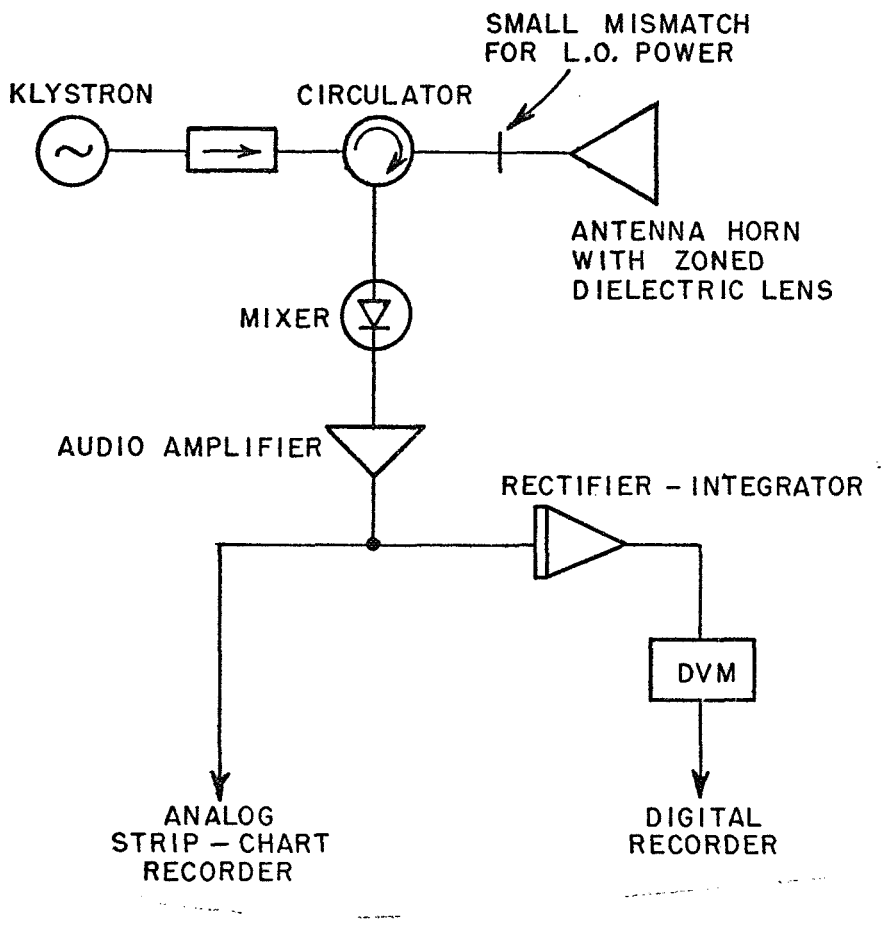

Fig. 2. Block diagram of a typical c-w doppler radar system.

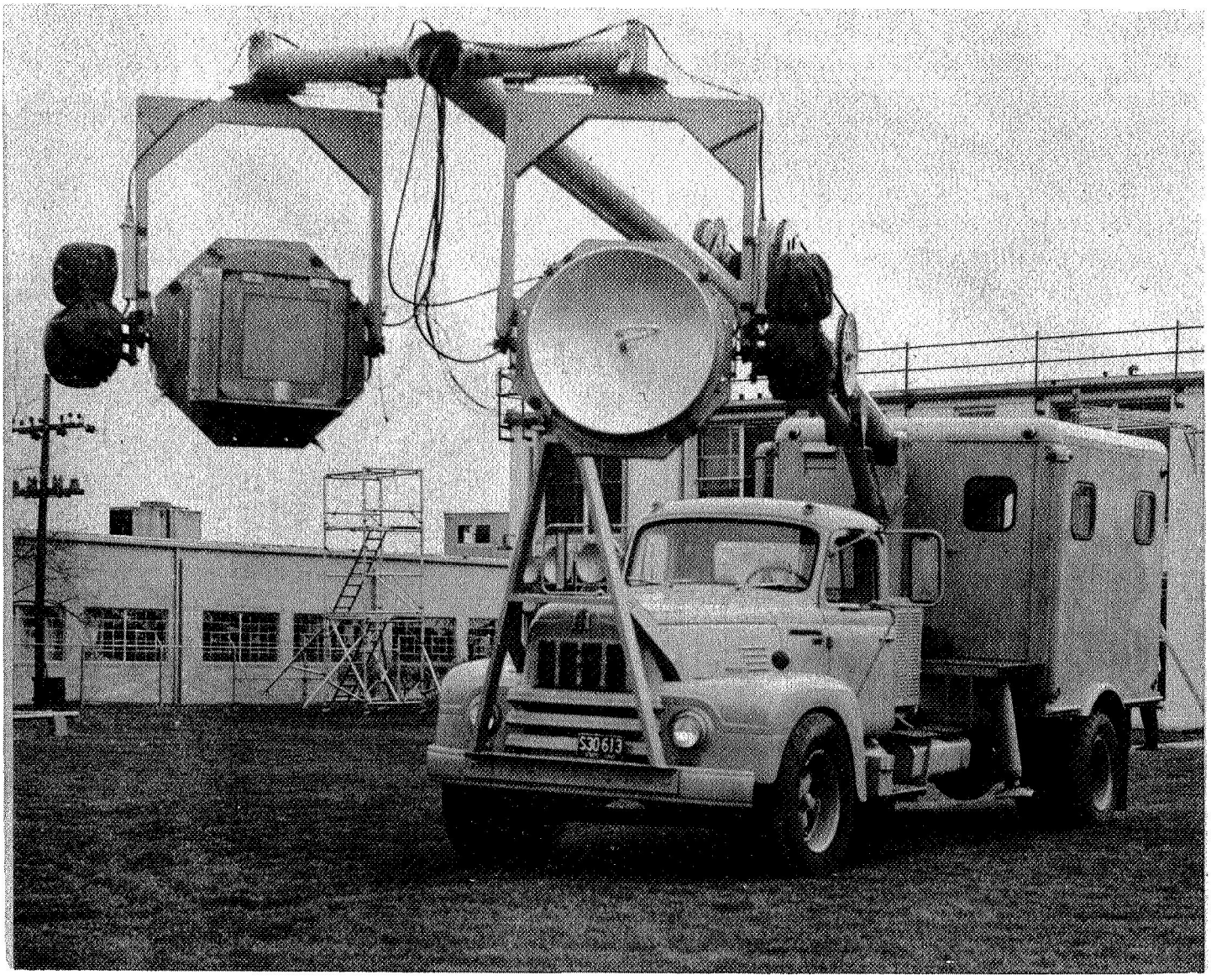

Fig. 3. The Ohio State University Mobile Radar-Radiometer Facility.

A summary of the radar system specifications, such as the antenna beamwidths, the local oscillator levels, and the smallest measured levels of the radar backscattering parameter, $\gamma(\theta_i)$, is given in Table I. The minimum detectable level of the radar backscatter, which is a more realistic index of system performance than system sensitivity, is less than the smallest measured values of γ for each radar system.

The radar systems are calibrated on an absolute basis by comparing the return from the terrain with the return from an 8" metal sphere, which is oscillated by a shaker (to provide the doppler shift) at the standard antenna-surface distance of 20 feet. All four radar systems are essentially similar to that shown in Fig. 2, except that the 1.8 GHz system uses a parabola instead of a horn, and the 10 GHz system receives both the direct and cross-polarized linear components of the return signal. The cross-polarized channel is calibrated relative to the direct channel by rotating an array of dipoles as a target. The rotation of the target modulates the reflected signal amplitude, and the sidebands provide the required frequency shifts for system operation.

The reduction of the radar data entails transformation of the integrated audio signal powers from the terrain and from the standard target to a normalized radar backscattering cross section per unit area, $\sigma^\circ(\theta)$, using the relationship

$$\sigma^\circ(\theta) = \frac{P_{rec(\theta)}}{P_{st}} \frac{\sigma_T}{R_o^2} \frac{1}{I_B(\theta)} \frac{B}{1100} \tag{3}$$

where P_{rec} = received power from terrain,

P_{st} = received power from standard target,

σ_T = radar cross section of standard target,

R_o = distance from antenna to target,

B = constant in exponent of one-way antenna power pattern,

I_B = value of integral tabulated by Barrick[7].

For a narrow beam antenna with one-way power pattern $f(\psi) = \exp(-B \frac{\psi^2}{2})$, one can show that $\gamma(\theta) \underline{\Omega} (P_{rec}/P_{st}) (\sigma_T/R_o^2) (B/\pi)$, i.e., γ depends only on the measured power levels, beamwidth, and σ_T/R_o^2. Details of the signal processing and data reduction are given in Reference 6.

TABLE I
Radar System Specifications

Frequency	1.8 GHz	10 GHz	15 GHz	35 GHz
Wavelength	12 cm	3 cm	2 cm	8.6 mm
Antenna Half-power Beamwidths	12°	5.2°	3.76°	2.00°
Antenna Type	3' parabolic	14" x 14" horn with lens	12" x 12" horn with lens	10" x 10" horn with lens
Polarization	any linear	any linear and 90° crossed linear	any linear	any linear
Transmitted Power	398 mw	75 mw	97 mw	28.9 mw
L. O. Level	1.5 mw	0.28 mw-direct 0.22 mw-crossed	1.0 mw	0.28 mw
Audio Amplifier Passband	0.8/250 Hz	8/250 Hz	8/250 Hz	8/250 Hz
Backscattering Cross Section, γ(dB) (Smallest measured values)	-35 dB	-30 dB-direct -45 dB-crossed	-20 dB	-18 dB

III. DESCRIPTION OF THE DATA

The data presented in Part IV of this report are of two kinds, first the description, or characterization of the various surfaces, (the "ground truth" data) and second the measurements of the normalized radar return parameter $\gamma(\theta)$, (the "sensor response" data). The measurements were made at four test sites, namely Mono Craters, Mono County, California; Pisgah Lava Flow and Lavic Dry Lake, San Bernardino County, California; Marble Cliff (Hobo) Quarry, Franklin County, Ohio; and Marblehead Quarry, Ottawa County, Ohio; in addition, data for a number of other surfaces are given for comparison purposes. In order to facilitate the correlation of sensor response with ground truth data, all of the data for an individual site are presented together, each site representing one section of Part IV. In each section, a general geological description of the site, supported where possible with topographic maps and radar imagery, is followed by more detailed descriptions of the particular surface elements of which the radar scattering properties were measured.

Following the surface descriptions, the actual radar data, in the form of graphs of the radar return parameter $\gamma(\theta_i)$ vs angle of incidence θ_i are given. The figures, with the exception of Figs. 24-26, are machine plotted from computer processed data averaged over terrain strips approximately 100 to 300 feet long. In the case of Figs. 24-26, it was not possible to average over sufficiently long terrain strips to produce meaningful averages. Thus for the latter surfaces, only strip chart records of the instantaneous values of the return, and some rather crude estimates of the average values of γ based on the chart records, are presented.

Each measurement is assigned a "group number" (groups 1-99 correspond to data obtained in 1965, groups 100-199 in 1966, and so forth), which was introduced to provide a convenient cross reference between the figures, and the surface identification ("ground truth"). The date on the figures gives the day, month, and last digit of the year of the measurement; for example, 16 Aug 6 corresponds to 16 August 1966. Computer printouts of the numerical values of $\gamma(\theta)$ and $\sigma^\circ(\theta)$ for each data group, identical in format to those included in Reference 2 are available, but have not been included in this report.

The accuracy of the data obtainable with the mobile radar system has been discussed in some detail in Reference 6 in which it was pointed out that the quality of the data depends not only on the instrumentation, but also the physical conditions under which the measurements were taken. In general, the errors which occur in the backscattering measurements arise from the following sources: (1) statistical fluctuations, which are insignificant here since the return is averaged over many independent samples; (2) calibration errors, due to alignment inaccuracies of the calibration target (especially at K_a-band) and ground effects (in the case of S-band); drift between pre- and post-calibration; and sporadic human errors in the recording of amplifier gains, etc. (Error in the absolute calibration will

affect only the absolute level of the cross sections, but not the relative values for a given measurement. Measurements on which absolute calibrations are in doubt have been indicated by "absolute calibrations in doubt."); (3) system geometry - since the truck is driven along the terrain, the look angle and antenna height can vary due to boom oscillation, truck bounce, etc. In addition, at a number of sites it was necessary to measure scattering by tilted walls of material rather than horizontal beds or surfaces, and some difficulty was encountered in maintaining constant range from radar to surface under these conditions, and in maintaining a constant angle of incidence with respect to the mean tilted surface.

It should be pointed out that the absolute level of the 1966-67 X-band cross-polarized data is in doubt since a suitable calibration was not available. An indication of the consistency of this data is provided by the reciprocity condition for the cross-polarized returns; that is, $\gamma^{\circ}_{VH}(\theta_i) = \gamma^{\circ}_{HV}(\theta_i)$. Particularly in the earlier measurements, apparent systematic differences between these two parameters are due to a small difference in gain between the two data processing channels. In practice, care has been taken to minimize the above sources of error, and it is felt that the reported measurements are accurate to within $\pm$ 1.5 dB although there may be occasional bad data points. Similarly, for the majority of measurements over relatively smooth horizontal surfaces, the accuracy in maintaining the angle of incidence is within $\pm$ 3°, although over rough terrain or tilted surfaces, poorer accuracy must be expected.

IV. SITES AND DATA

A. Mono Craters[8]

Mono Craters occur in east-central California in Mono County, just south of circular Mono Lake and 6-7 miles east of the Sierra Nevada front. The area is one of NASA's fundamental test sites (lunar analog) for remote sensing techniques. The craters are comprised of a series of spectacular obsidian domes and flows (coulees), and pumice cones. Their geologic youthfulness (Late Pleistocene or Recent) is attested to by the essentially unmodified volcanic forms that they display. The main body of the craters is a continuous arc concave toward the west that is nearly ten miles long. Isolated obsidian domes extend for nearly an equivalent distance to the south. The Lapilli Surface, which is one of two surfaces on which radar data was gathered, occurs between two tongues of an obsidian flow (North Coulee) (see location map, Fig. 4). Presumably, the Lapilli Plain resulted from a violent explosion from one of the crater flanks that spewed out material in horizontal fashion. The pumice Surface occurs near the crest of the craters within the vent of the South Coulee (see Fig. 4). This surface occurs on the property of the U. S. Pumice Company whose permission to enter is gratefully acknowledged. The location of surfaces is also designated on Fig. 5, which is a K-band, side-looking airborne radar image of Mono Craters and the adjoining area.

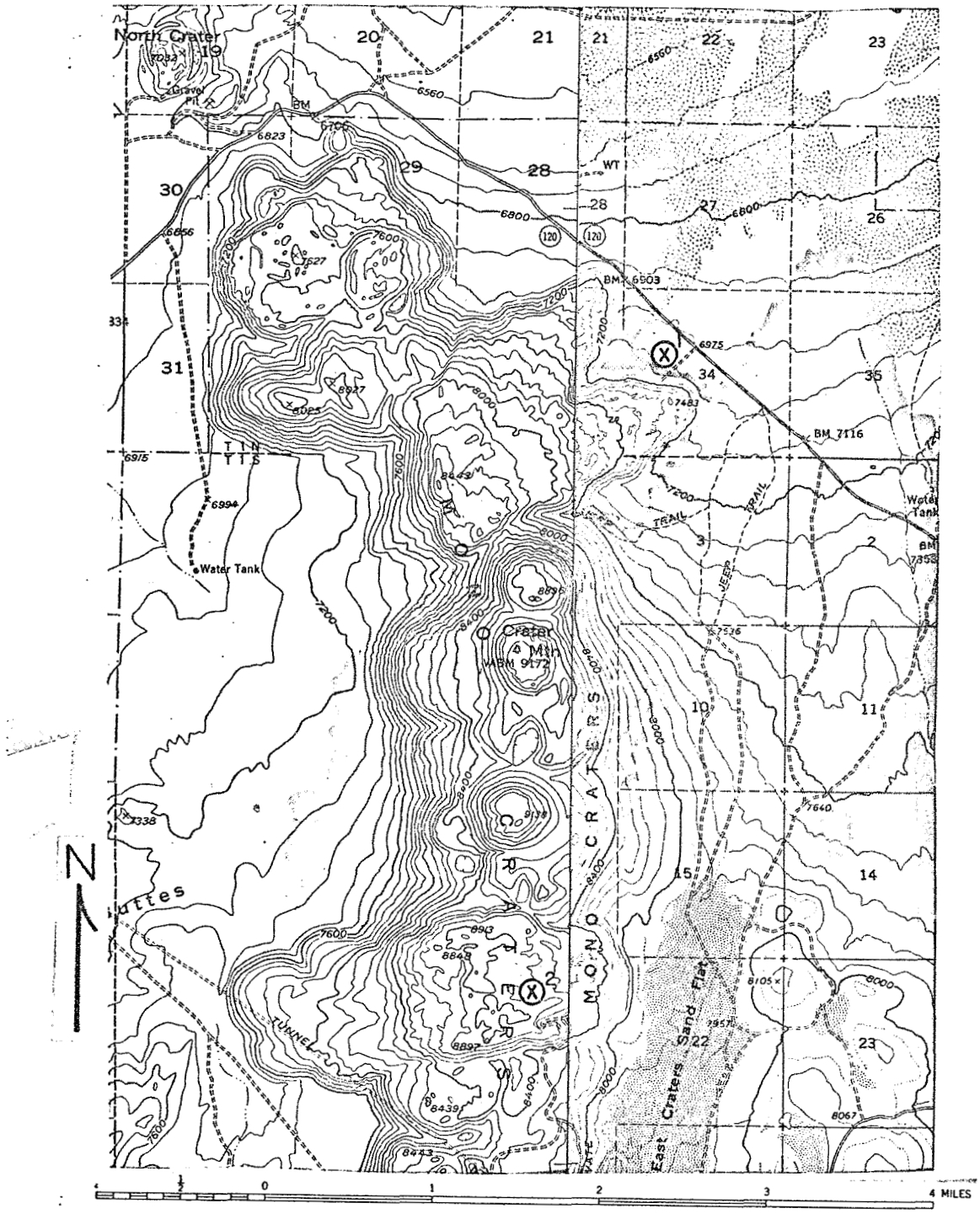

Fig. 4. (Location map). This topographic map of Mono Craters, California shows the location of the Lapilli Surface ⊗[1] and the Pumice Surface ⊗[2]. The map was constructed from the east-central portion of the Mono Craters, California 15-minute topographic quadrangle and the west-central portion of the Cowtrack Mountain, California 15-minute topographic quadrangle.

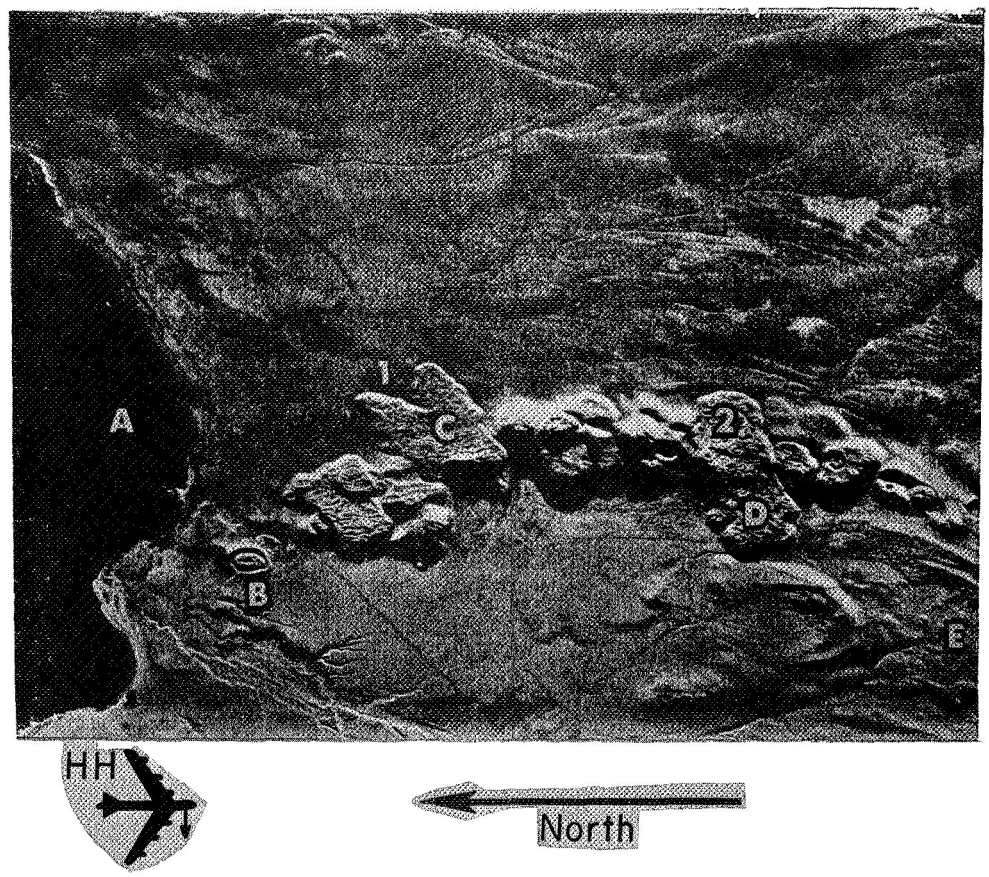

Fig. 5. SLAR Image of Mono Craters Area, California. Direct return, K-band, side-looking, airborne radar image of the Pisgah Craters area showing location of radar test surfaces. Notations are "A" Mono Lake, "B" North Crater, "C" North Coulee, "D" South Coulee, "E" U.S. 39 , "1" Lapilli test surface, and "2" Pumice test surface.

1. Lapilli Surface (Mono 1)

Group Nos. 1, 2, 3, 4

Location. Mono Craters, California

Description. The lapilli surface was measured at a site on a topographically flat plain that slopes gently north toward Mono Lake (see Fig. 4). The material is a mixture of lapilli-sized particles (diameter > 4.0 mm) and volcanic ash, with the latter predominating. The bimodal character and poor sorting coefficient are obvious from Table II. The largest particles rarely exceed 30 mm and there is almost a total lack of clay-sized particles (0.0039 mm). There is some concentration of coarser particles at the surface and finer particles at depth caused by the eluviation effect of rain. The material was perfectly dry and uncompacted in the first few inches, but some moisture was evidently present at shallow depths, because the surface supported a sparse ground vegetation (see Figs. 6 and 7).

Texturally and compositionally, the particles are very simple. Below 0.5 mm in diameter most of the particles are angular, clear to light-gray, rhyolitic glass with some admixture of organic fibers and spherical bodies. Above 0.5 mm there is a gradual increase in the number of white to light-gray grains showing lineated to non-lineated, microvesicular to vesicular structure. These grains dominate the size samples greater than 2.0 mm. All of these vesicular grains and particles can be classified as pumice and are probably rhyolitic in composition.

Radar data are plotted in Figs. 8 and 9.

TABLE II

Size distribution by Weight % in a layer from the surface to two inches below the surface.

Diameter (mm)	Weight %
> 12.7	1.5
12.7-5.0	16.8
5.0-4.0	1.1
4.0-2.0	20.4
2.0-1.0	24.3
1.0-0.5	23.3
0.5-0.25	8.4
0.25-0.125	2.4
0.125-0.063	0.9
< 0.063	0.9
	100.0

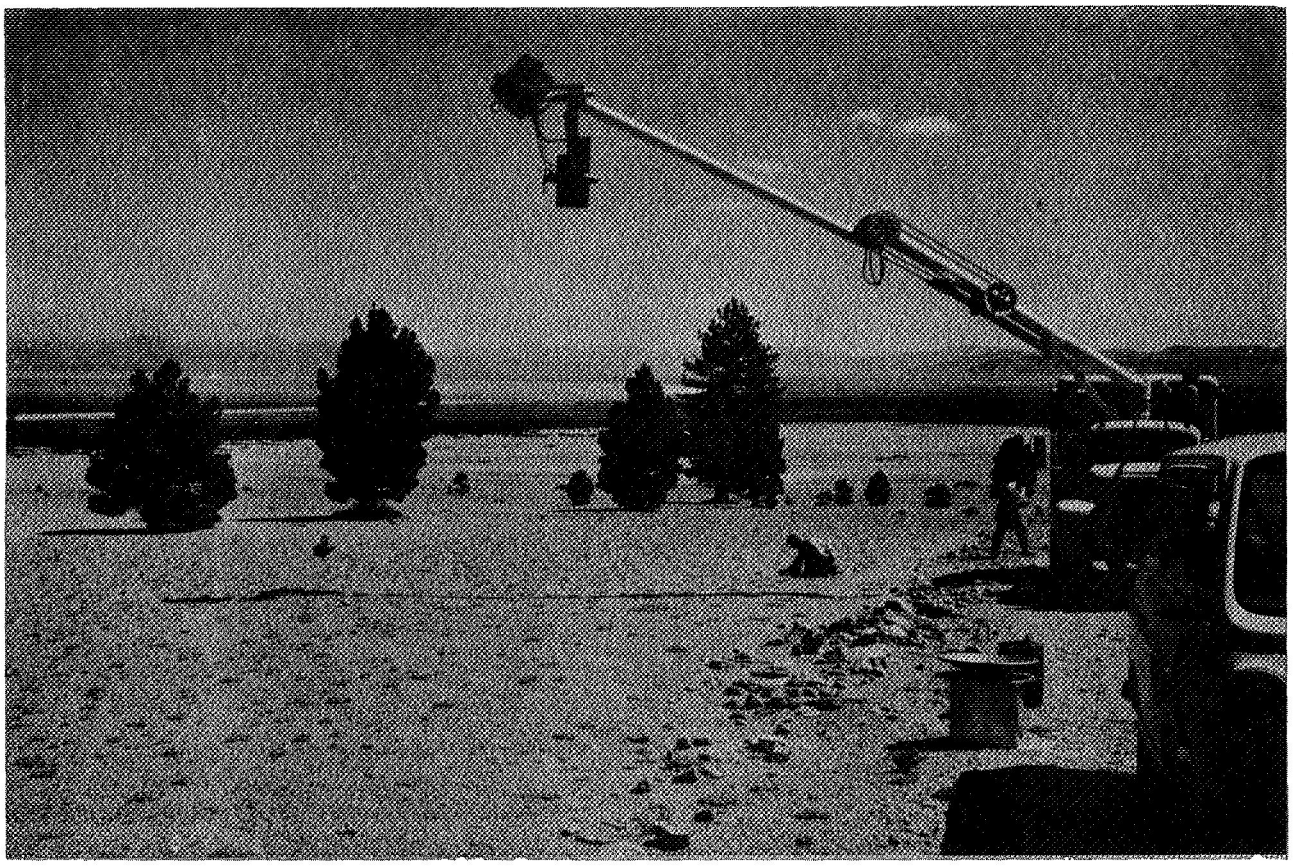

Fig. 6. Radar truck taking measurements on the lapilli plain. The view is to the northeast toward Mono Lake (center, left). Note the general flatness of the plain and lack of vegetation except for scattered trees and small ground plants.

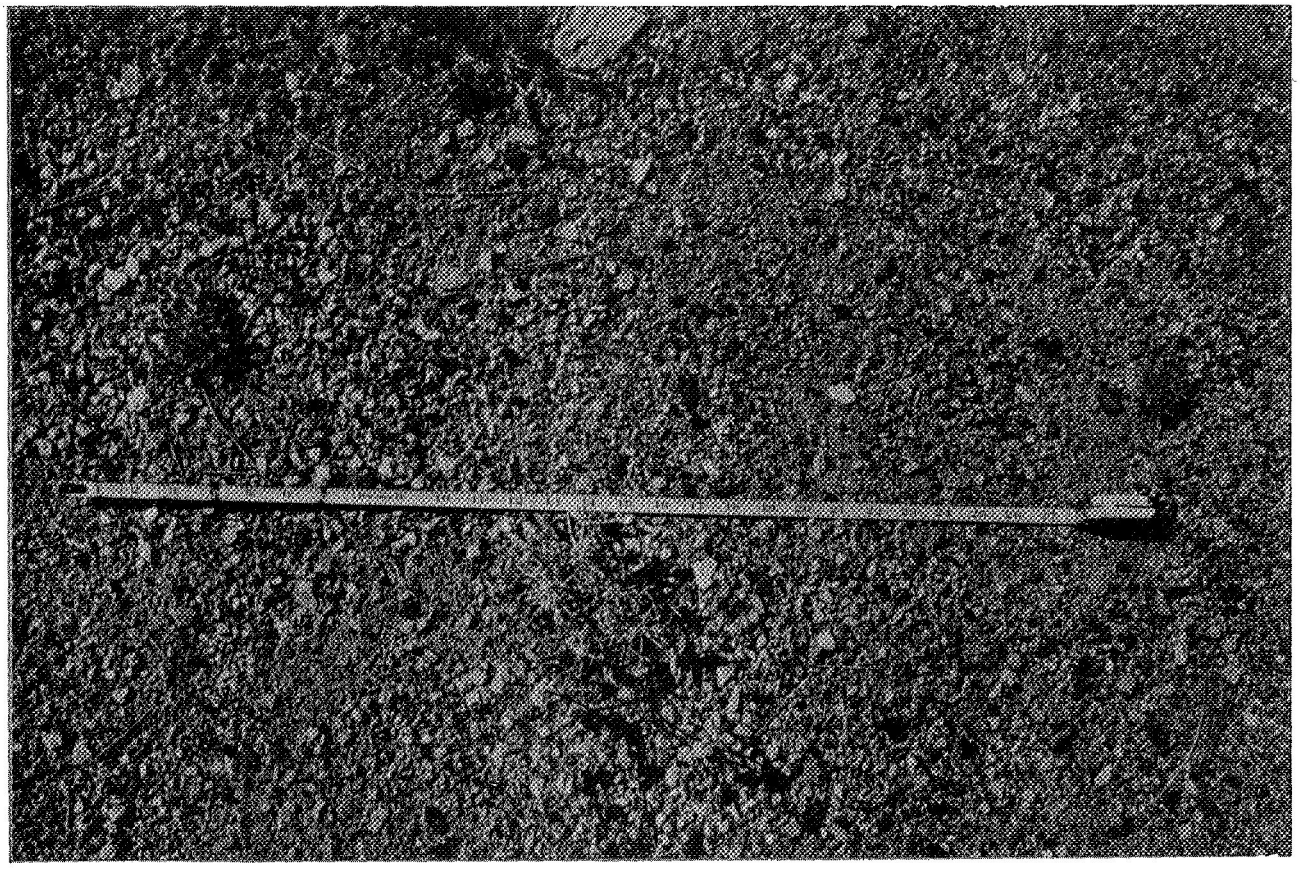

Fig. 7. Close-up of lapilli surface. Note the concentration of coarse pumice lapilli in botches and bands, and the sparse ground vegetation and scattered pine needles. Scale is in inches.

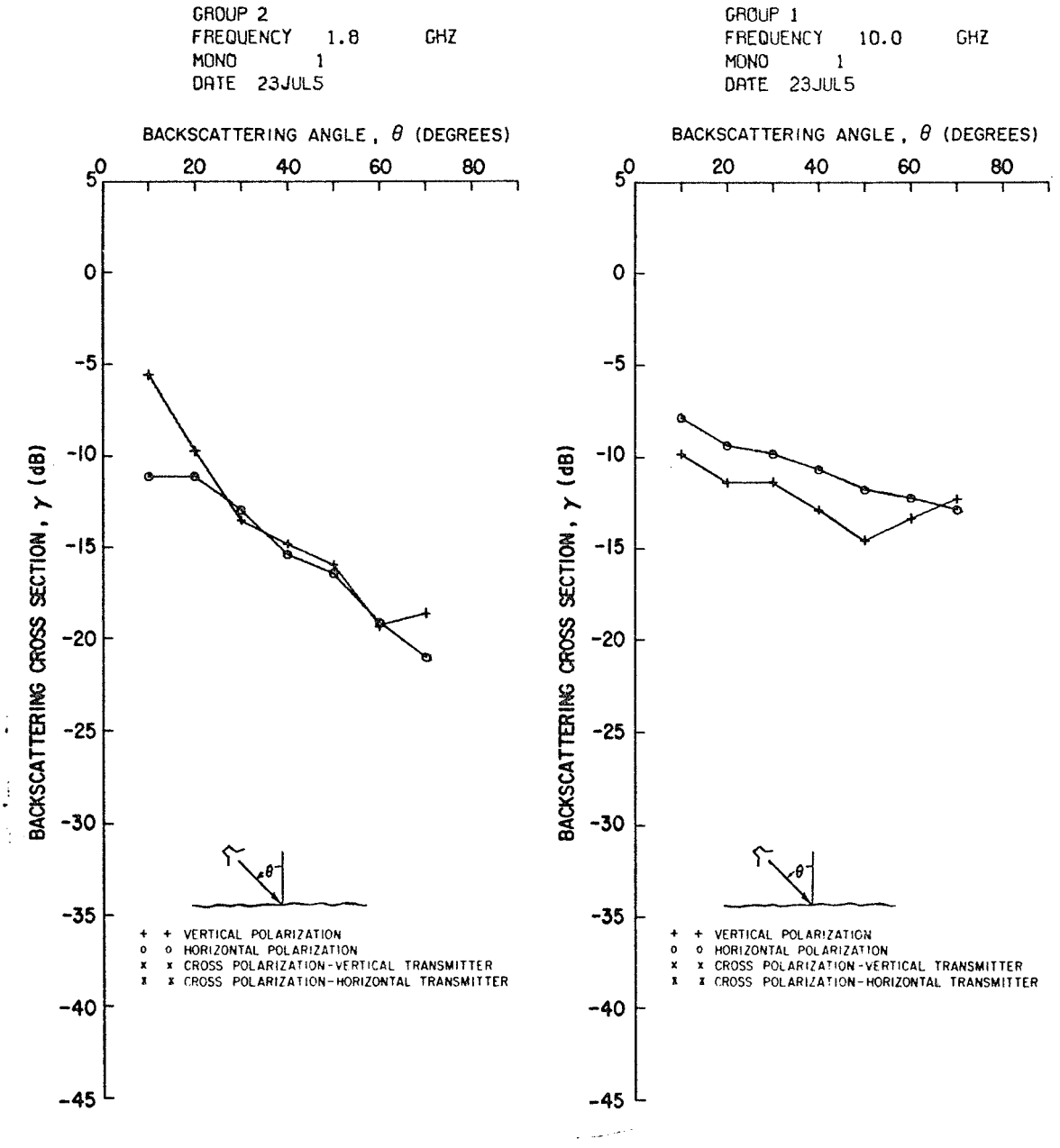

Fig. 8. Lapilli Surface (Mono 1).

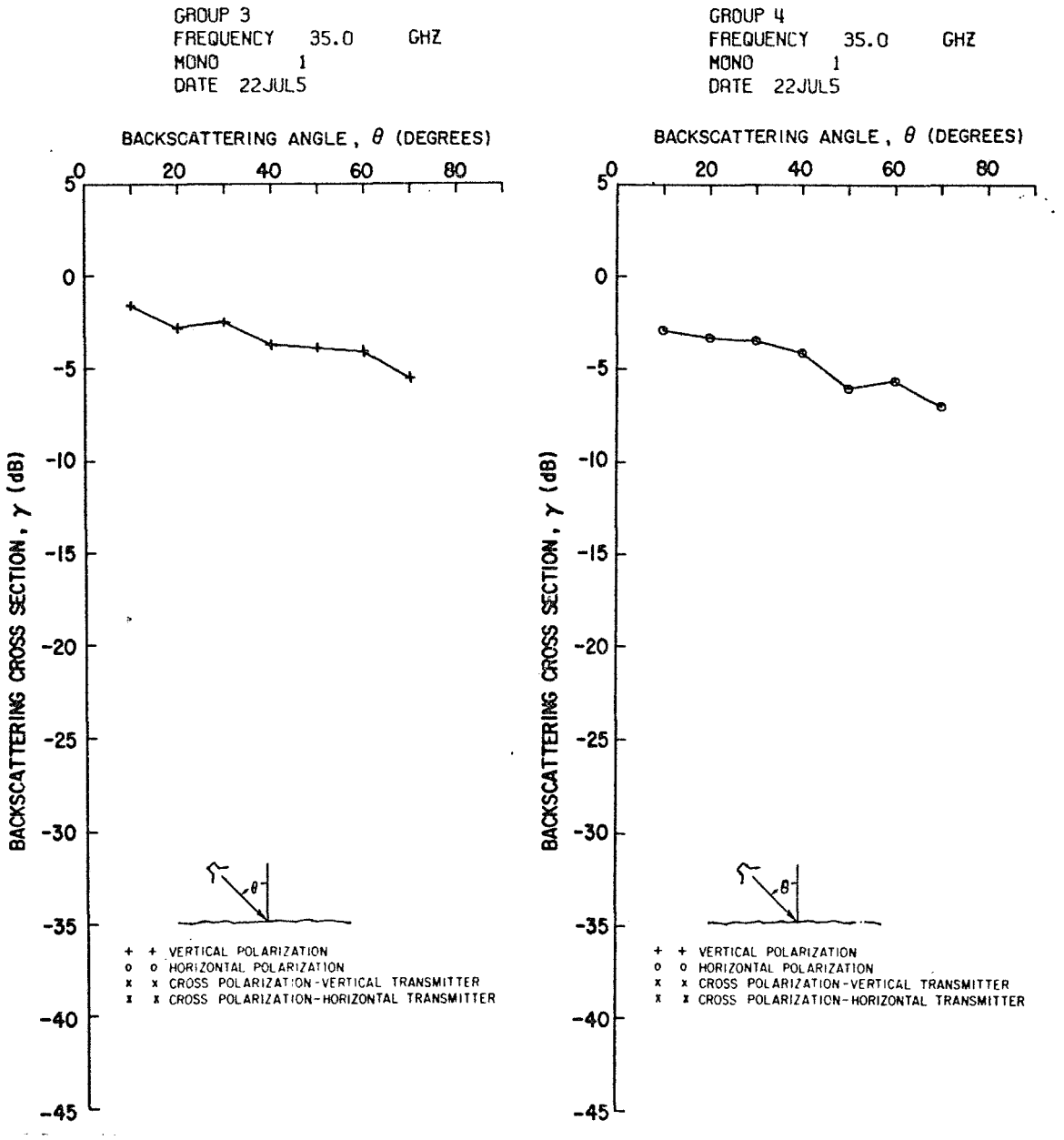

Fig. 9. Lapilli Surface (Mono 1)

2. Pumice Surface (Mono 2A)

Group Nos. 17, 18, 19

Location. Mono Craters, California

Description. The radar response to pumice was measured within the chain of volcanoes that make up Mono Craters. Specifically, the site was within the probable vent area of the so-called South Coulee (a short, blocky, steep-sided lava flow, generally composed of glassy rhyolitic material) (see Fig. 4).

The test site is in an area of extremely rough macrotopography that is completely devoid of vegetation and made up of a jumble of large pumice blocks and spines of pumice lava showing vertical flow structure. The particular area illuminated by radar is along a bulldozed access road. In spite of this activity it is believed that the blocks examined are approximately in their natural state. The average cross-sectional area of the blocks is 131 square inches and the average diameter is 11.5 inches (see Fig. 10). The range in diameters is 4 to 34 inches. The pumice itself is medium-dark gray, translucent glass that shows unusually coarse vesicular structure and almost always some flow structure. Vesicles are typically several millimeters in diameter. The blocks are all very angular and are unweathered, although yellowish discolorations on some surfaces indicate minor hydrothermal (deuteric) alteration.

Radar data for this surface are shown in Figs. 11 and 12.

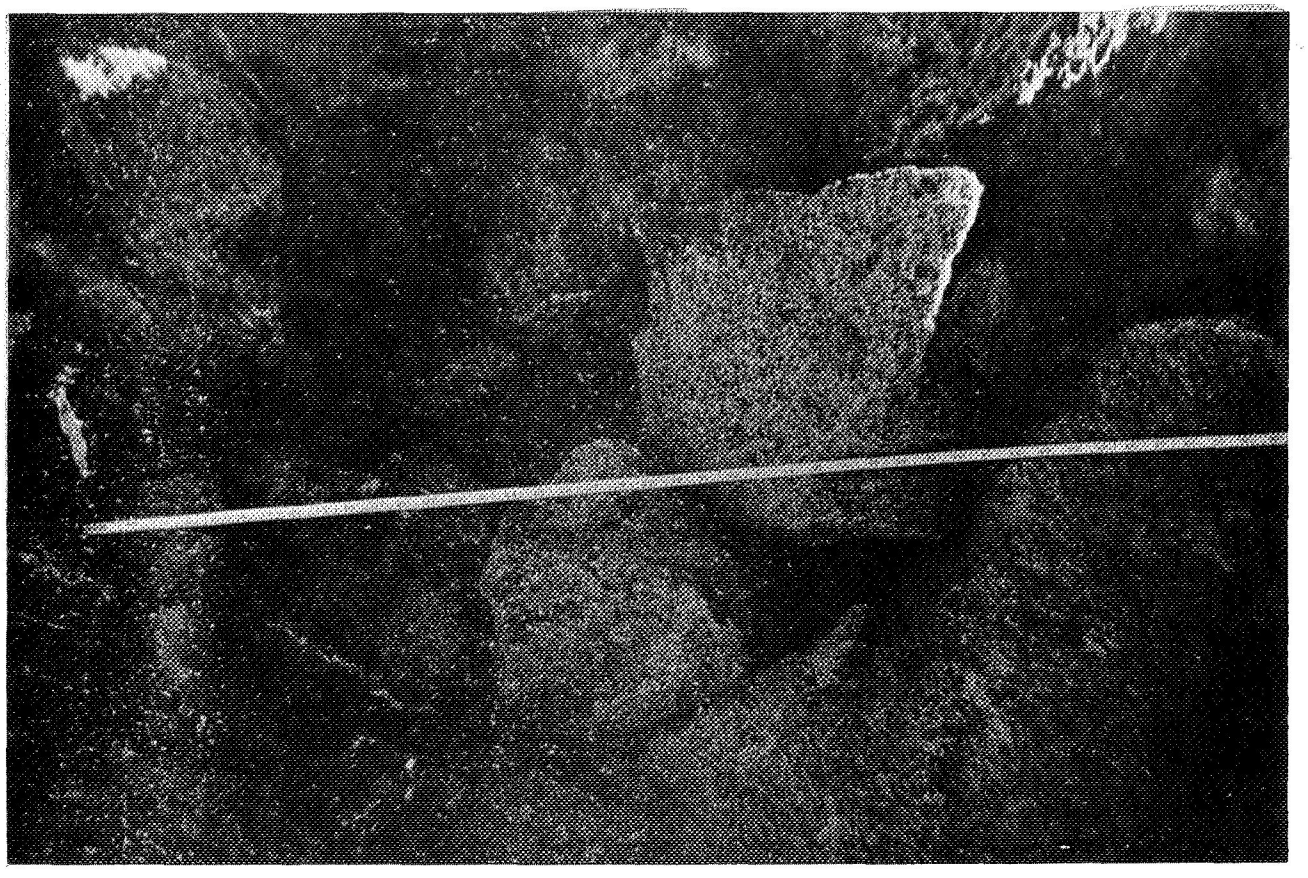

Fig. 10. Pumice blocks at Mono Crater. The photograph shows the large angular blocks of pumice that underlie the rugged topography near the summit of one of the Mono Craters. Note the large size of the vesicles. The scale is in inches.

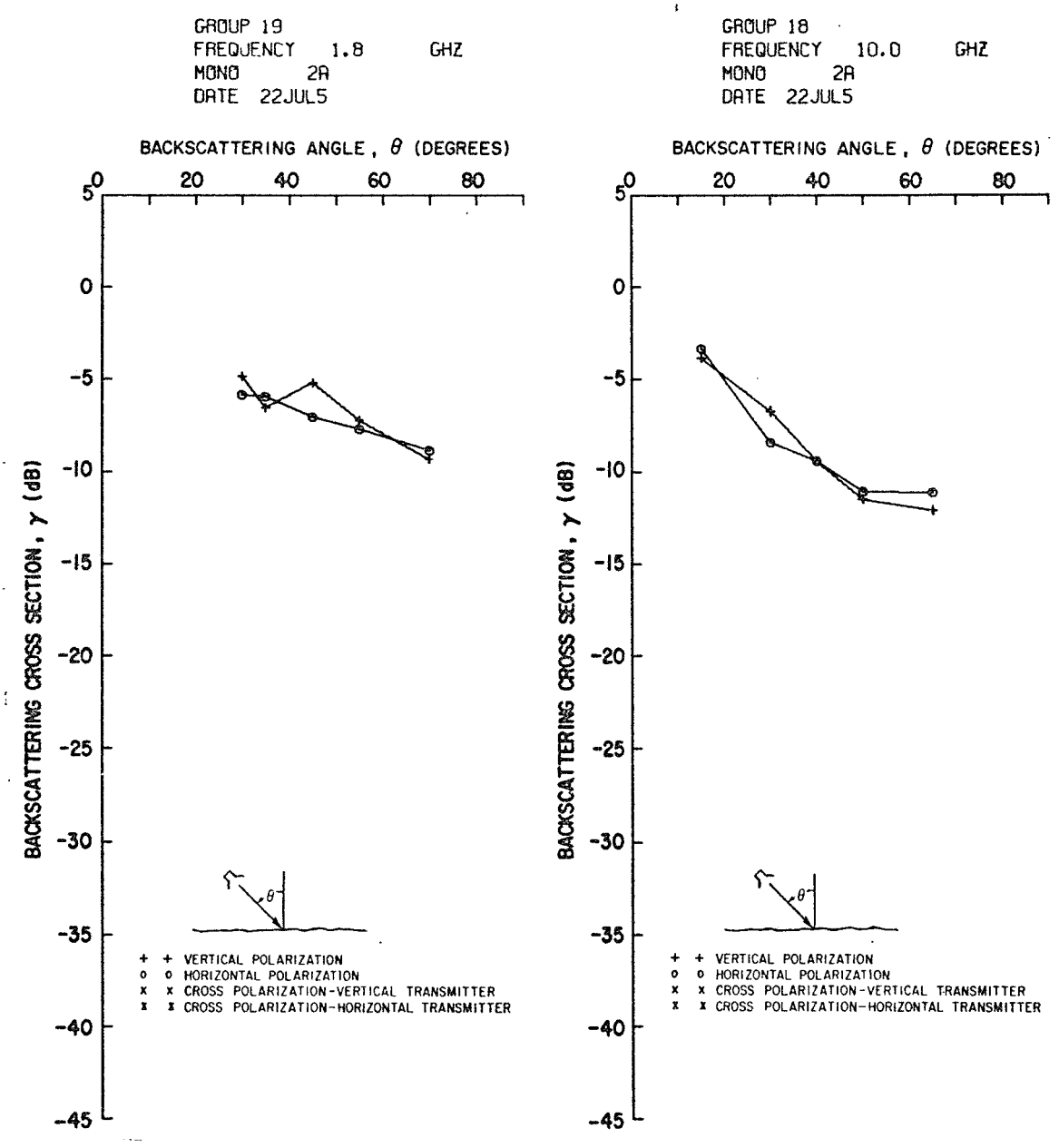

Fig. 11. Pumice Surface (Mono 2A)

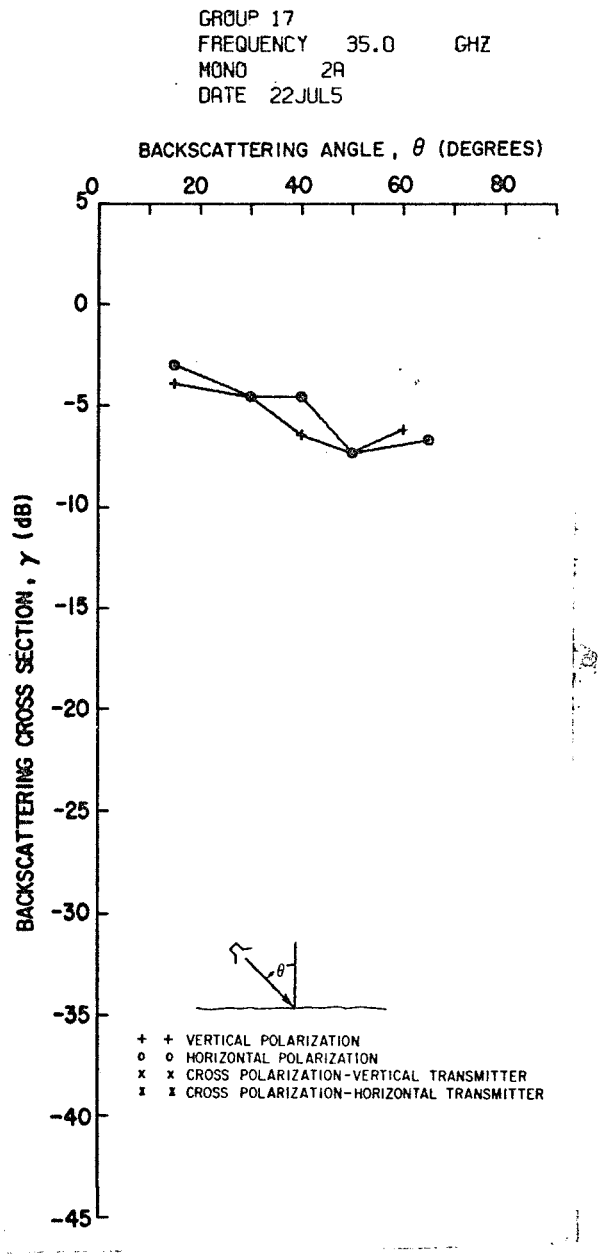

Fig. 12. Pumice Surface (Mono 2A)

B. Pisgah Crater, Pisgah Lava Flow, and Lavic Dry Lake[9]

Pisgah Crater, Pisgah Lava Flow, and Lavic Dry Lake occur in San Bernardino County, California, approximately 30-35 miles east-southeast of Barstow and just south of highway U.S. 66. The area lies well within the Basin and Range physiographic province and the Mojave Desert subprovince, and is one of NASA's fundamental test sites (lunar analog) for remote sensing techniques. The Pisgah Lava Flow is composed of a series of thin sheets of olivine basalt lava, which merge to a single sheet near the margin. They were erupted over a short period of time in the Late Pleistocene or Recent, and thus, primary volcanic features are well preserved. The flows extend from a 300-foot high cinder cone called Pisgah Crater, which is the probable vent area, a distance of approximately 14 miles downslope into the Lavic Dry Lake basin. The dry lake is a playa dating from pluvial periods during the latter part of the Pleistocene, and was near the head of the local drainage system at that time. The playa surface is nearly perfectly flat and is prominently mud cracked. The Pisgah Lava Flow in part overrides the playa, and is in part buried by playa clay.

All of the surfaces on which radar data was gathered for this report occur at the southern terminus of the Pisgah flow at its junction with Lavic Dry Lake. This part of the flow is characterized by large collapse areas and tilted blocks of lava crust resulting from underflow of liquid lava and withdrawal of support from the solid crust shortly after the time of eruption. Location of the specific surfaces tested is marked on a location map, Fig. 13. The same locations are marked on Figs. 14(a) and 14(b), which are K-band, side-looking airborne radar images of the Pisgah area.

NOTE: The playa surface L1 was measured near the center of square 27.

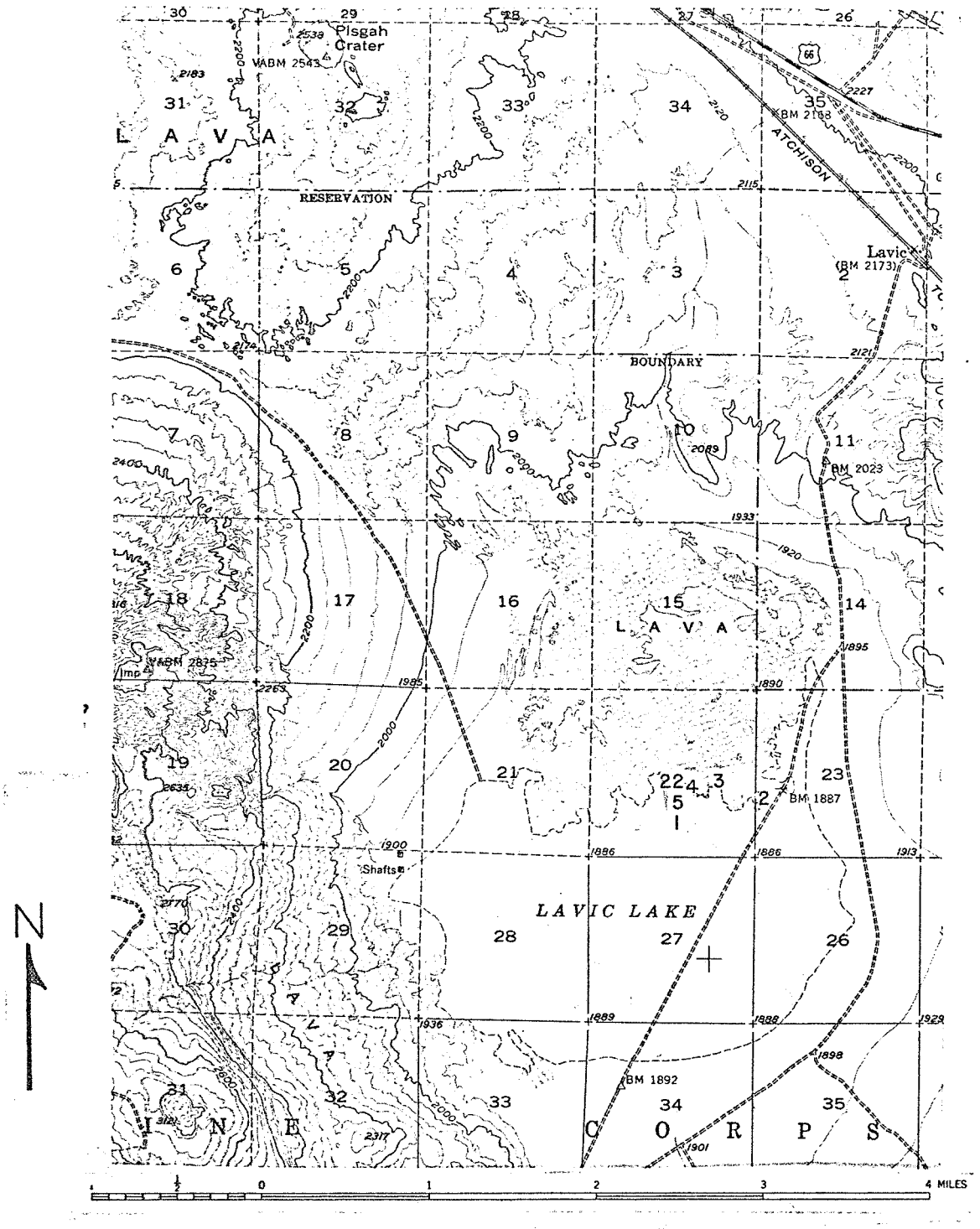

Fig. 13. (Location Map). This topographic map of the Pisgah Flow-Lavic Dry Lake test site shows the location of surfaces on which radar data was gathered. These surfaces are:

1 - Playa and cinder-covered playa surfaces
2 - Mosaic cinder surface
3 - Pahoehoe lava surface
4 - Smooth basalt lava and aa lava surfaces
5 - Smooth basalt lava surface with squeeze-up

The map is from the north-central portion of the Lavic, California 15-minute topographic quadrangle.

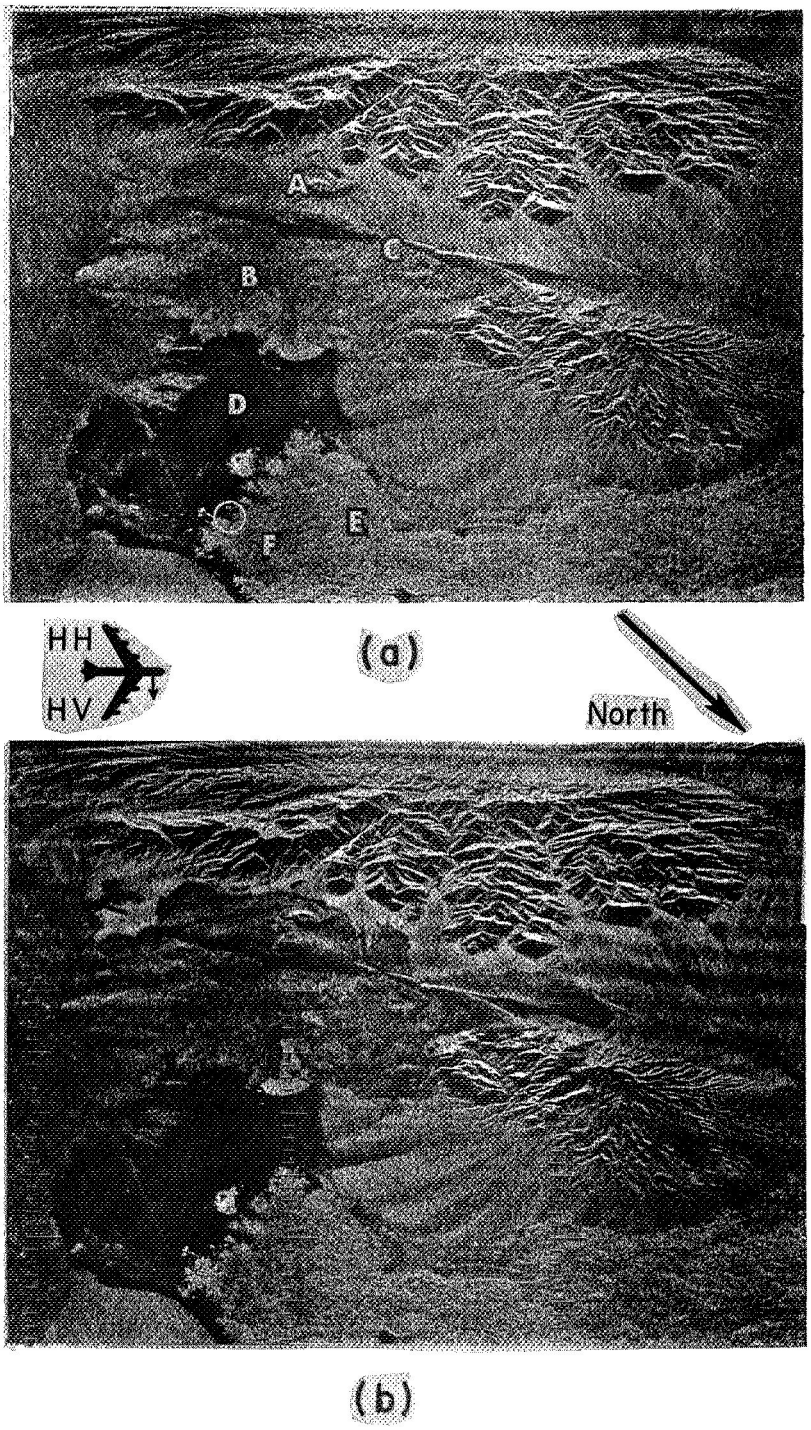

Fig. 14. SLAR Images of Pisgah Crater Area, California. Direct return and cross-polarized return, K-band, side-looking, airborne radar images of the Lavic Dry Lake-Pisgah flow test site showing the area of radar test surfaces. Letter notations are "A" Sunshine Crater, "B" Sunshine flows, "C" Pisgah fault, "D" Lavic Dry Lake playa, "E" Pisgah Flow, and "F" area of test surfaces.

1. Playa Surface (Pisgah L1)

Group Nos. 5, 6, 11, 12, 13, 14, 15, 16

Location. Lavic Dry Lake, California

Description. Radar properties of playa surfaces were determined on Lavic Dry Lake at the south end of the Pisgah Lava Flow in the Mojave Desert, California (see Fig. 13). A playa is the flat central basin of a desert plain, which at rare and irregular intervals becomes a broad, shallow lake. Lavic Dry Lake (playa) is classed as a playa of the dry-surfaced type with a hard, dry, compact crust (Neal, 1965[10]). The crust is broken by contraction (dessication) cracks and divided into polygons of three general dimensions (see Fig. 15). The largest of these polygons are 20 feet or more in diameter, and are bounded by contraction cracks that produce depressions up to one foot in depth. Intermediate polygons are about one foot in diameter, and the smallest polygons are one to three inches in diameter. The latter show upturned edges and are readily extracted from the playa floor although they are friable. Bulk physical properties of Lavic Lake playa samples are as follows (Kerr and Langer, 1965[11]):

Specific gravity	2.08
Bulk density	1.67 g/cc
Compaction ratio (1.0 = 0 porosity)	0.80
Nonstructural water	5.8%

Playa material is light tan and shows a dull to almost waxy luster. Mechanical analysis showed that 96.6% of the grains in the surface layer (about one inch thick) are less than 0.074 mm in diameter, indicating a great predominance of silt- and clay-sized particles. About 74% of bulk playa samples from Lavic Lake are clay according to Kerr and Langer (1965). Grains are crudely graded in the top one-inch layer with the finer ones near the surface. This surface layer is also very porous in appearance on a microscopic scale. Compositionally, the clay fraction is dominated by montmorillonite (12.5 Å), with secondary amounts of interlayered montmorillonite-illite and some illite (10 Å) according to X-ray analyses (Kerr and Langer, 1965). Grains coarser than 0.25 mm, but less than 1.0 mm (the maximum grain size) are mostly scoriaceous basalt, but comprise less than 1% of the samples by weight. Glassy grains of quartz, some feldspar and olivine, and an abundance of a white to pale bronze mica-like mineral dominate the material between 0.25 and 0.074 mm. Salines, which make up about 0.2% of bulk samples, are dominated by halite (Kerr and Langer, 1965). Calcite is a common constituent judging by the persistent, vigorous reaction of playa samples in dilute HCl.

Radar data for this surface are shown in Figs. 16-19.

Fig. 15. Lavic Lake Playa. The surface of the playa is almost perfectly flat except for small scale roughness generated by contraction (dessication) cracks. These cracks break the playa surface into polygons of three distinct sizes: A - measured in terms of 10's of feet; B - measured in terms of a few feet; and C - measured in terms of a few inches. In the intermediate distance is the radar truck being used to make calibration measurements and in the far distance to the left are the black basalt lava flows from Sunshine Crater. The view is to the northwest.

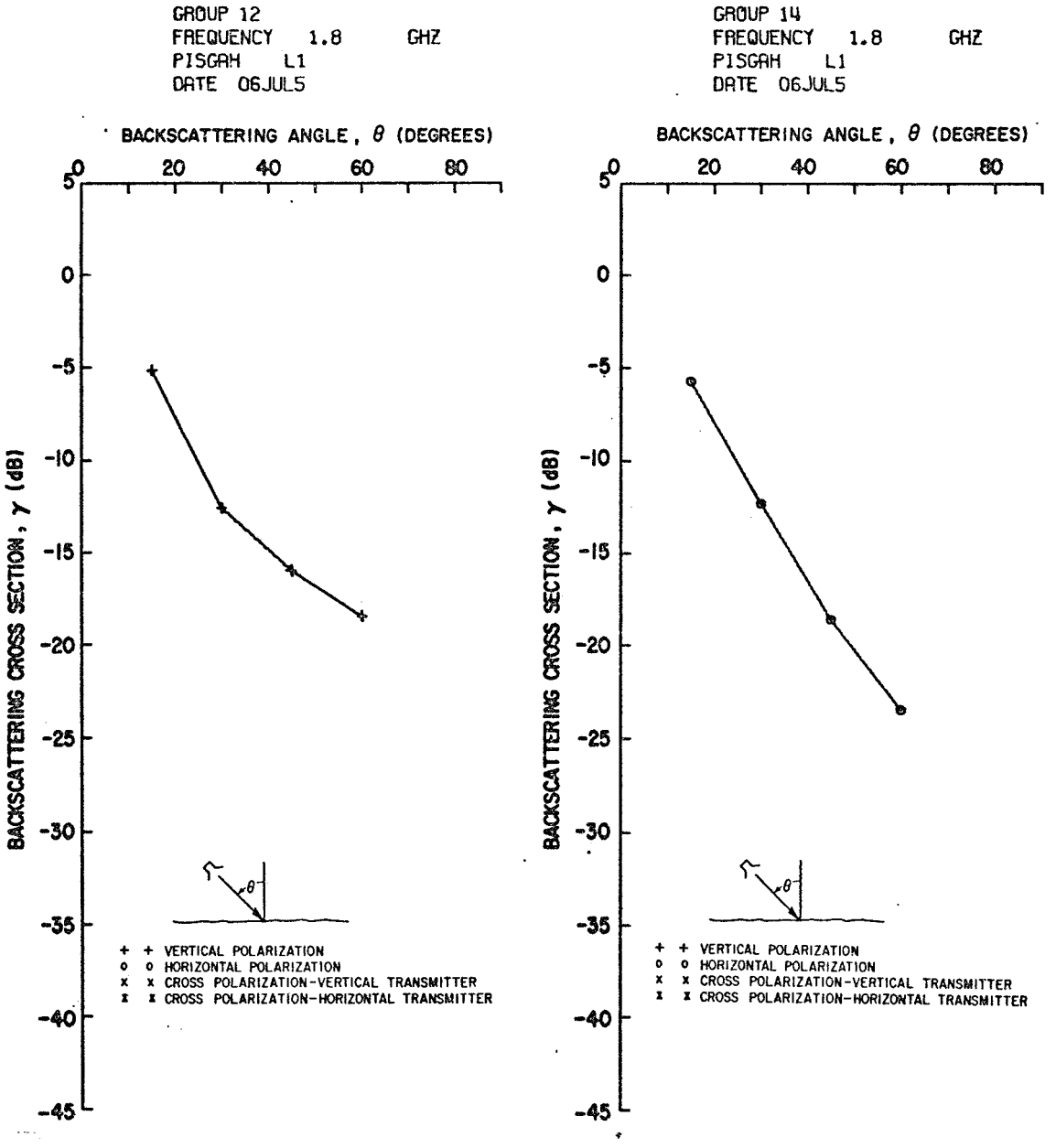

Fig. 16. Playa Surface (Pisgah L1).

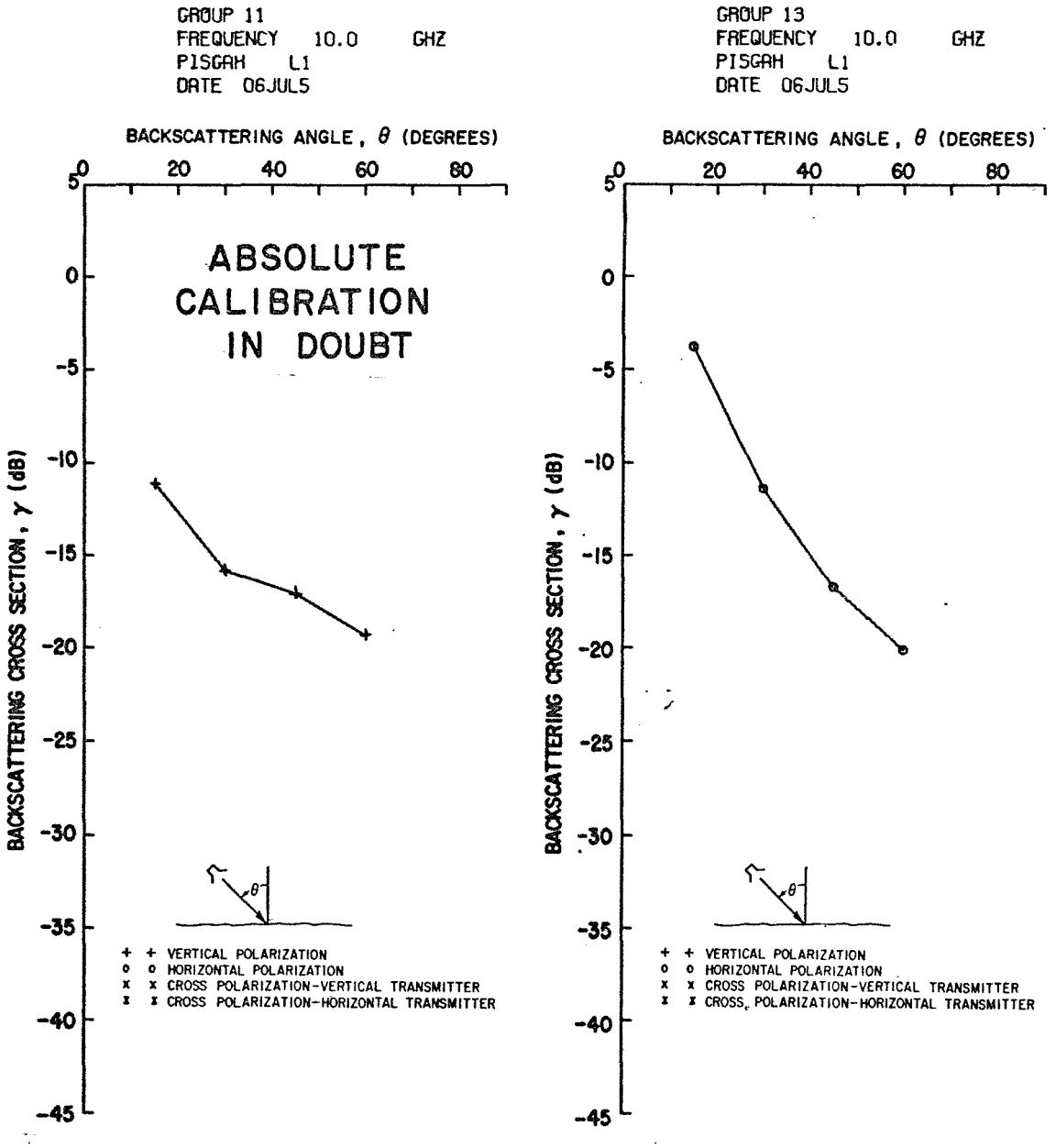

Fig. 17. Playa Surface (Pisgah L1).

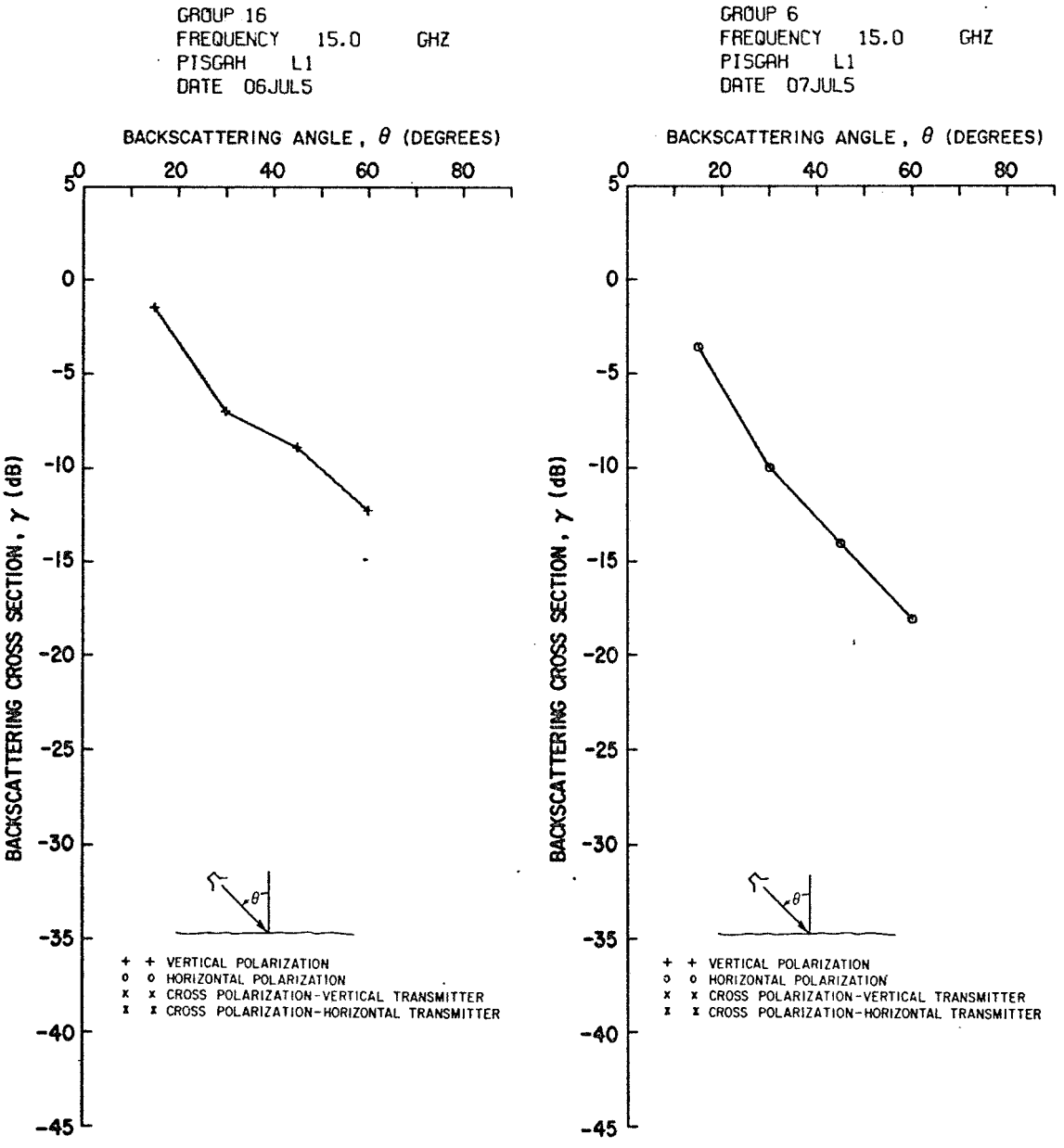

Fig. 18. Playa surface (Pisgah L1).

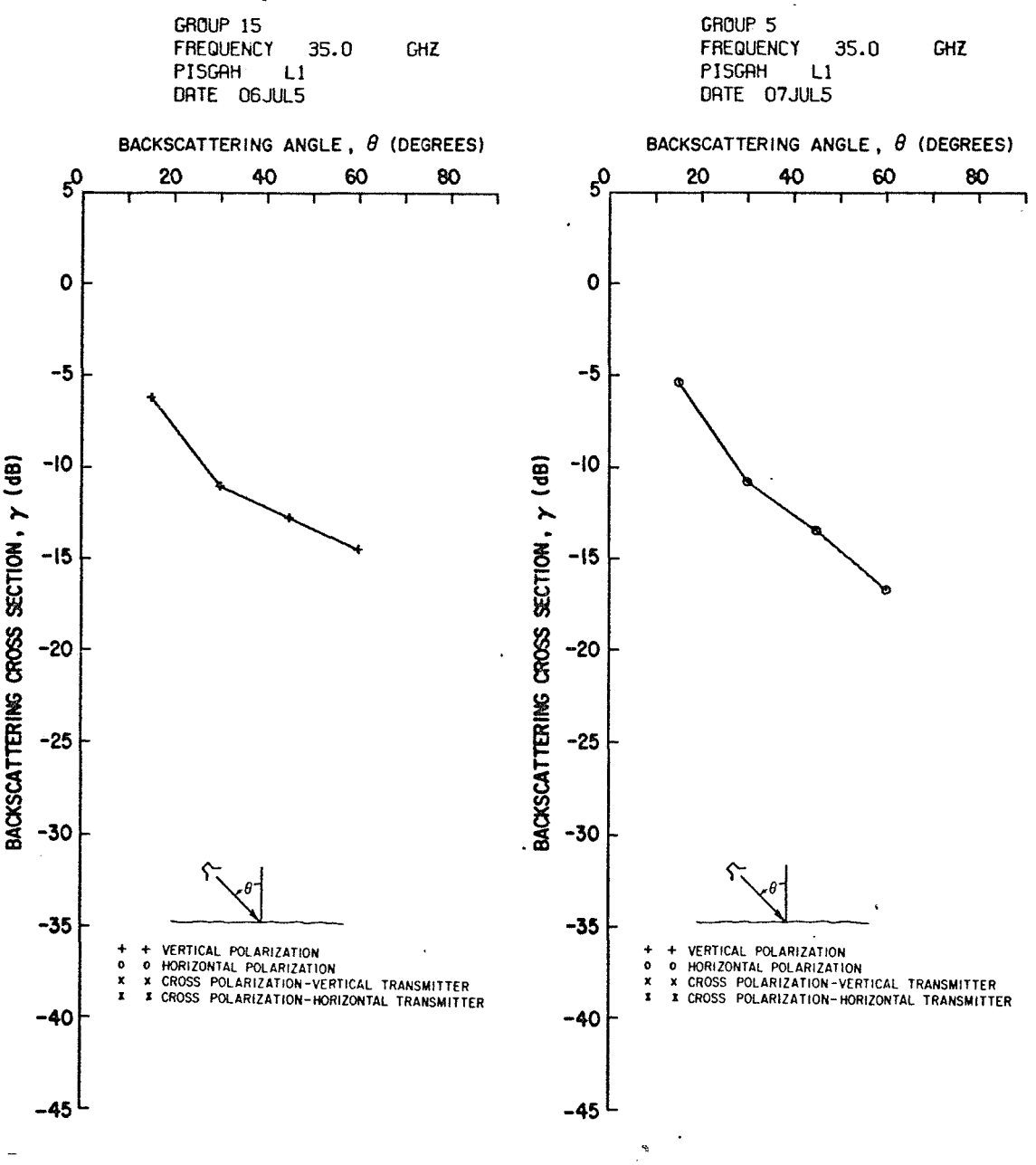

Fig. 19. Playa surface (Pisgah L1).

2. Playa Surface with Partial Cover of Basalt Cinders

Location. Lavic Dry Lake, California

Description. The playa surface in this set of measurements is identical to the previous one except that it is covered in part by basaltic cinders, derived from the Pisgah Crater Lava Flow. The cinders are rather jagged and angular in shape, and are generally one to three inches in diameter (see Fig. 20). They are fairly uniformly distributed and usually are not in contact with one another. The photograph (Fig. 20), which represents a typical cinder population, was used to determine the area covered by cinders. The method employed indicated that the surface is 29.7% cinders and 70.3% clay-rich playa from a vertical look-angle. The area covered by cinders apparently increases as the look-angle decreases, of course, since the cinders stand above the essentially flat playa surface. For instance, at a look-angle a few degrees above horizontal, the surface appears to be completely covered with cinders (see Fig. 21). The cinders are scoriaceous, aphanitic, olivine basalt (for a more detailed description, see the following section of this report). It is believed that they have been deposited in their present position by ice rafting. Because of the relatively short runs represented by the cinder covered area, and because it was not possible to drive parallel to the lava shown in Fig. 21, average values of γ could not be obtained for these surfaces. However, strip chart recordings of the instantaneous value of the return signal (with pen deflection proportional to the scattered electric field) were made, to illustrate the nature of the variations in signal strength from the playa, lava, and cinder covered surfaces illustrated in Fig. 21. For example, Fig. 22 shows the record from a run at 45° angle of incidence, vertical polarization, (upper trace, 1.8 GHz, lower trace 10 GHz). The return signal is a narrow band noise signal, with center frequency at the doppler frequency characteristic of a point at the center of the illuminated spot, and bandwidth (approximately the inverse of the fading rate for the envelope) determined by the difference in doppler between the leading and trailing edges of the spot. The difference in level between the return from the lava (large signal), cinders, and playa (smooth surface, small signal) is clearly shown. One may note on the record the short strip of playa clear of cinders (at the position of the human figure in Fig. 21) between the lava and the cinders. A similar run is shown in Fig. 23, for the high frequency pair of radars at 15 and 35 GHz.

It is rather difficult to analyze these brief samples in a quantitative way. However, an attempt has been made to plot relative (not absolute) values of $\gamma(\theta)$ vs θ, based on a visual estimate of the signal strengths in a number of runs similar to those shown in Fig. 22 and Fig. 23. The results are shown in Figs. 24-26. Reference levels for γ are arbitrary, but have been chosen so that the return from the playa surface agrees roughly with that measured in the center of Lavic Lake (surface L1). The rather large values for the lava material may be due partly to the fact that the outcrop was several feet high (thus reducing

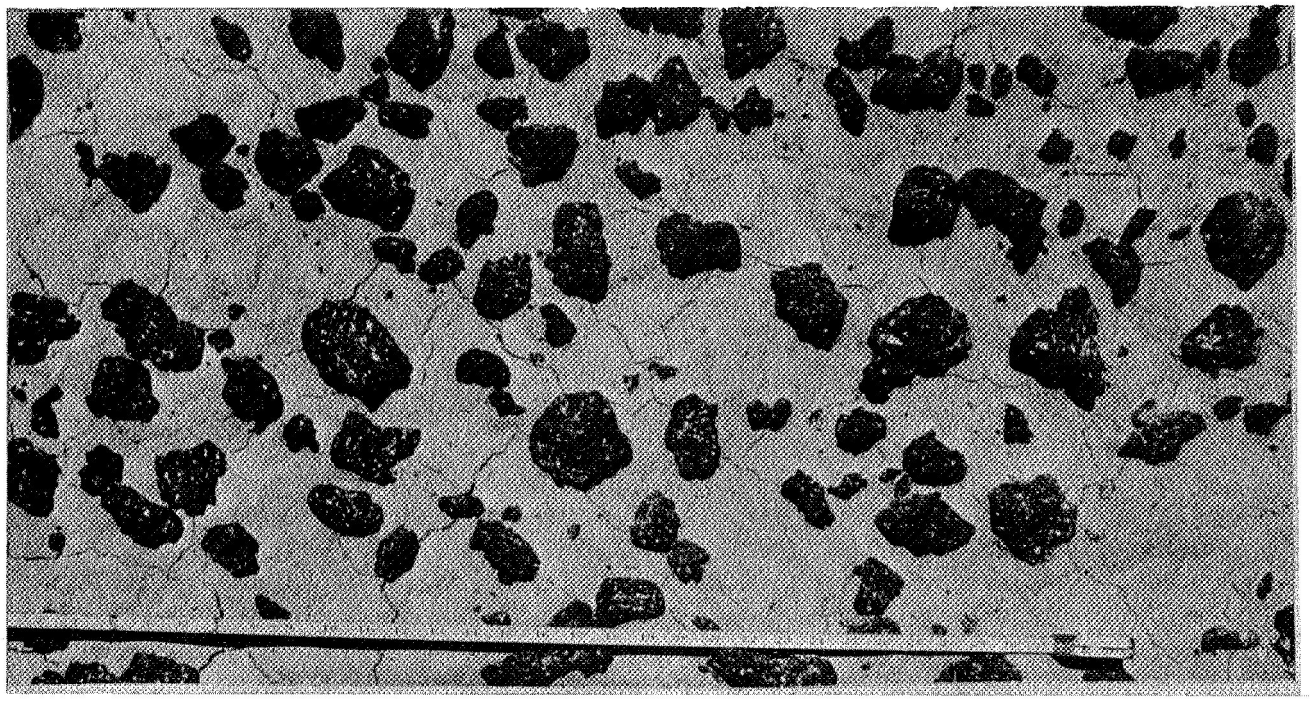

Fig. 20. Lavic Lake playa covered by basaltic cinders. This is a vertical view of vesicular basalt fragments sitting on playa surface, which is broken by small-scale dessication cracks. The size of the mud-crack polygons and the cinders can be judged from the inch-scale at the bottom of the photograph.

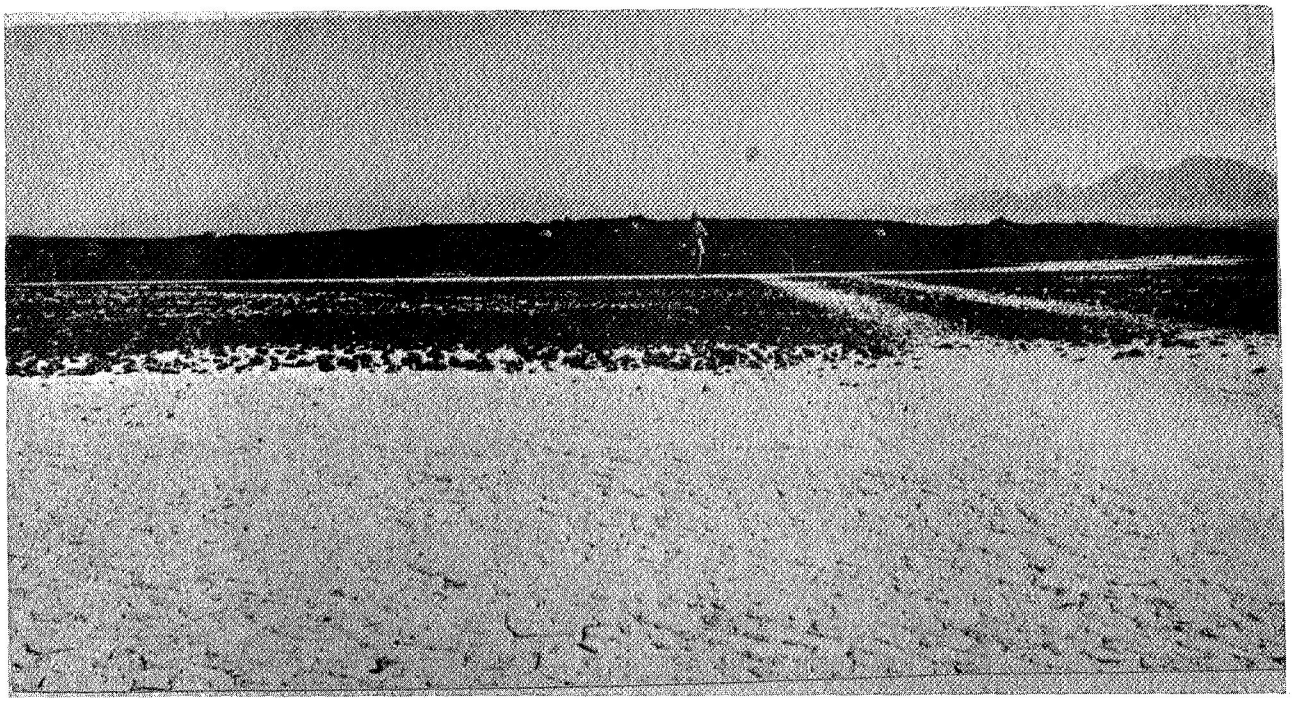

Fig. 21. Lavic Lake playa covered by basaltic cinders. A low angle view from cinder-free playa, across partially cinder-covered playa, to the front of the Pisgah basalt flow. Notice that at this angle the playa surface appears to be almost completely covered with cinders, whereas in actual fact, only approximately 30% is cinder covered. The track in the right-center of the photograph is the path of the radar truck as it moved back and forth "scanning" the surface. Notice that the wheels of the 10-ton vehicle hardly made an indentation in the hard, compact playa surface. The figure in the center of the photograph is standing on the contact between lava flow and playa.

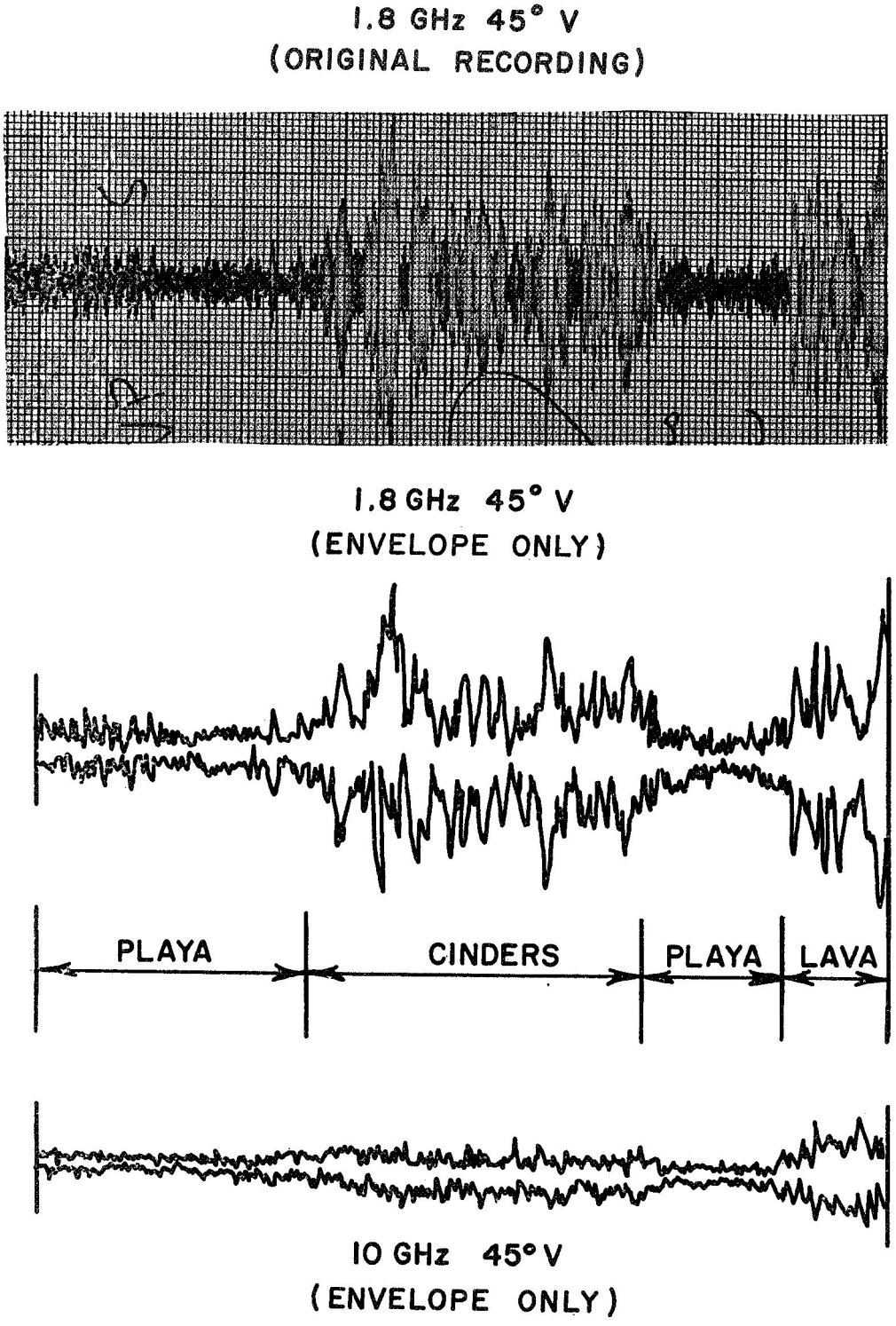

Fig. 22. Strip chart record of amplitude of the return from the area shown in Fig. 21, constituting playa, a cinder covered region, a short strip of playa, and a lava outcrop. Frequencies 1.8 GHz and 10 GHz; polarization V, angle of incidence = 45°.

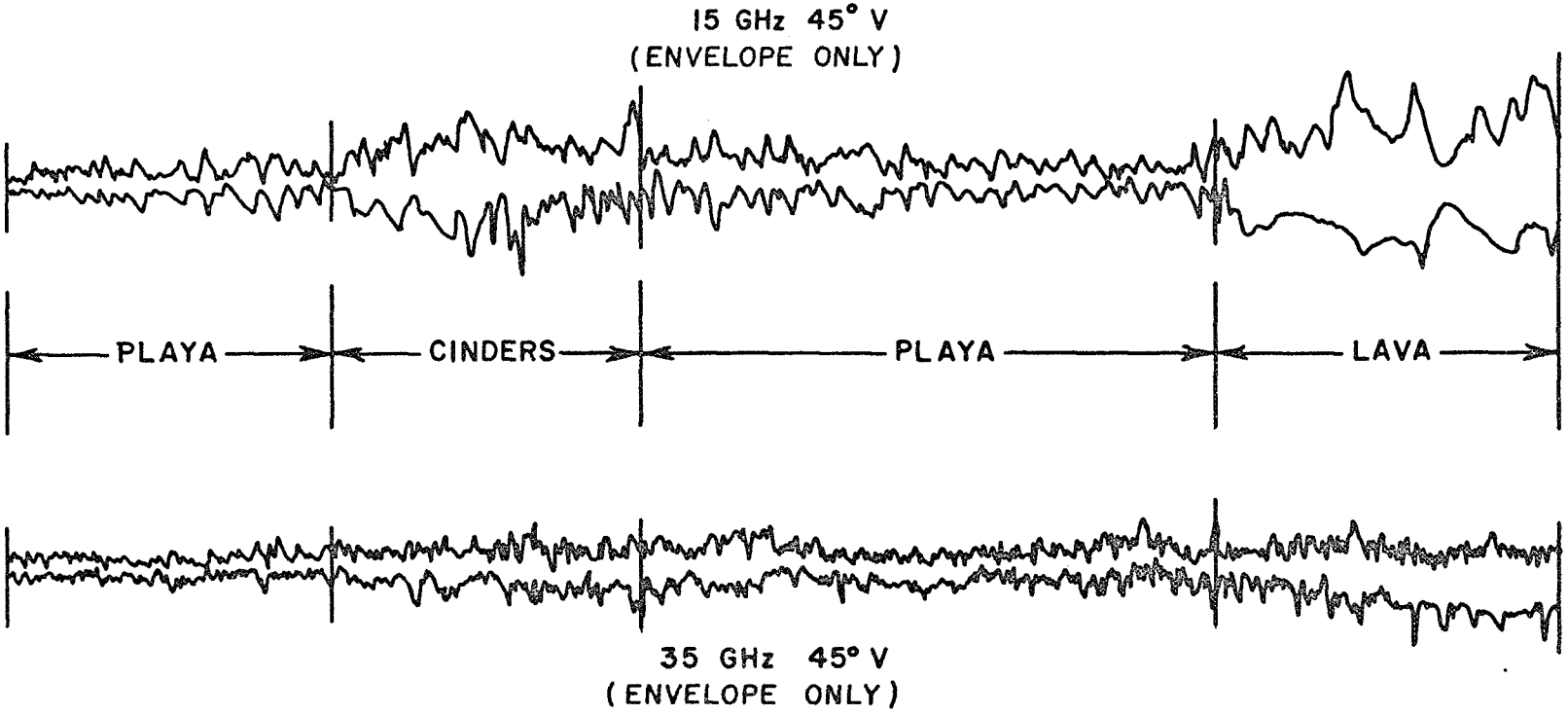

Fig. 23. Strip chart record of amplitude of the return from the area shown in Fig. 21, constituting playa, a cinder covered region, a short strip of playa, and a lava outcrop. Frequencies 15 and 35 GHz; polarization V, angle of incidence = 45°.

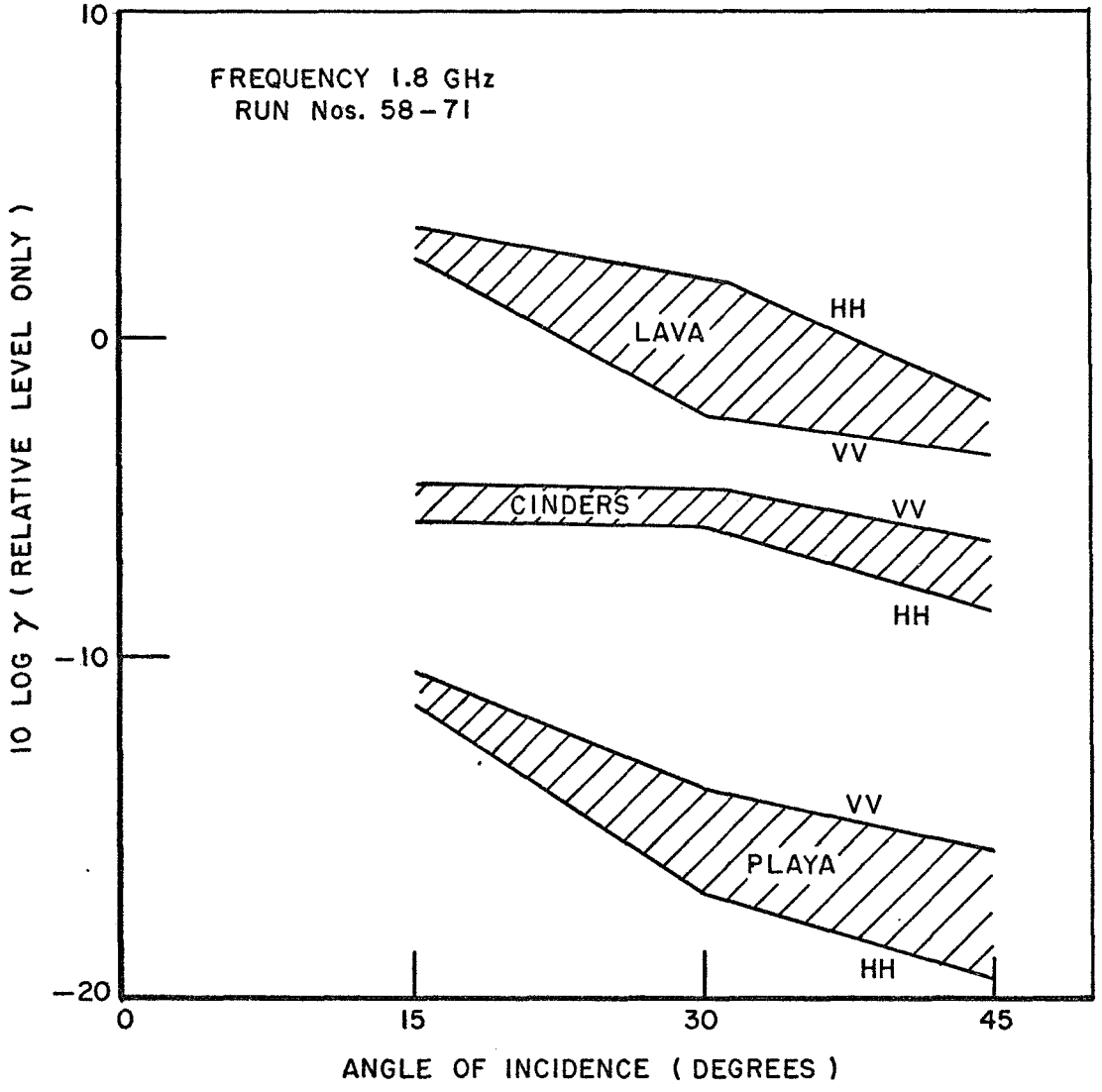

Fig. 24. Relative radar return parameter γ vs angle of incidence for lava, cinders, and playa at 1.8 GHz. (Relative level only.)

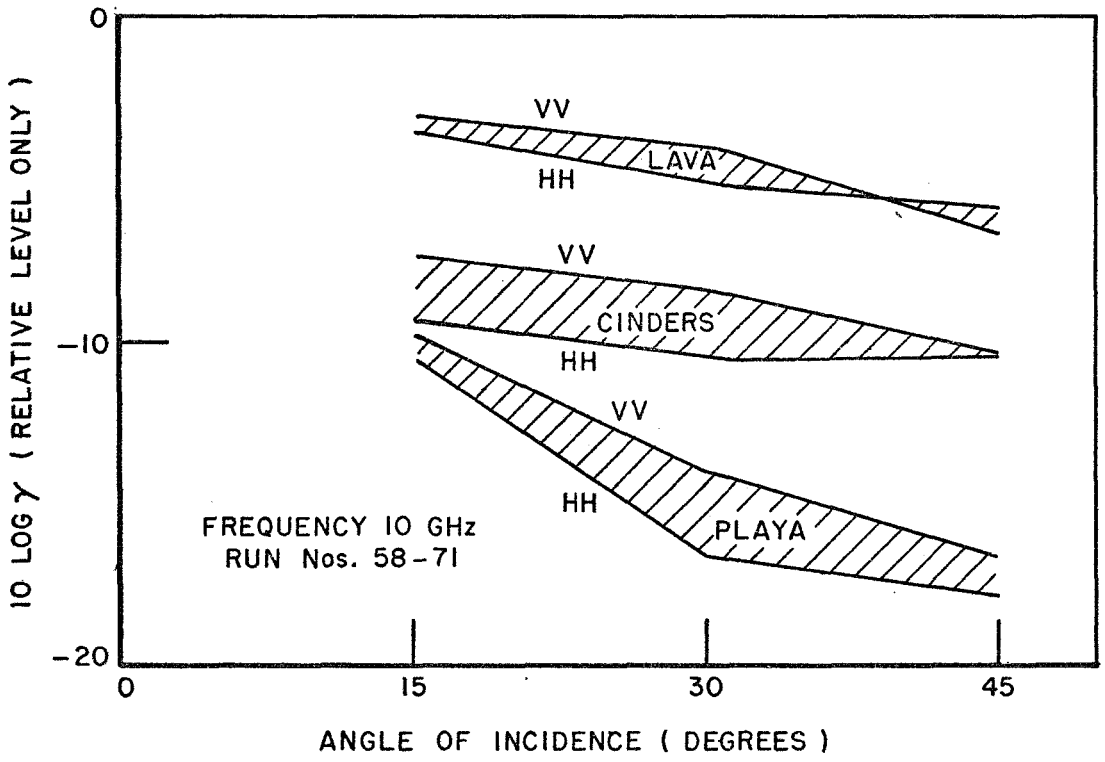

Fig. 25. Relative radar return parameter γ vs angle of incidence for lava, cinders, and playa at 10 GHz. (Relative level only).

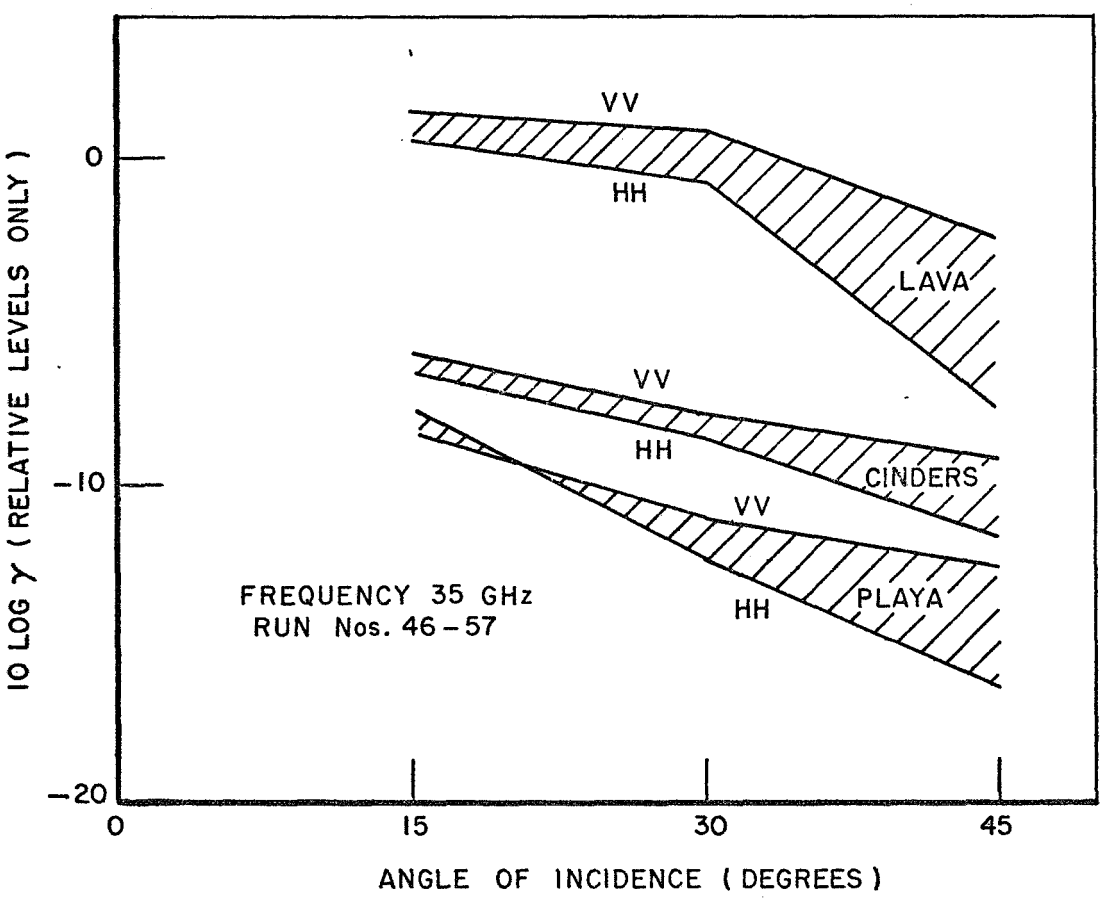

Fig. 26. Relative radar return parameter γ vs angle of incidence for lava, cinders, and playa at 35 GHz. (Relative level only.)

3. Mosaic Cinder Surface (Pisgah 1B)

Group Nos. 7, 8, 9, 10

Location. Pisgah Lava Flow, Pisgah Crater, California

Description. The mosaic cinder surface is nearly horizontal and lies approximately eight feet above the playa surface on basalt lava bedrock near the southern terminus of the Pisgah flow. It is smooth on a gross scale (feet), but extremely rough on a small scale (1-2 inches). The surface is made up of clean, vesicular basalt fragments neatly packed together into what at first glance appears to be a solid surface (see Fig. 27). However, this material is easily loosened exposing a concentration of playa-like material on which the surface fragments seem to be "floating" above the lav bedrock.

Approximately 97% by weight of the loose surface material is coarser than 1 mm. The median size is 17.4 mm and the maximum diameter is about 45 mm. Almost all of this material is black, vesicular basalt that is slightly porphyritic with an aphanitic ground-mass. The basalt fragments at the very surface show some desert varnish. The material between the surface layer of cinders and bedrock (between approximately one and three inches below the surface) is bimodal in character with approximately 70% by weight less than 0.074 mm (silt and clay), and with most of the remainder greater than 1.0 mm. Mineralogically, this sample is identical to playa samples except that calcite seems more abundant. Typically, playa material is cemented with calcite onto the underside of surface cinders and within individual vesicles.

The mosaic cinder surface was probably made when the playa was covered by turbulent water at least eight feet deep. Gentle wave action on the surface of the lake over a brief period of time organized the cinders into a neatly packed arrangement. Following evaporation and runoff of the lake, eluviation by later rains concentrated playa clay and silt just below the surface leaving a lag or residue of "clean" cinders.

Radar data are shown in Figs, 28 and 29.

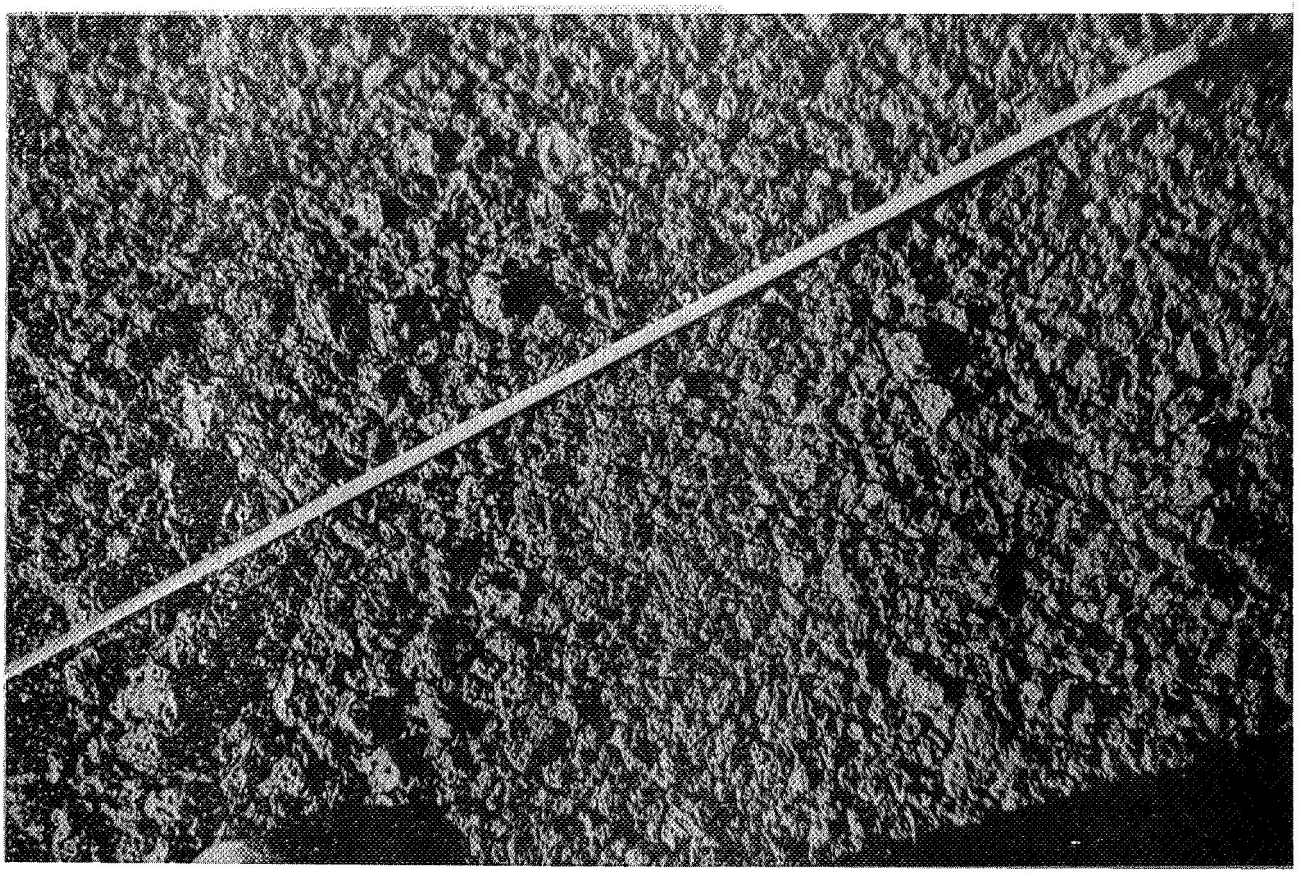

Fig. 27. Mosaic Cinder Surface. Neatly packed vesicular basalt cinders present the appearance of a solid surface, but are actually loose. Beneath this veneer of cinders there is a concentration of playa clay and silt before more or less solid basalt bedrock is encountered one to three inches below the surface. Size of the fragments can be judged from the scale, which is in inches.

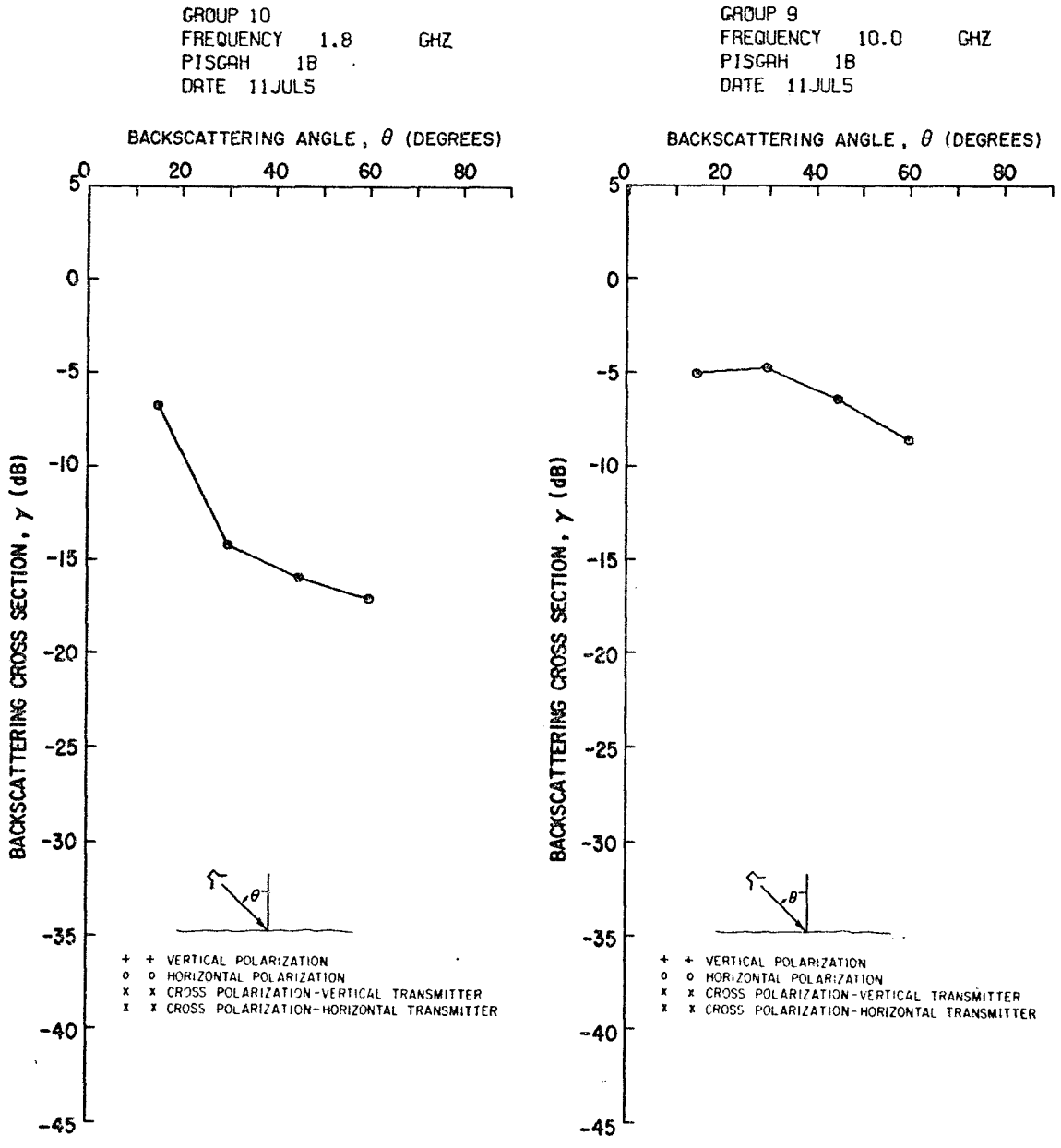

Fig. 28. Mosaic cinder surface (Pisgah 1B).

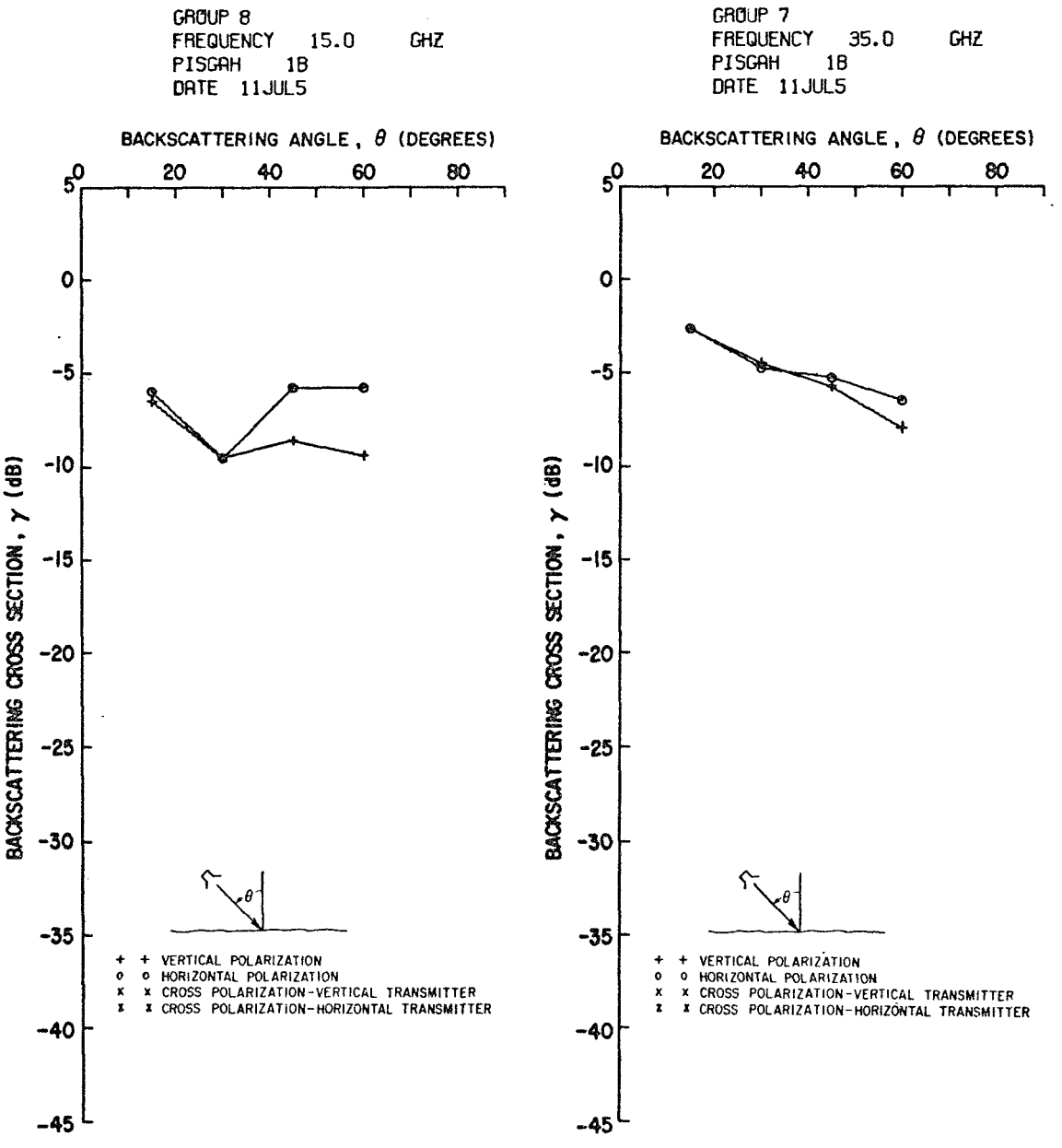

Fig. 29. Mosaic cinder surface (Pisgah 1B).

4. Pahoehoe Lava Surface (Pisgah 1A)

Group Nos. 28, 30, 31, 33, 35

Location. Pisgah Lava Flow, Pisgah Crater, California

Description. The pahoehoe surface measured is near the southern terminus of the Pisgah flow at the contact with the playa. The lava surface has been tilted as a result of collapse caused by withdrawal of molten lava from beneath the hardened crust (surface examined) shortly after eruption. The surface dips approximately 40° SW toward the playa and strikes east-west. The lava surface is solid and presents a smooth, ropy appearance typical of pahoehoe lava. The western part of the surface is well lineated as a result of flow and contains a few imbedded scoriaceous blocks (see Fig. 30). The eastern part of the surface is poorly lineated and contains an abundance of embedded cindery blocks, and thus is much rougher than the west side. The lava itself is scoriaceous basalt with elongate vesicles (elongation parallel to the flow surface) 2 to 20 mm long. It is medium-dark gray on fresh surfaces and slightly porphyritic. Surfaces exposed to the atmosphere show a resinous luster and brownish-black color due to desert varnish. Microscopic examination of thin sections shows a porphyritic-intersertal texture with euhedral phenocrysts of perfectly fresh olivine embedded in a nearly opaque glassy groundmass containing euhedral laths of labradorite and granules of clinopyroxene and magnetite. Flow structure shown by parallel arrangement of feldspar laths is evident in sections normal to the flow surface, but not in parallel sections. A typical mode is listed below:

Groundmass (opaque glass)	55.2%
Plagioclase (labradorite)	20.4%
Olivine (forsteritic)	8.4%
Clinopyroxene and Magnetite	2.5%
Vesicles (partly filled with playa clay cemented with calcite)	13.5%
	100.0%

Radar data are given in Figures 31, 32 and 33.

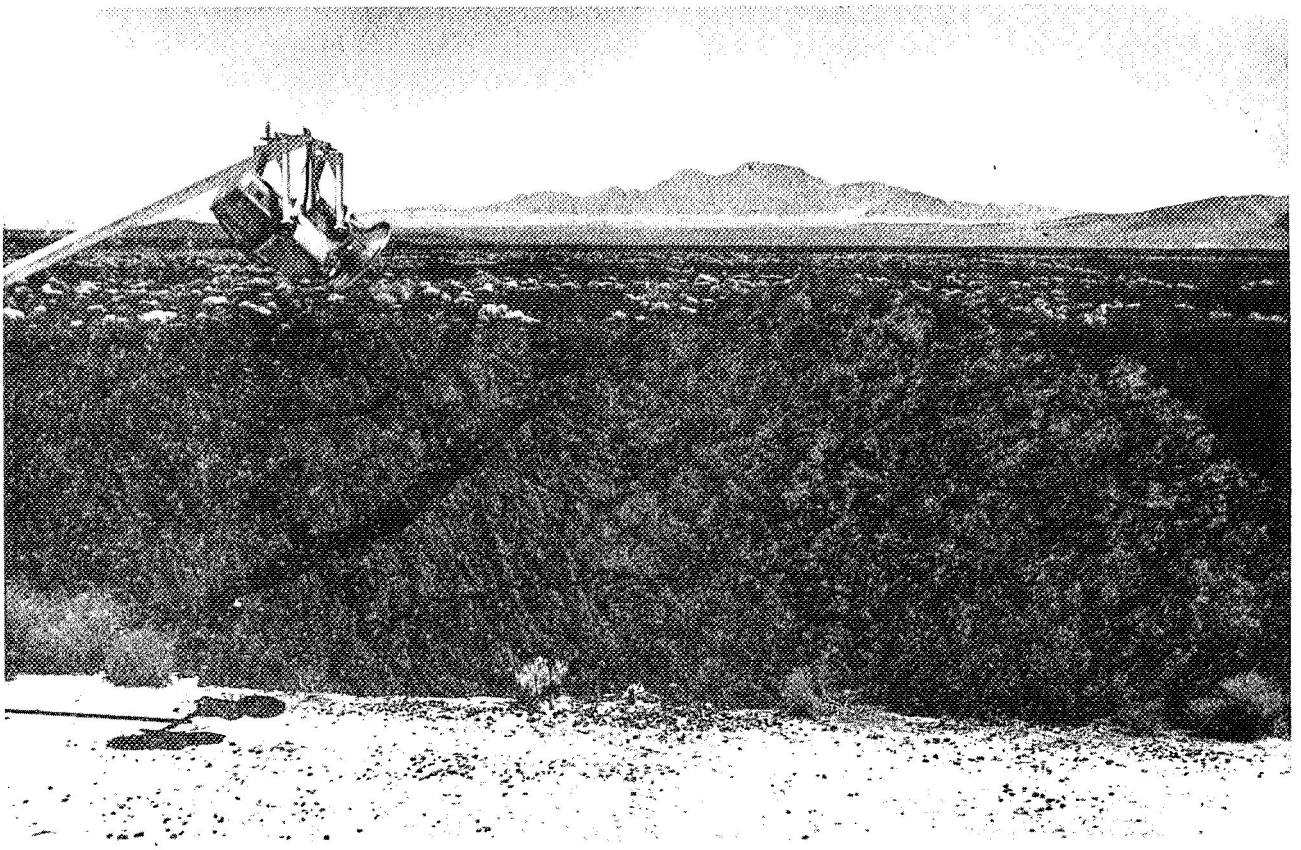

Fig. 30. Pahoehoe Lava. A tilted slab of hardened pahoehoe lava at the contact with the white playa surface is shown being illuminated by radars attached to a hydraulic boom. The western part (left) shows well lineated ropy structure resulting from flow. The eastern part (right) does not show this structure as well, and contains an abundance of embedded scoriaceous blocks. The dark band on the surface sloping to the west is a crack about four feet wide. In the distance, framed by the boom and the radar units, is Pisgah Crater from which the basalt lava flows emanated.

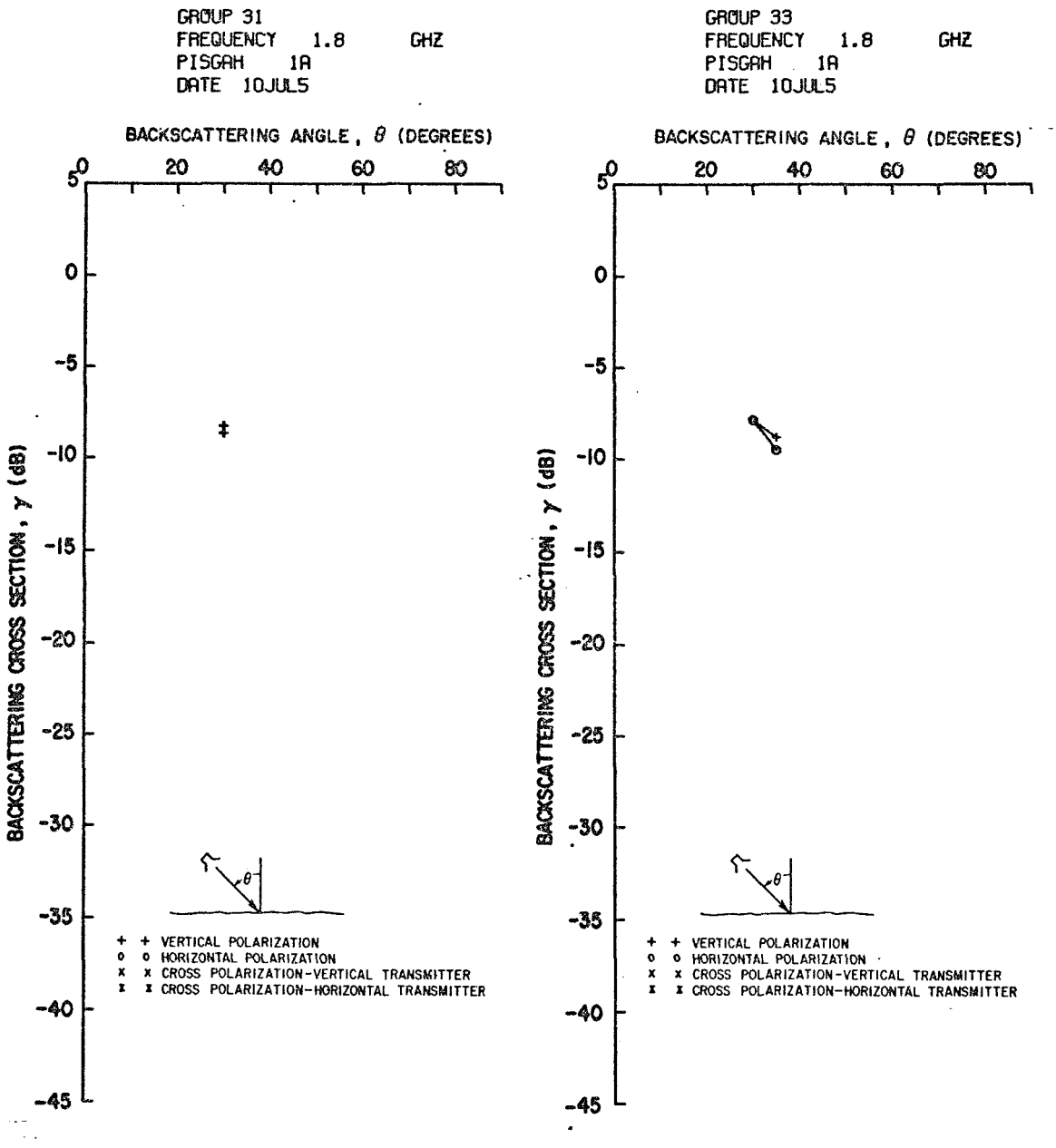

Fig. 31. Pahoehoe lava surface (Pisgah 1A).

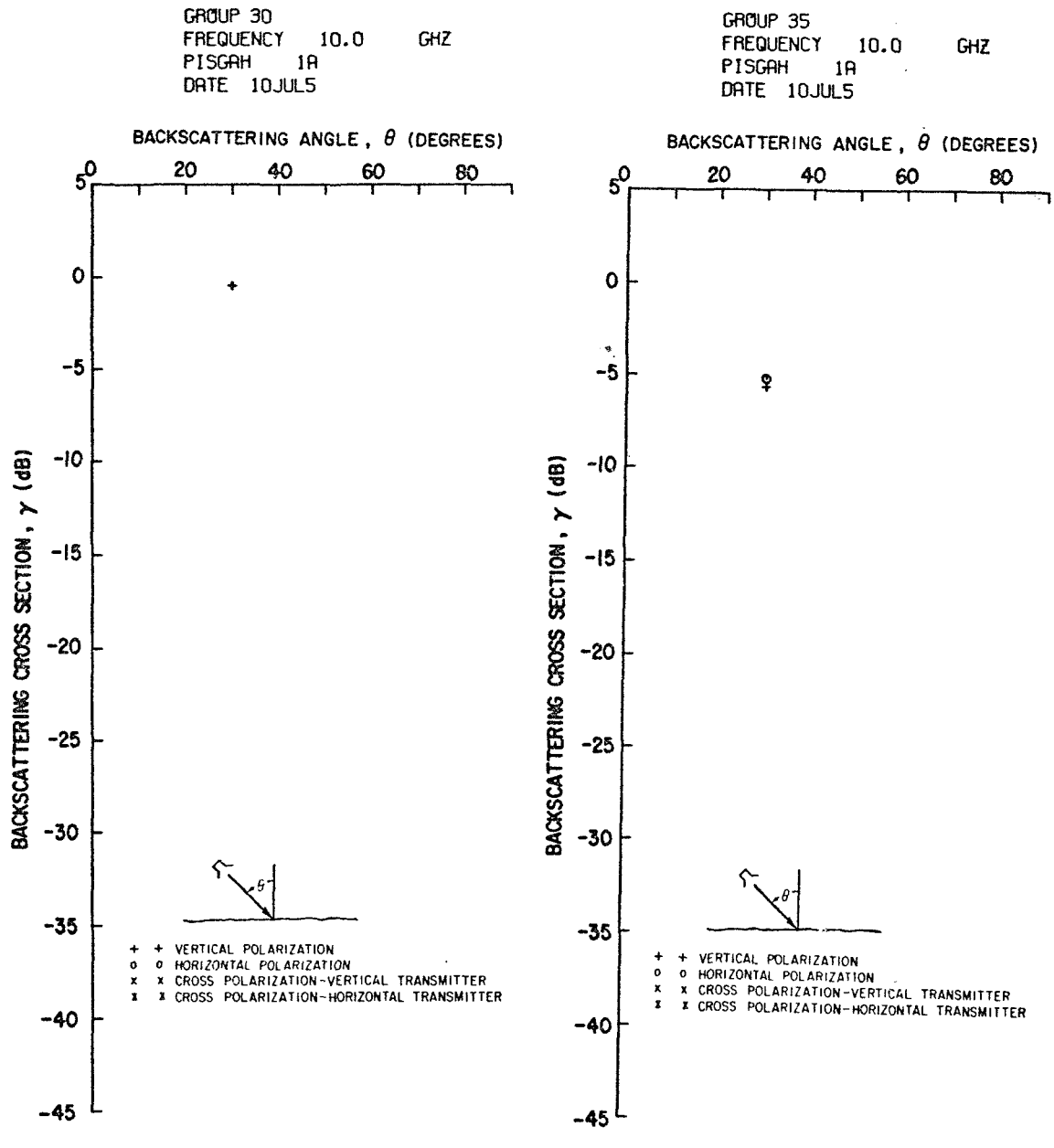

Fig. 32. Pahoehoe lava surface (Pisgah 1A).

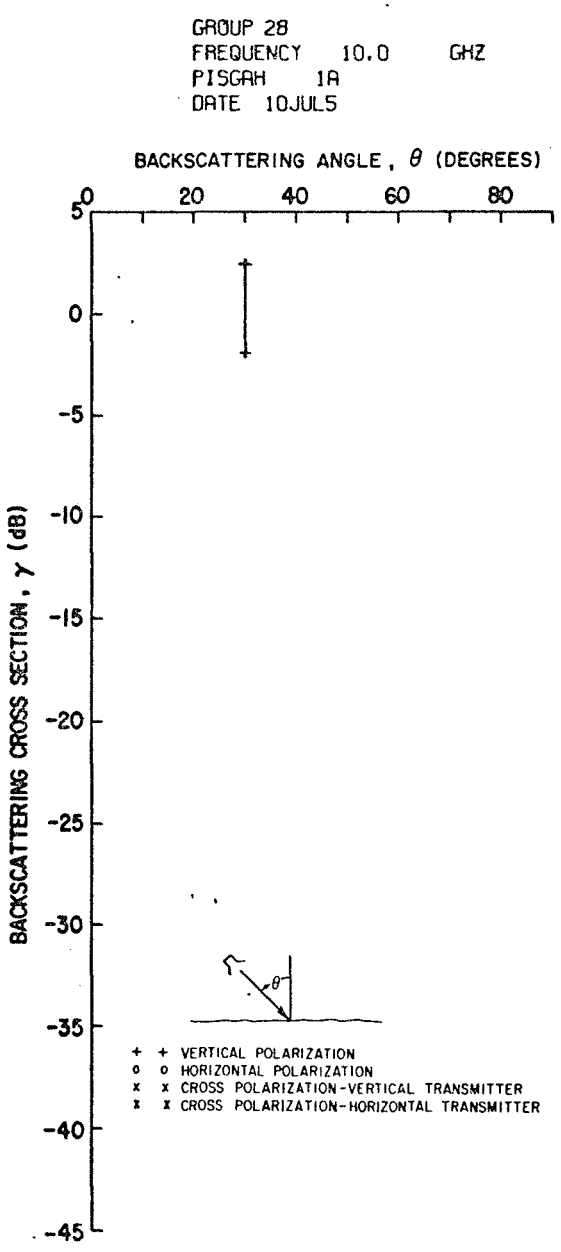

Fig. 33. Pahoehoe lava surface (Pisgah 1A).

5. Smooth Basalt Lava Surface (Pisgah 2A)

Group Nos. 21, 24, 26

Location. Pisgah Lava Flow, Pisgah Crater, California

Description. The smooth basalt lava surface is similar in all respects to the Pahoehoe Surface except that it is nearly perfectly flat and does not show the typical ropy structure of pahoehoe. The surface dips about 25° SE and strikes N 45° E. It contains a few embedded cinders, and is composed of the same vesicular, slightly porphyritic olivine basalt as the Pahoehoe Surface.

Radar data are given in Figs. 34 and 35.

6. Aa Basalt Lava Surface (Pisgah 2B)

Group Nos. 22, 25, 27

Location. Pisgah Lava Flow, Pisgah Crater, California

Description. The aa Basalt surface is a continuation of the Smooth Basalt Lava Surface, but is demarcated from it along a very sharp boundary. The surface is extremely rough on a scale of a few inches to one foot, but is flat on a gross scale (see Fig. 36). The surface developed on the lava flow when the crust was semi-brittle and the main body of the flow was still molten. The stress set up by underflow disrupted the weak, partially cooled surface, but the broken surface was still hot enough to "weld" into a more or less solid mass.

Radar data are given in Figs. 37 and 38.

7. Smooth Basalt Lava Surface with Squeeze-up (Pisgah 1C)

Group Nos. 20, 23

Location. Pisgah Lava Flow, Pisgah Crater, California

Description. This surface is identical in all respects to the Smooth Basalt Surface described previously except that there is a lava squeeze-up in the center of the surface. The squeeze-up occurred along a fracture in brittle crust (the major portion of this surface) that overlaid molten lava. The lava welled up from below, carrying many fragments of crust with it, and overflowed the older crust. The nature of this surface, therefore, is essentially a tilted (N 5° W, 21° NE), smooth, basalt lava slab with a strip of aa-like lava across it.

Radar data are given in Fig. 39.

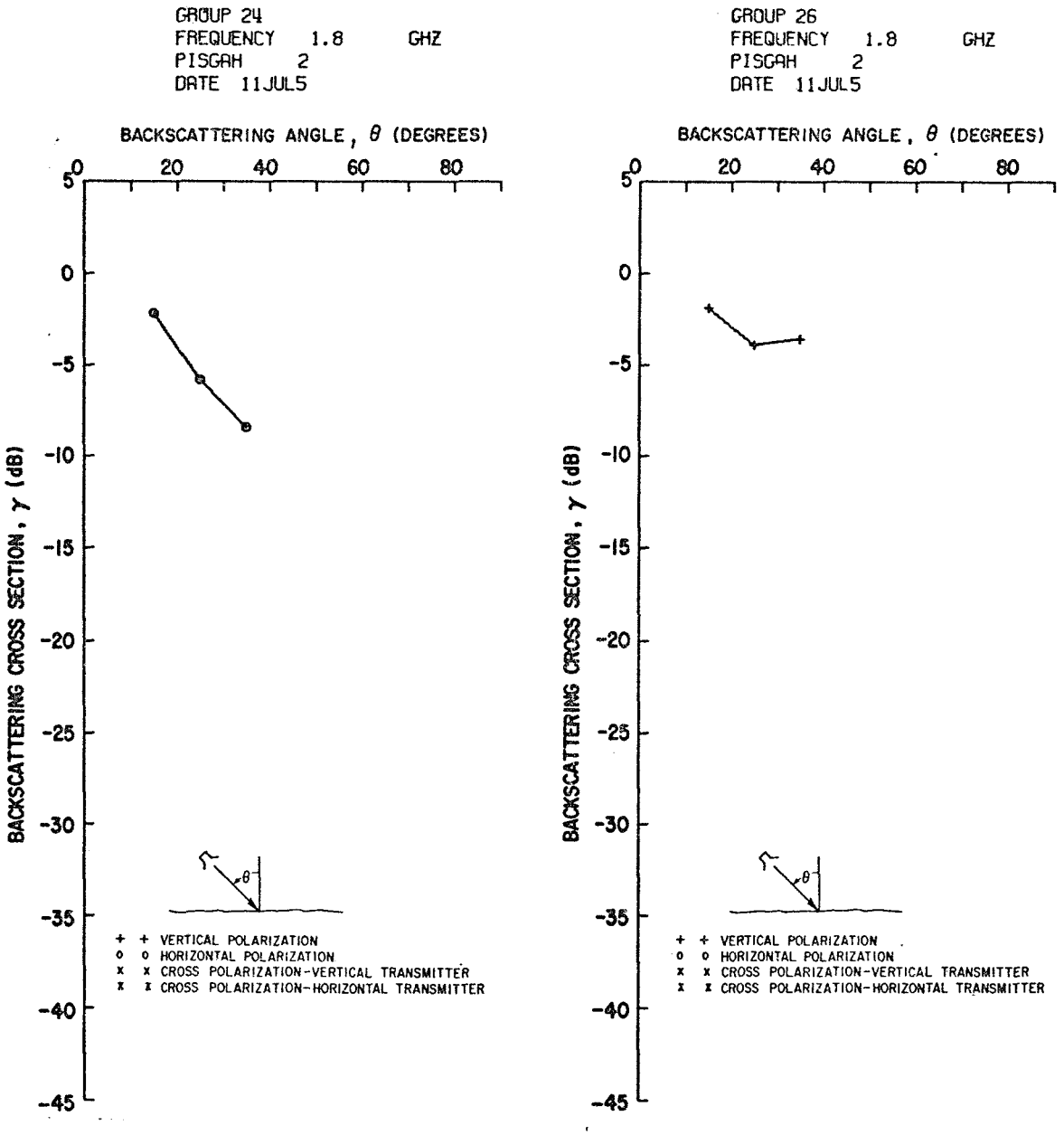

Fig. 34. Smooth basalt lava surface (Pisgah 2A).

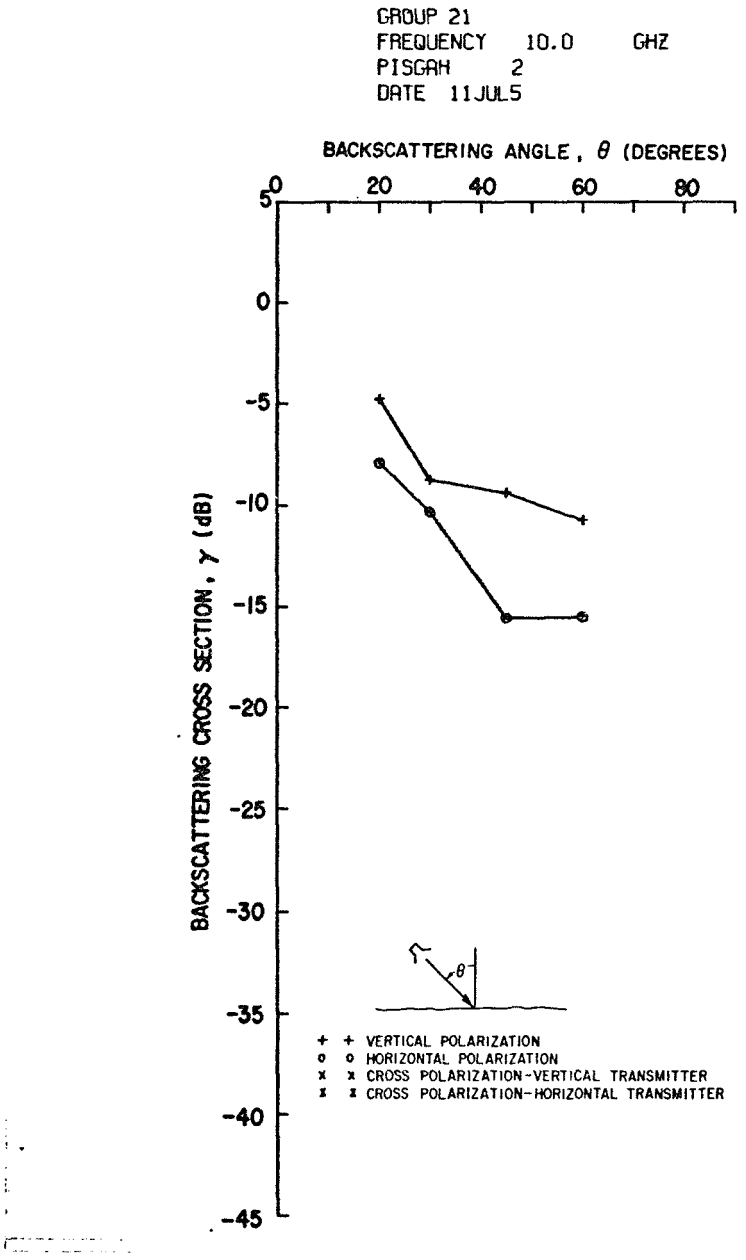

Fig. 35. Smooth basalt lava surface (Pisgah 2A).

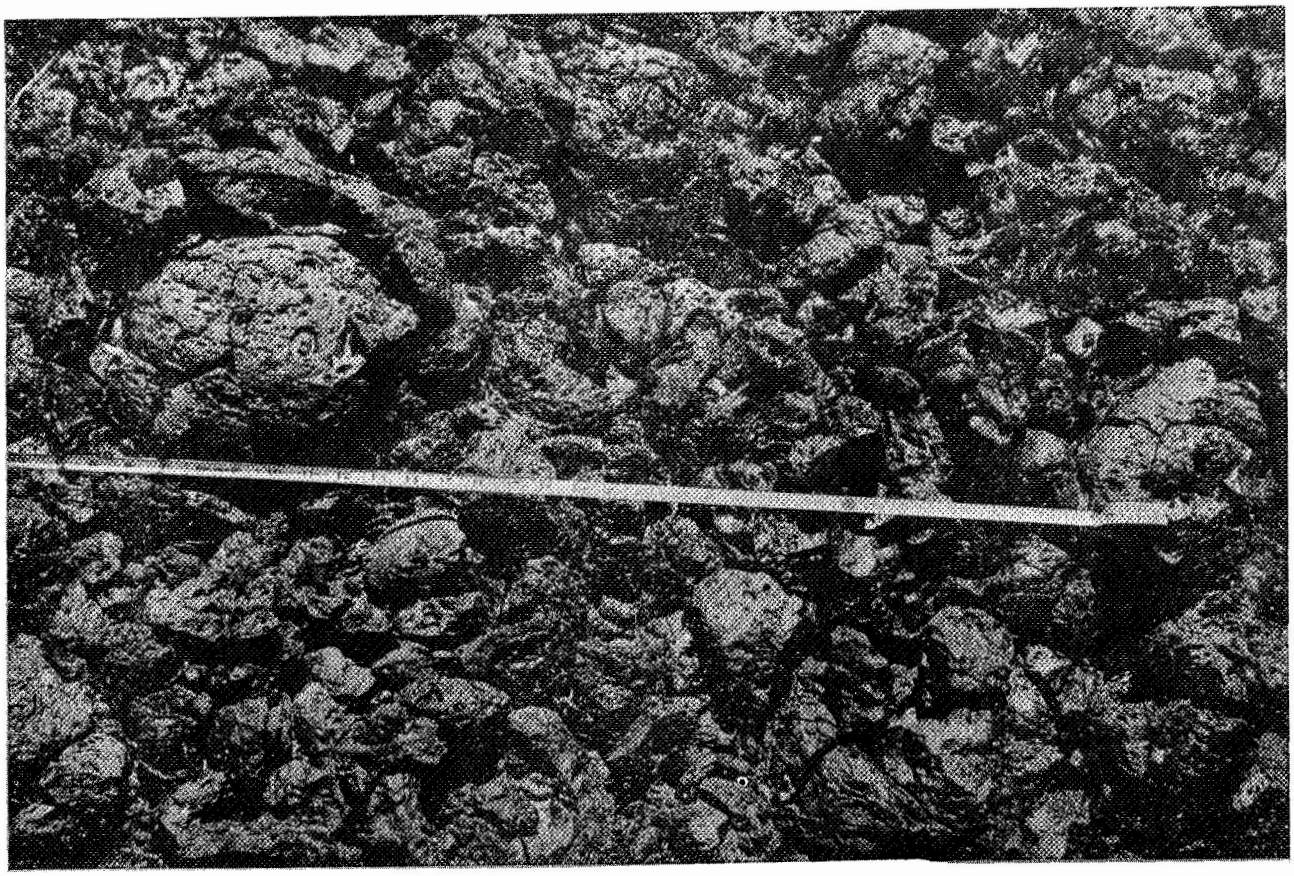

Fig. 36. Aa Basalt. The photograph shows the extremely rough surface characteristic of aa lava. Although the surface appears to be composed of loose rubble, it is actually fairly solid. The reason for this is that after the original lava crust was broken by underflow, there was still enough heat to "weld" the fragments together. Scale is provided by the tape, which is in inches.

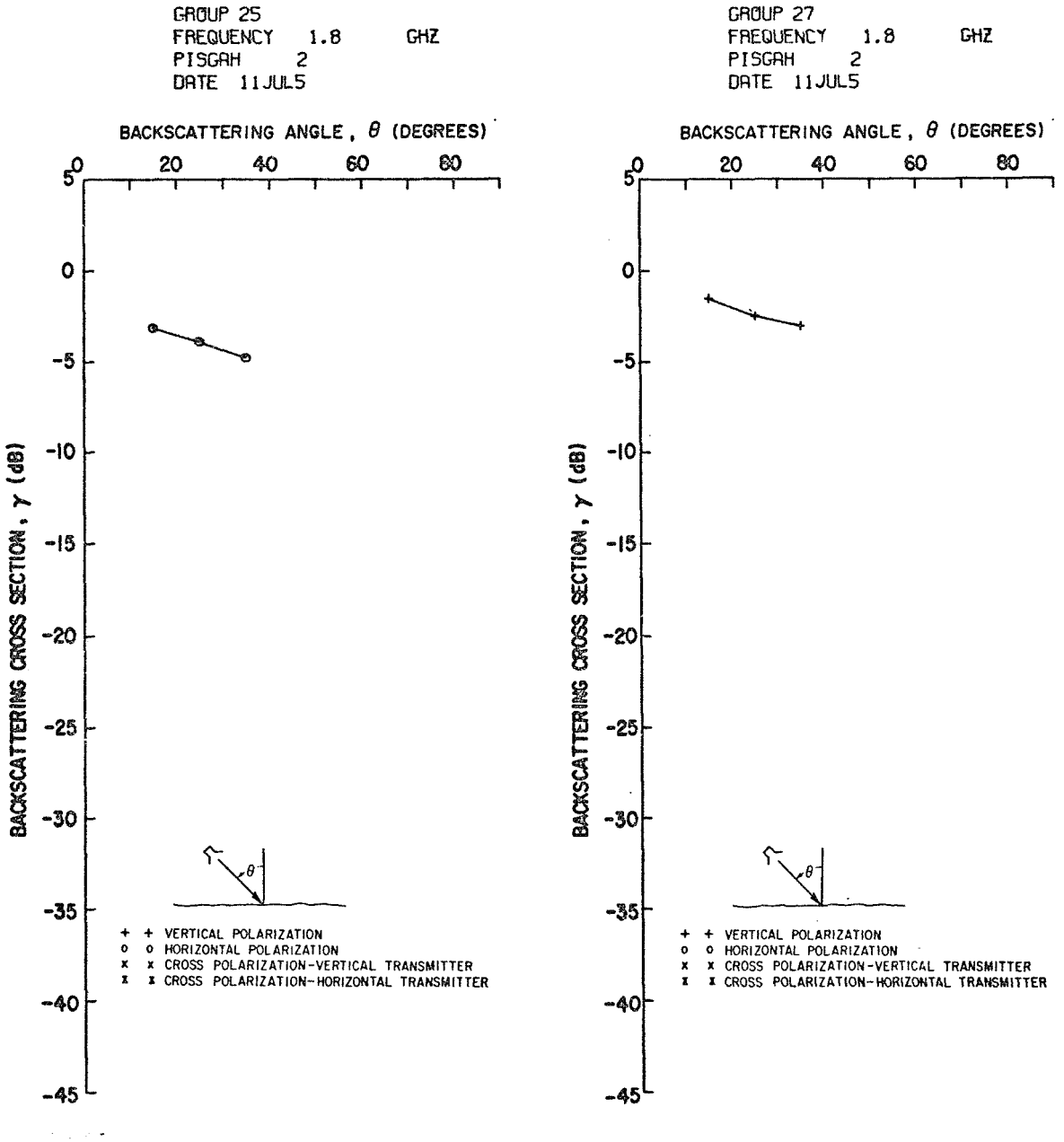

Fig. 37. As basalt lava surface (Pisgah 2B).

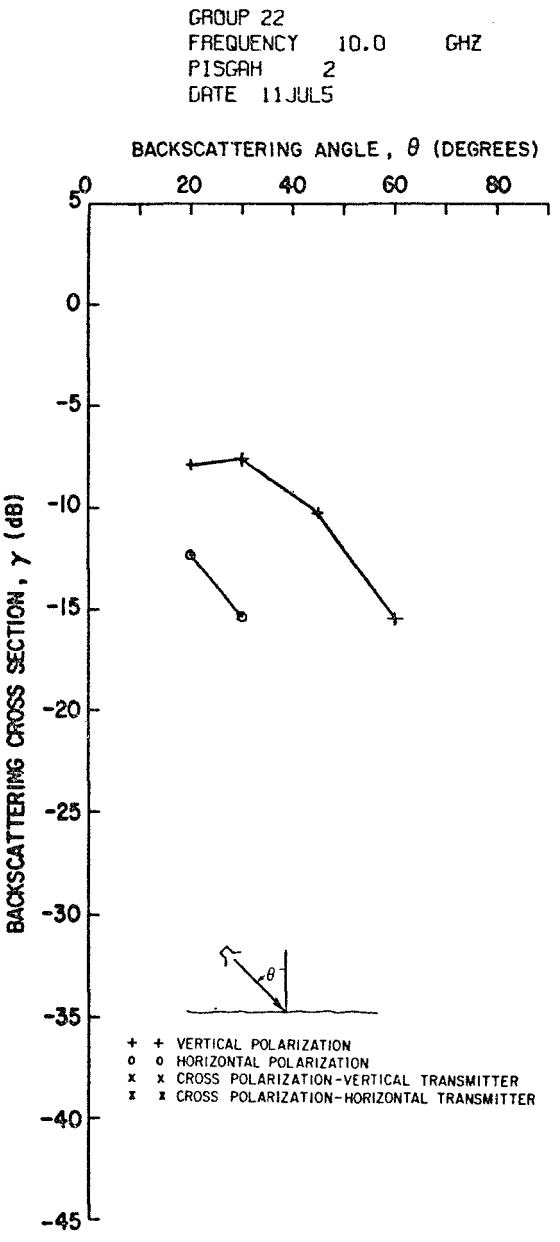

Fig. 38. As basalt lava surface (Pisgah 2B).

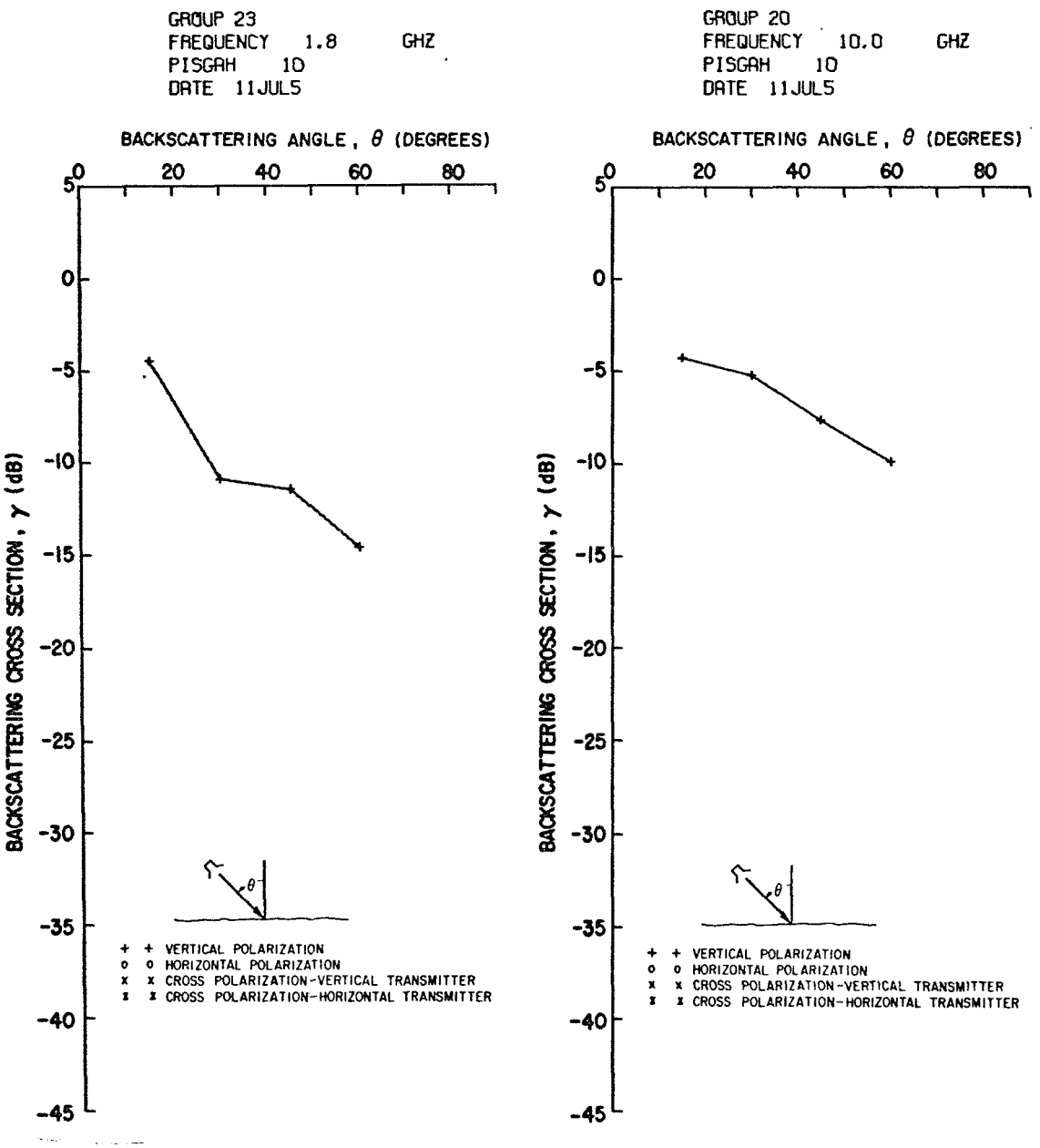

Fig. 39. Smooth basalt lava surface with squeeze-up (Pisgah 1C).

C. Marblehead Quarry[12]

The Marblehead quarry occurs in Ottawa County, Ohio on the eastern terminus of Marblehead Peninsula, which lies north of Sandusky Bay and south of Lake Erie proper (see Location Map, Fig. 40). It is operated by The Standard Slag Company, who generously permitted access to their property. The rock being quarried and the material on which radar data was gathered is Columbus limestone of Devonian age. Physiographically, the site is on the Columbus-Delaware cuesta within the Interior Lowlands, and structurally it lies just east of the crest of the Findlay Arch. The strata dip imperceptibly a few tens of feet per mile to the east, but for all practical purposes they are flatlying and undeformed. The main point of interest at this site, however, is that within the area there are acres of glacially abraded limestone that has been laid bare by stripping as part of the quarrying operation. The glacially abraded surface is smooth, almost polished, and is marked by parallel glacial striations.

1. Columbus Limestone Surface (MARHD PARGV and MARHD PPGV)

Group Nos. 149, 150, 151, 152, 159, 160, 161, 162

Locations. Standard Slag Co., Marblehead Stone Division, Marblehead, Ohio

Description. Two sets of radar data were collected in the famous Marblehead Quarries at the eastern end of Marblehead Peninsula, Ohio. The rock is fossiliferous, light-gray Columbus limestone, which is nearly identical to that of the Marble Cliff quarries in Columbus. However, the surface examined resulted from glacial abrasion and is not an unmodified bedding plane such as the surfaces examined at Marble Cliff. The Marblehead surface was originally covered by a thin layer of till, but this was cleared in the course of quarrying operations. Rain has since washed the surface perfectly clean of all debris. The surface was dry when measured and free of any obvious weathering effects. It is flat except for some glacial grooves, which were avoided. The surface is smooth almost to the extent of being polished, and is characterized by parallel, very narrow and shallow glacial scratches. The orientation of the scratches (direction of ice movement) is generally S 73° W. One set of measurements was made parallel to these scratches (Group No. 149-150, 161-162), labelled MARHD PARGV, and the other perpendicular to the scratches (Group No. 151-152, 159-160), labelled MARHD PPGV. The rock is broken by a few tight joints, which bear no relationship to the glacial scratches.

Radar data are given in Figs. 41-44.

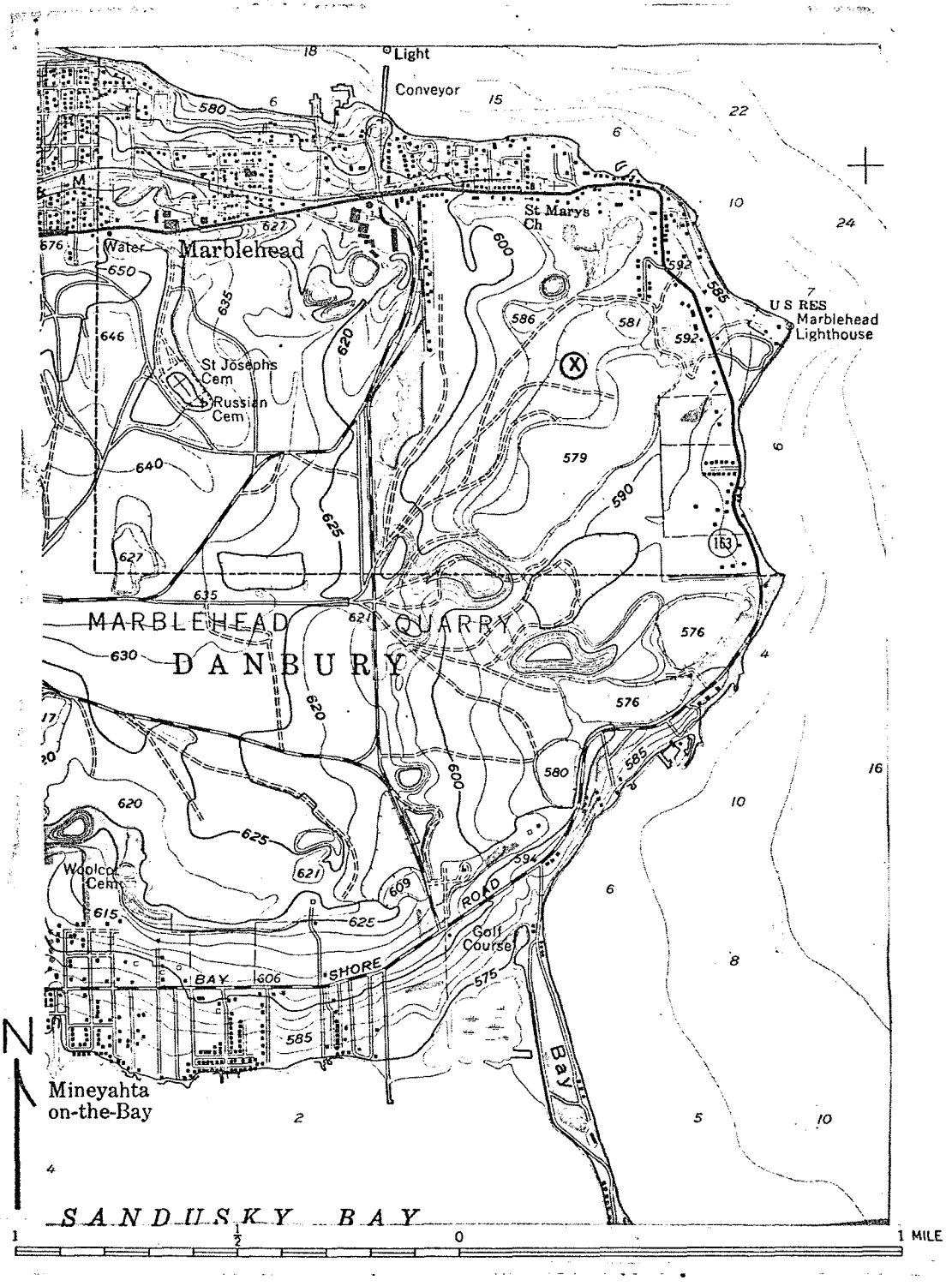

Fig. 40. (Location Map). The area where radar data was acquired in the Marblehead quarries on Marblehead Peninsula is marked (x) on the location map. The map is part of the Kelleys Island, Ohio 7 1/2 minute topographic quadrangle.

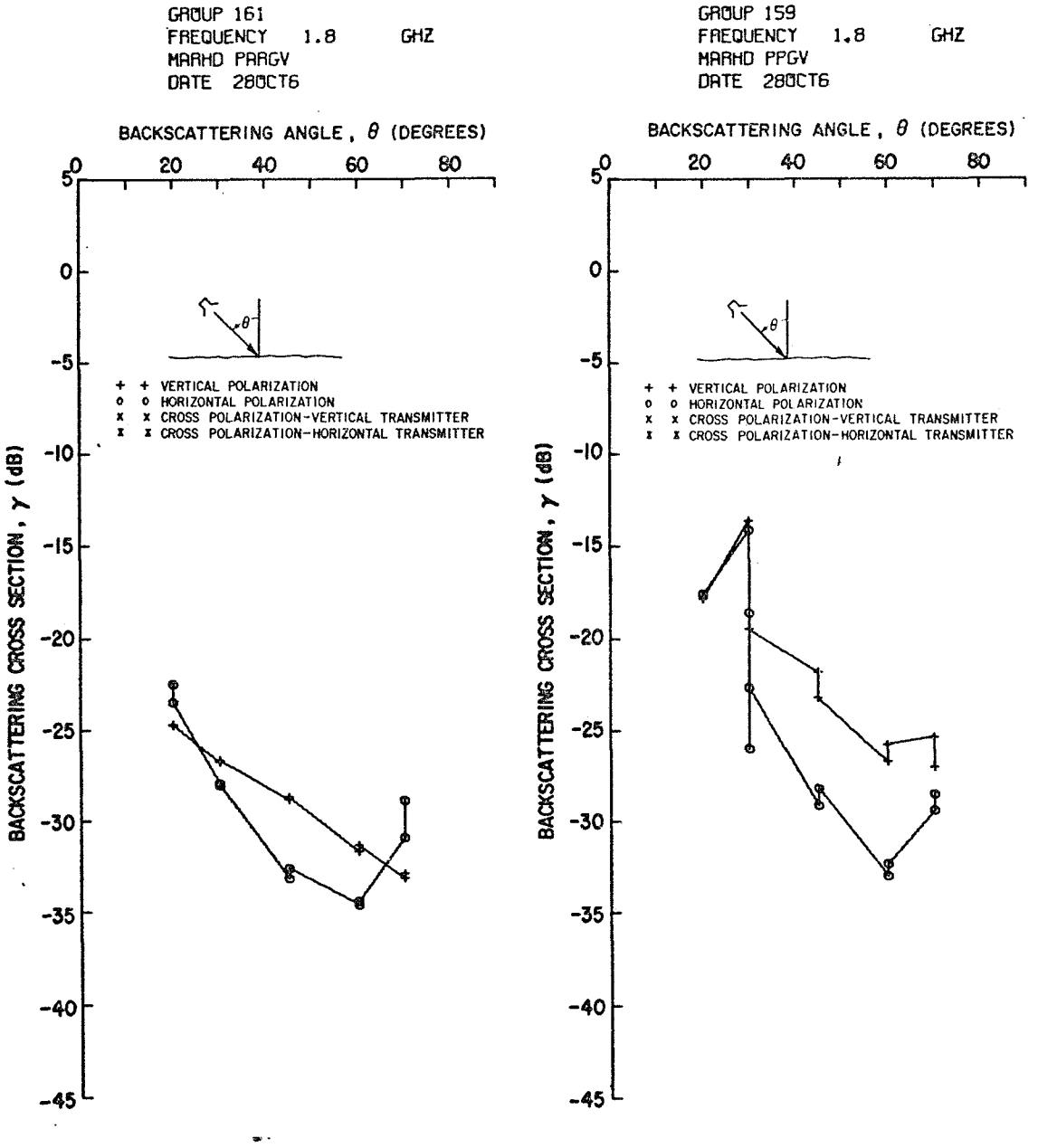

Fig. 41. Columbus limestone surface (MARHD PARGV and MARHD PPGV).

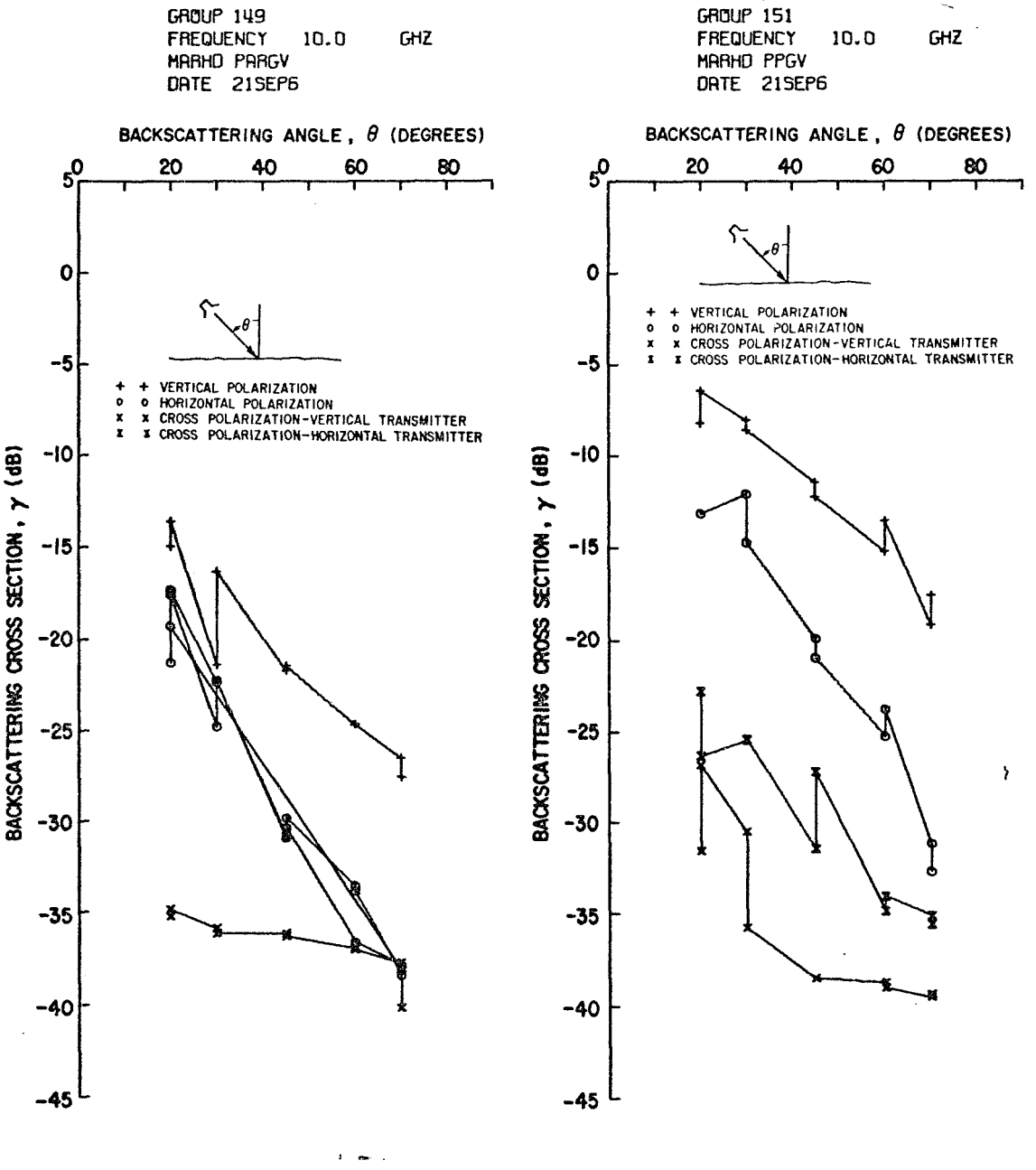

Fig. 42. Columbus limestone surface (MARHD PARGV and MARHD PPGV).

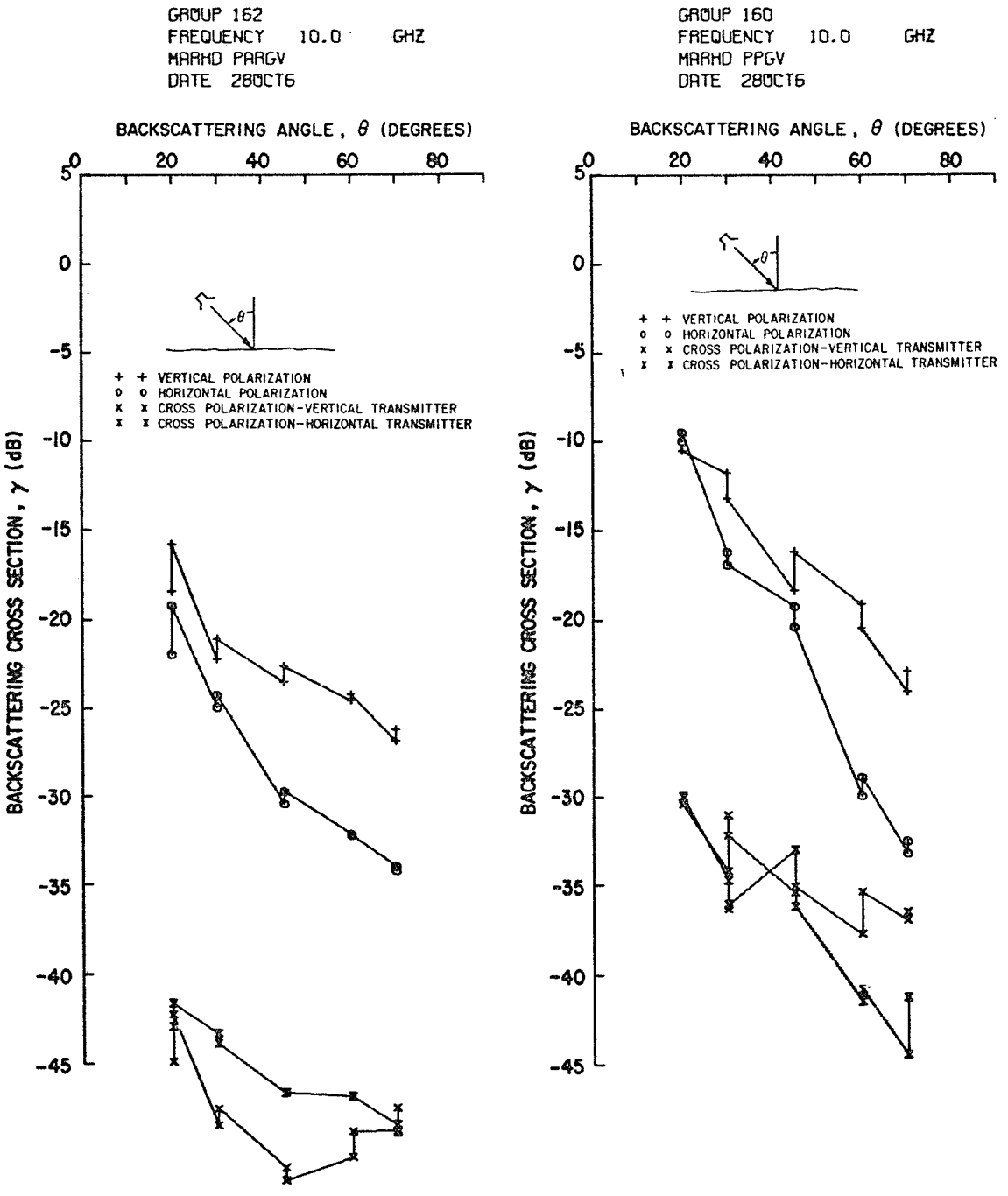

Fig. 43. Columbus limestone surface (MARHD PARGV and MARHD PPGV).

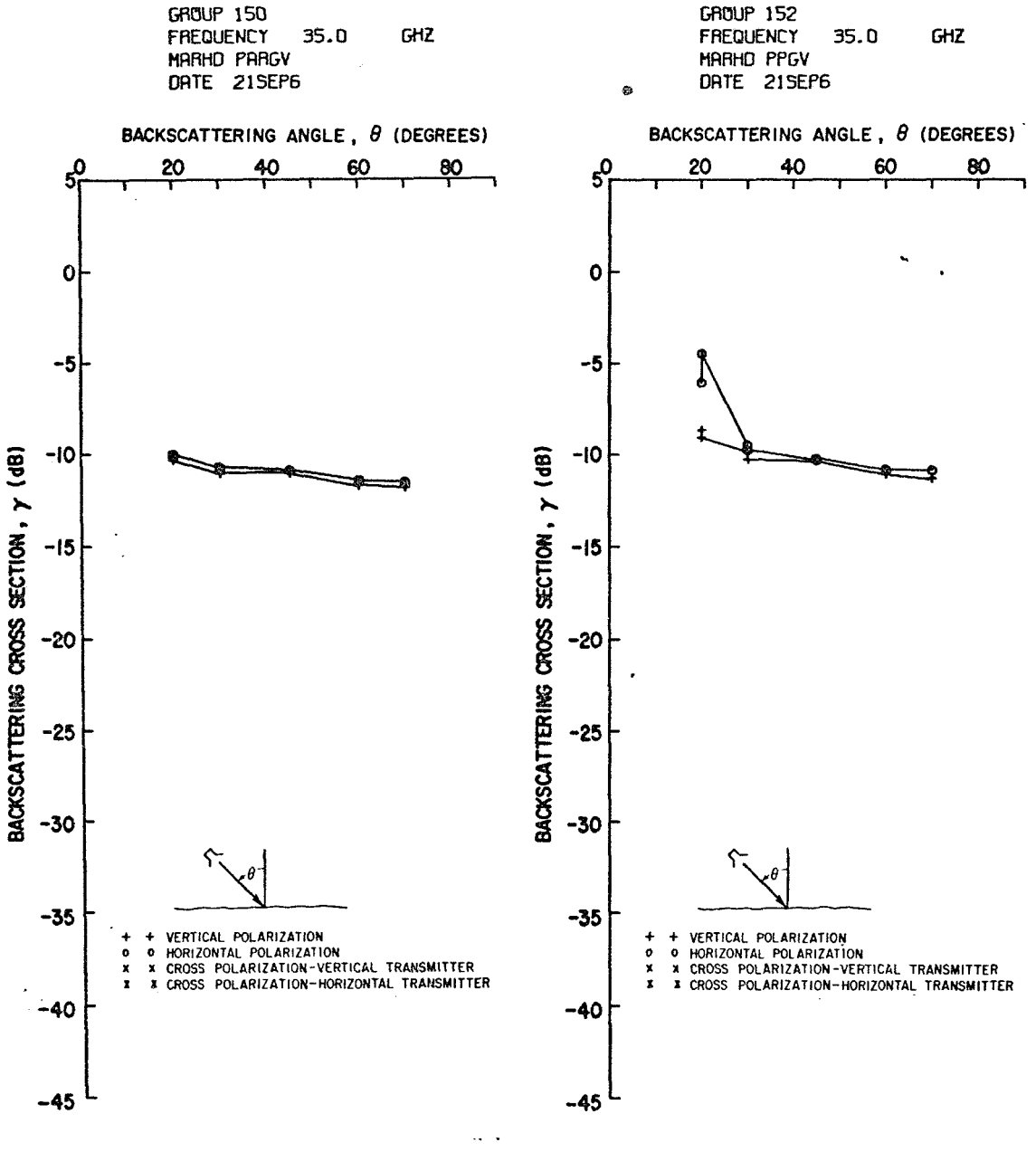

Fig. 44. Columbus limestone surface (MARHD PARGV and MARHD PPGV).

D. Marble Cliff (Hobo) Quarry

The Marble Cliff (Hobo) Quarry occurs in Franklin County, Ohio along the west bank of the Scioto River approximately five miles west-northwest of downtown Columbus (see Location Map, Fig. 45). The quarry is owned and operated by the Marble Cliff Quarries Company, who kindly permitted us access to the property. The rock on which radar data was gathered is the Columbus limestone of Devonian age. In the quarry the Delaware limestone (Devonian) is also exposed, but it lies above the Columbus and is inaccessibly high on the quarry wall. The Delaware in turn is overlain by Wisconsin drift, which is the natural surface material in this area. The strata dip imperceptibly to the east and are, therefore essentially flatlying and undeformed. The quarrying operation has exposed bedding planes of the massive Columbus limestone along several prominent benches. It is these natural surfaces of Devonian sedimentation that were investigated at this site.

1. Columbus Limestone Surface (MARBLE ST 1)

Group Nos. 139, 142

Location. Marble Cliff Quarries, Columbus, Ohio

Description. Two sets of measurements were made on the Columbus limestone in the Hobo Quarry. This one was made on a horizontal bedding plane exposed during the quarrying operation, and occurs 47 feet below the contact with the Delaware limestone on a prominent quarry bench. The rock is a massive, white to very light-gray, highly fossiliferous, exceptionally pure limestone. The limestone is broken by several sets of tight joints. Most of these are vertical, but some dip at low angles (see Fig. 46). No effects of weathering were noted and the surface was perfectly dry. The actual area illuminated by radar is a runway 7 to 10 feet wide and 85 feet long that was swept perfectly clean, except for a patch that was thinly covered with fine-grained quarry rubble (see Fig. 47). The surface is somewhat rough primarily due to the protruberance of fossil shells (see Fig. 48). In addition, the surface shows a very shallow rolling topography with randomly distributed, equant peaks and basins, which are probably primary features of the original surface of sedimentation. The macrotopography rarely exceeded one inch in total relief.

Radar data are given in Figs. 49 and 50.

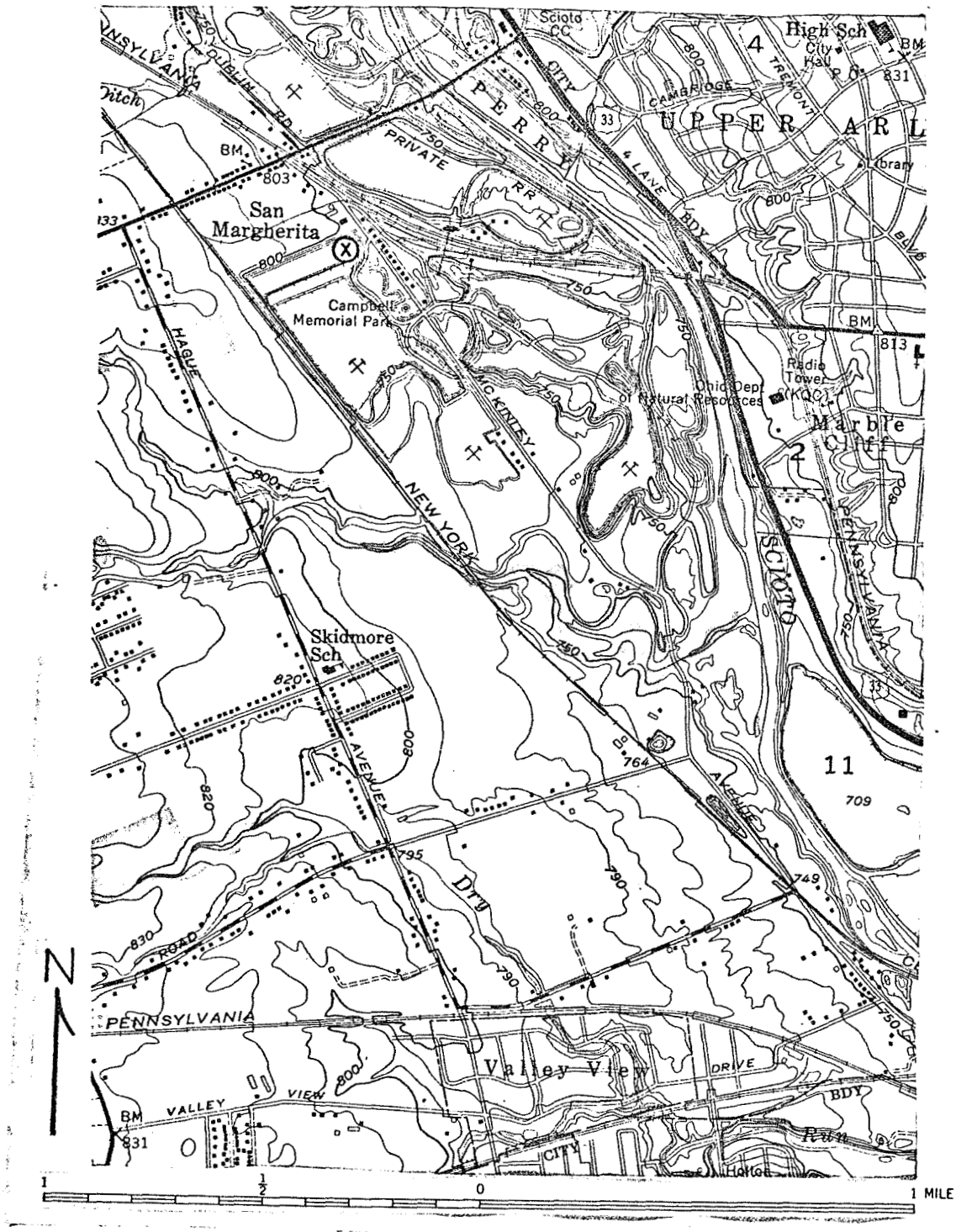

Fig. 45. (Location Map). The test site area within the Marble Cliff (Hobo) Quarry is marked ⓧ on the location map. The map is part of the Southwest Columbus, Ohio 7 1/2 minute topographic quadrangle.

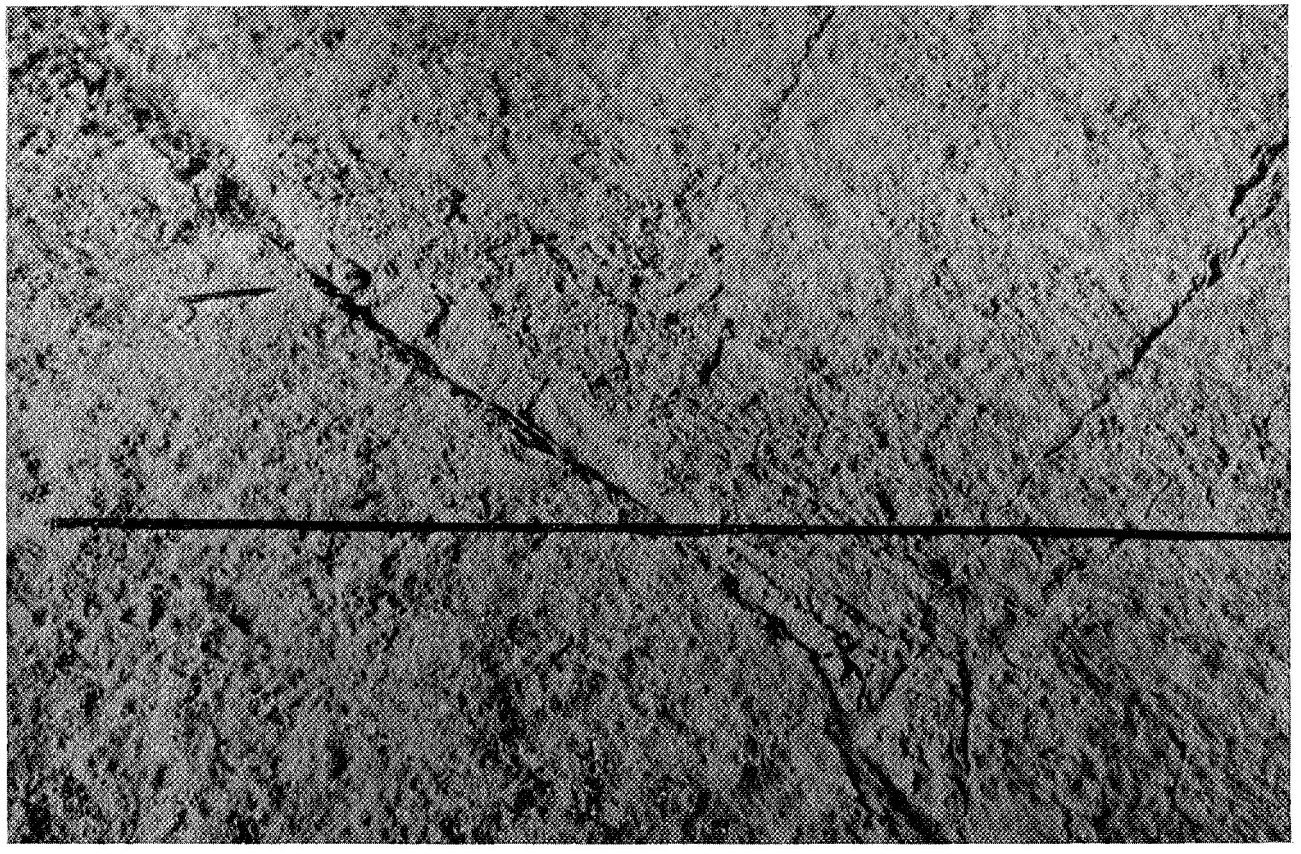

Fig. 46. Joints Cutting Columbus Limestone (Site 1). Most joints in the Columbus limestone are tight and nearly vertical, although there are exceptions. Of the two sets of joints illustrated by this photograph, the one extending from the upper-left corner dips 45° toward the lower left corner. The other set is vertical. The tape scale is in inches, and the pen is about five inches long.

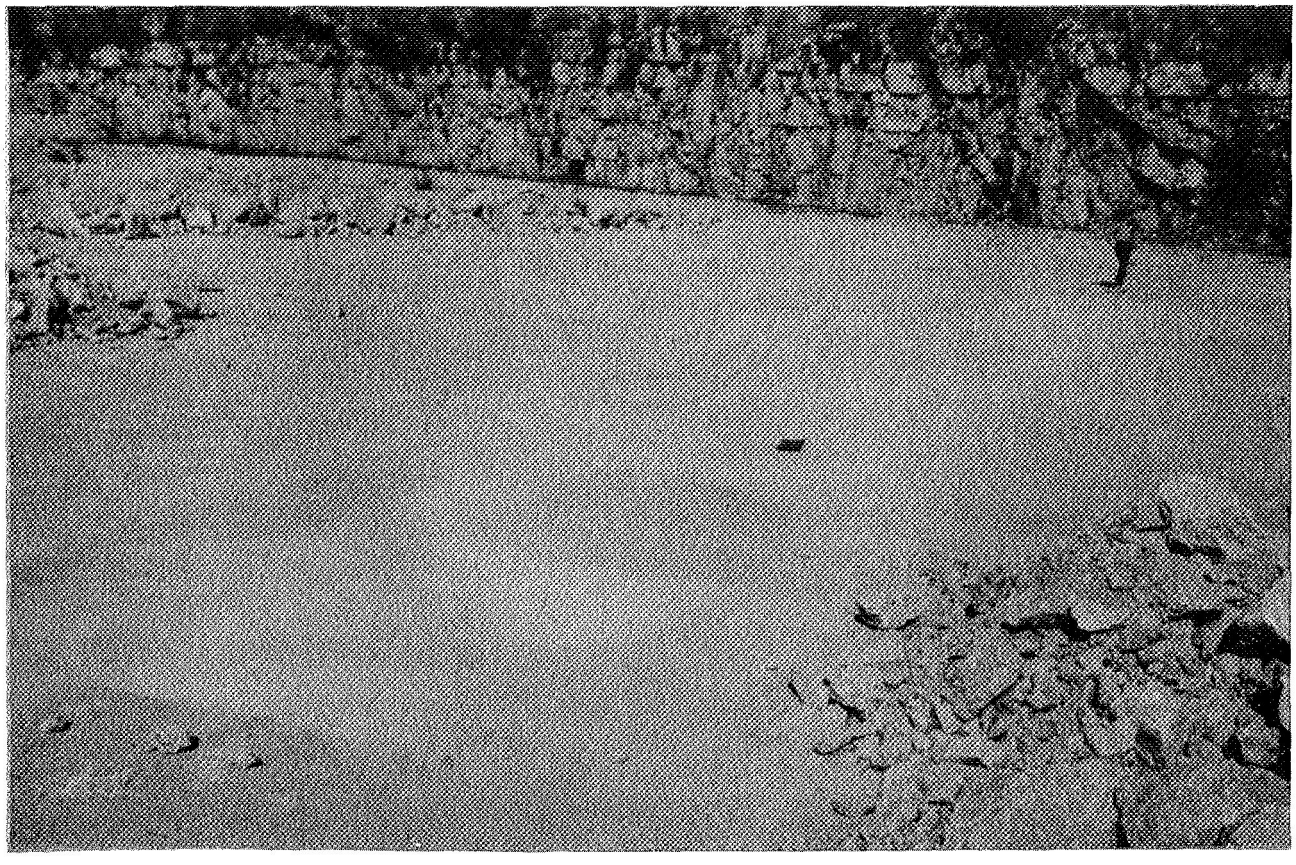

Fig. 47. Radar Test Strip, Site 1. The first Columbus limestone surface examined occurs on a bench 47 feet below the Delaware-Columbus contact. The test strip was swept clear of quarry debris except for a small patch toward one end. Tracks made by the radar truck as it scanned back and forth can be seen to the left of the runway.

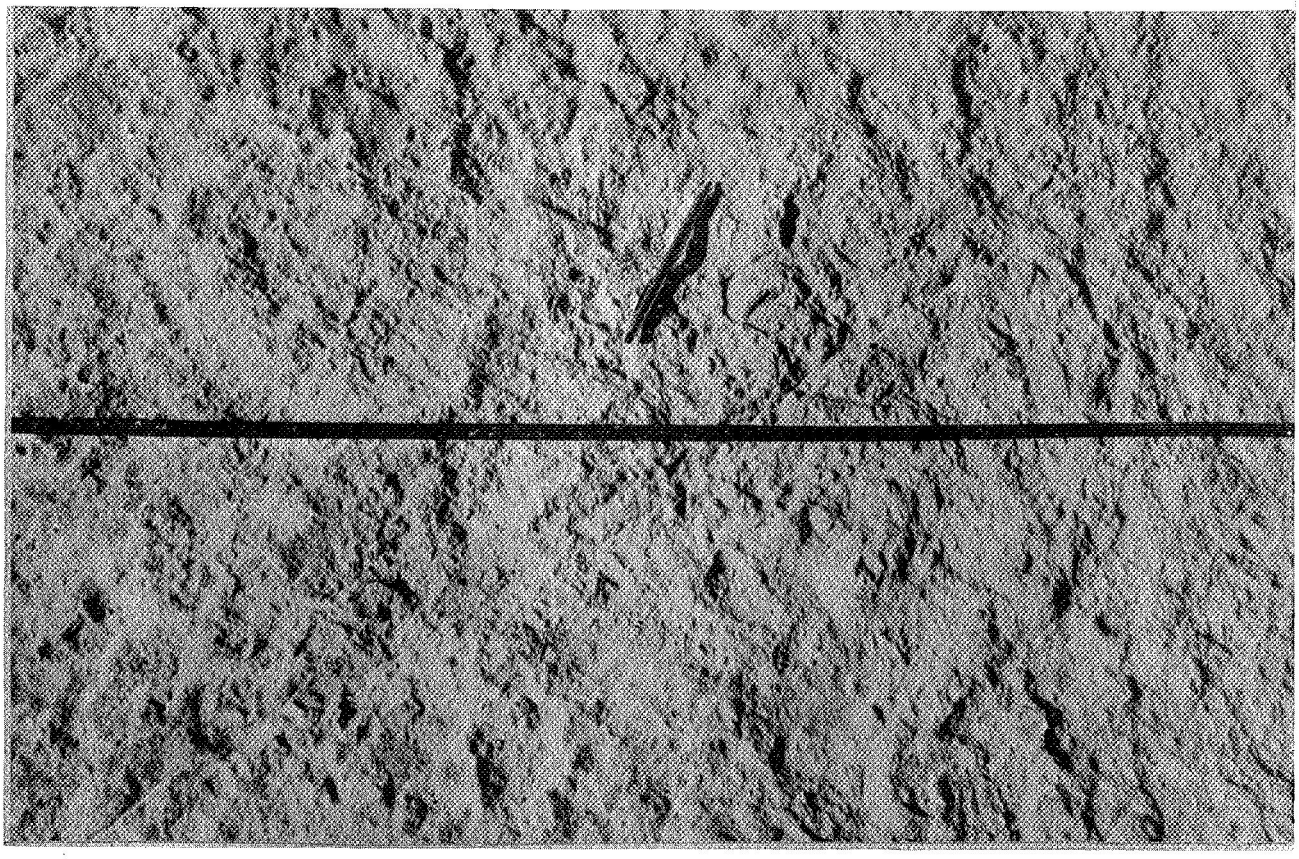

Fig. 48. Roughness of the First Surface (Site 1). This rough, irregular surface results from protruberance of fossil structures from the bedding plane (note the coiled cephalopod just to the right of the pen). The tape scale is in inches.

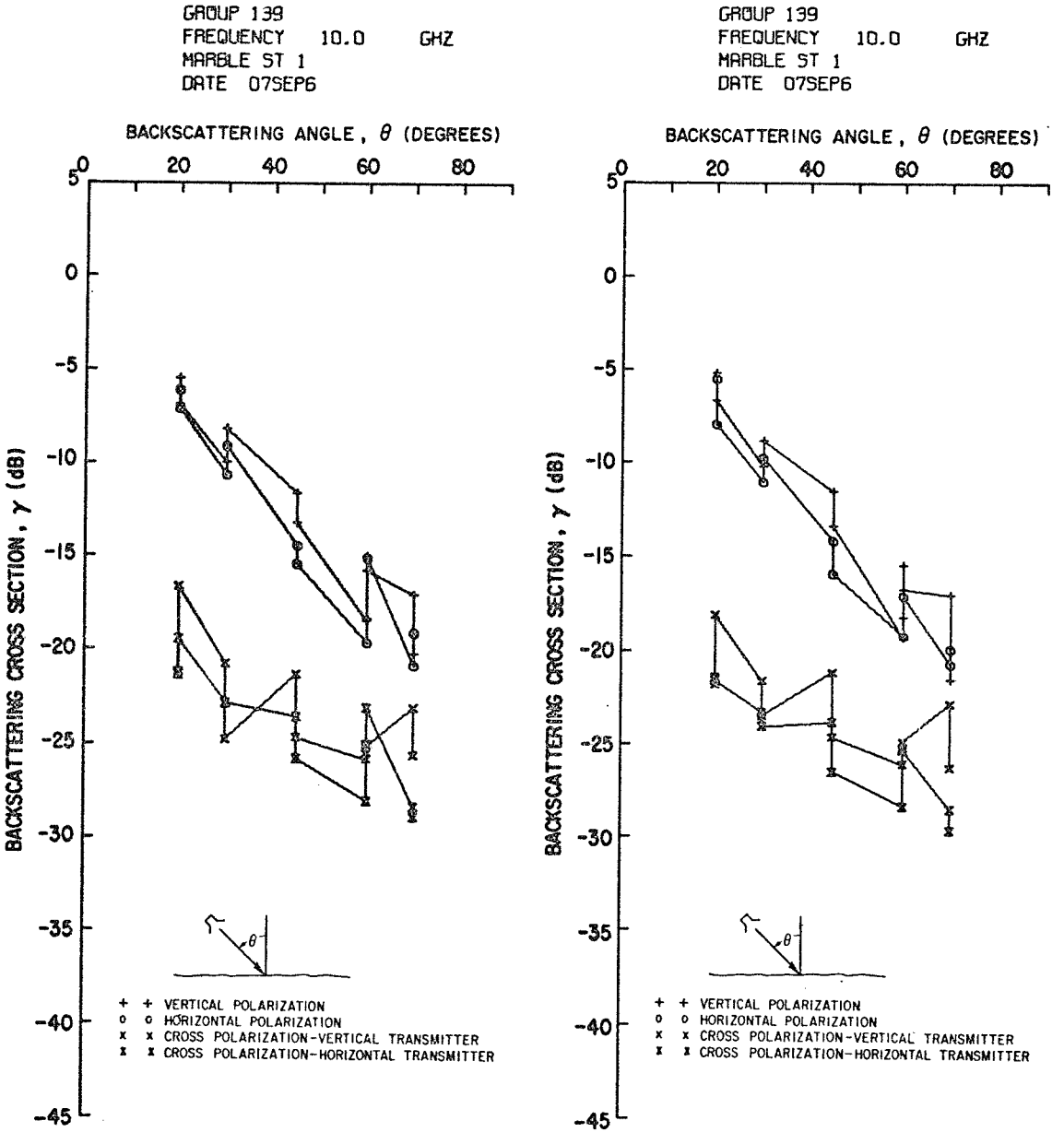

Fig. 49. Columbus limestone surface (MARBLE ST1).

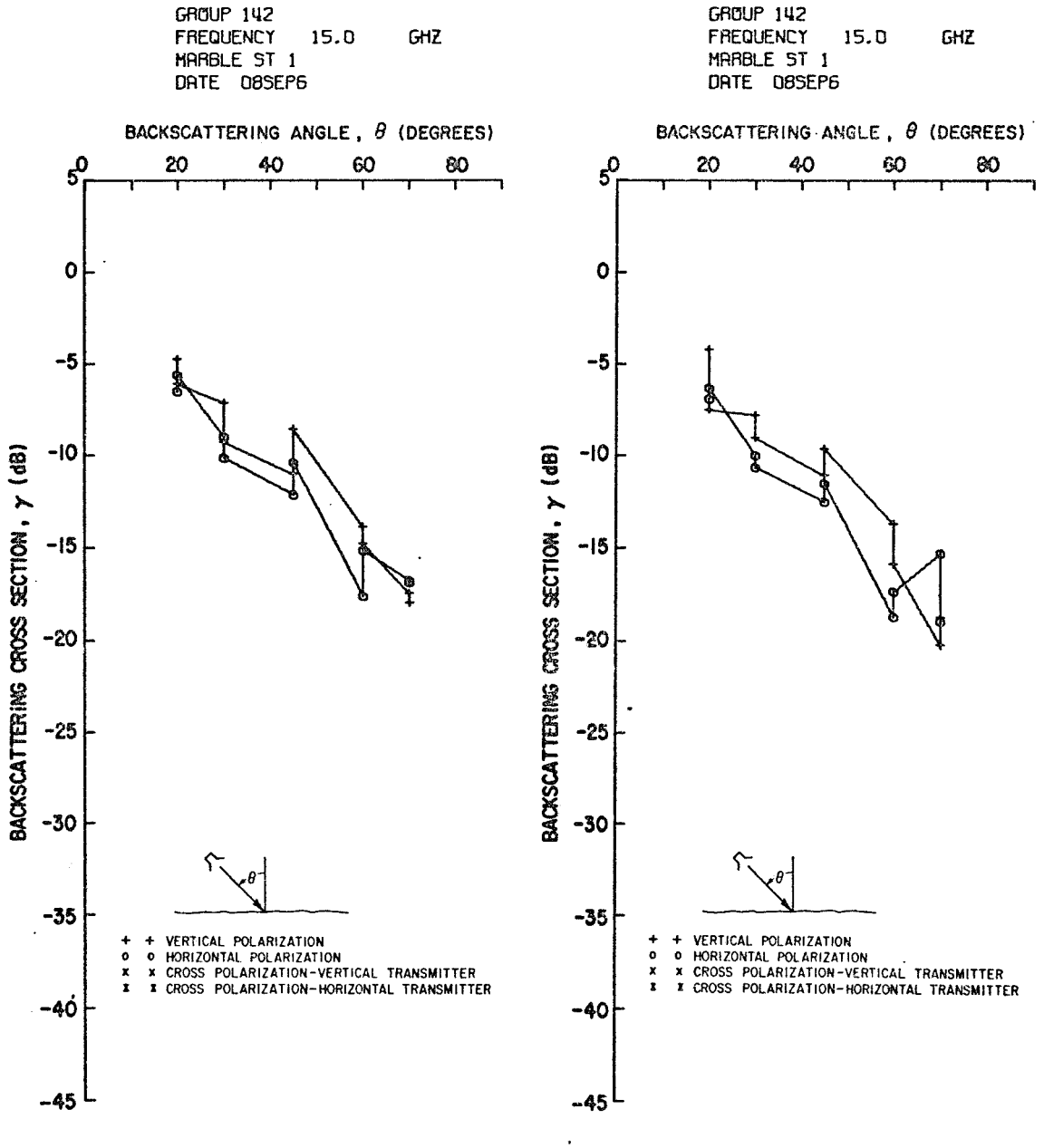

Fig. 50. Columbus limestone surface (MARBLE ST1).

2. Columbus Limestone Surface (MARBLE ST 2)

Group Nos. 141, 143, 144, 145, 146, 148

Location. Marble Cliff Quarries, Columbus, Ohio

Description. The second surface measured on the Columbus limestone in the Hobo Quarry occurs 23 feet below the first, or 64 feet below the Columbus-Delaware contact. The physical conditions and properties of this surface are very similar in many respects to the first. Again, the surface is on a prominent bench developed in the quarry operation. The surface is significant stratigraphically in that it represents the contact between the upper part of the Columbus limestone, which is very pure (high lime), and the lower part, which is dolomitic (magnesian). As in the first surface, the particular area utilized was swept clean of all loose debris. The rock is a very light gray to beige, finely crystalline, dolomitic limestone containing fairly abundant fossils. Since fossils are not as abundant as in the first surface, the second is notably smoother (see Fig. 51). Furthermore, the second surface lacks the shallow pitch and swell macrotopography of the first.

Radar data are given in Figs. 52-57.

Fig. 51. Smoothness of the Second Surface (Site 2). The second surface on the Columbus limestone measured with radar is notably smoother than the first. This is presumably due to the presence of less abundant fossils. Note the poor development of joints. The tape scale is in inches.

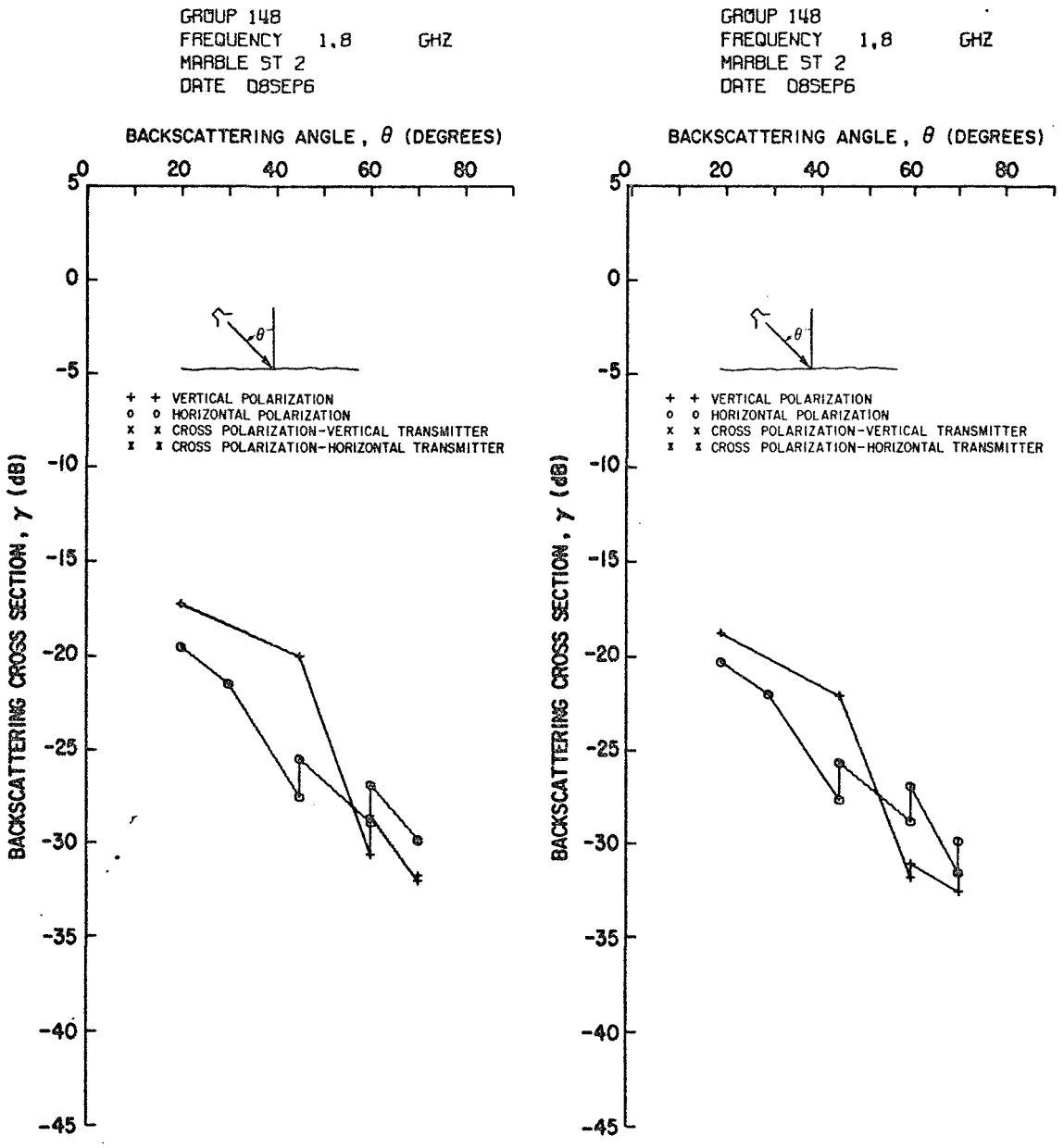

Fig. 52. Columbus limestone surface (MARBLE ST2).

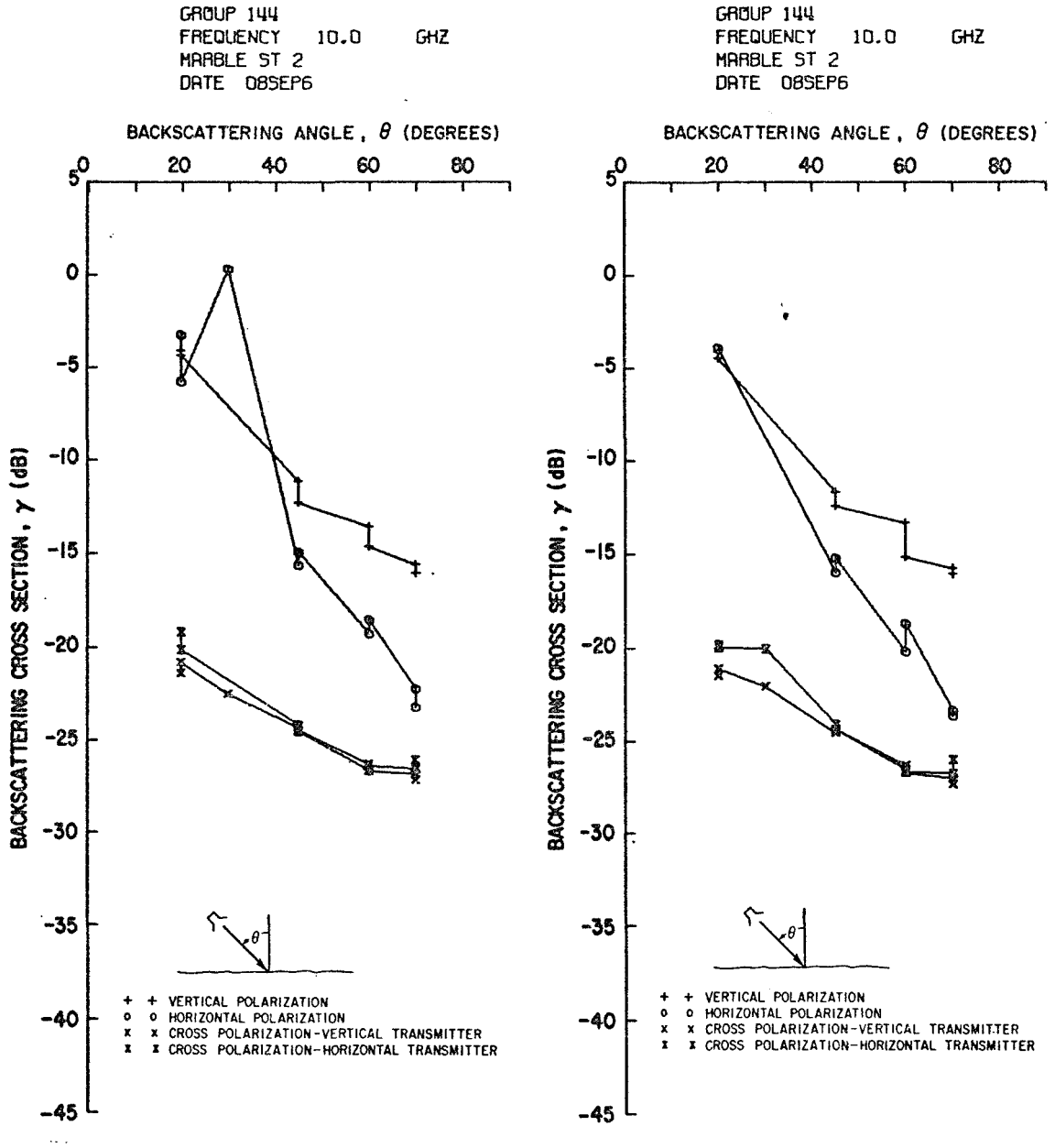

Fig. 53. Columbus limestone surface (MARBLE ST2).

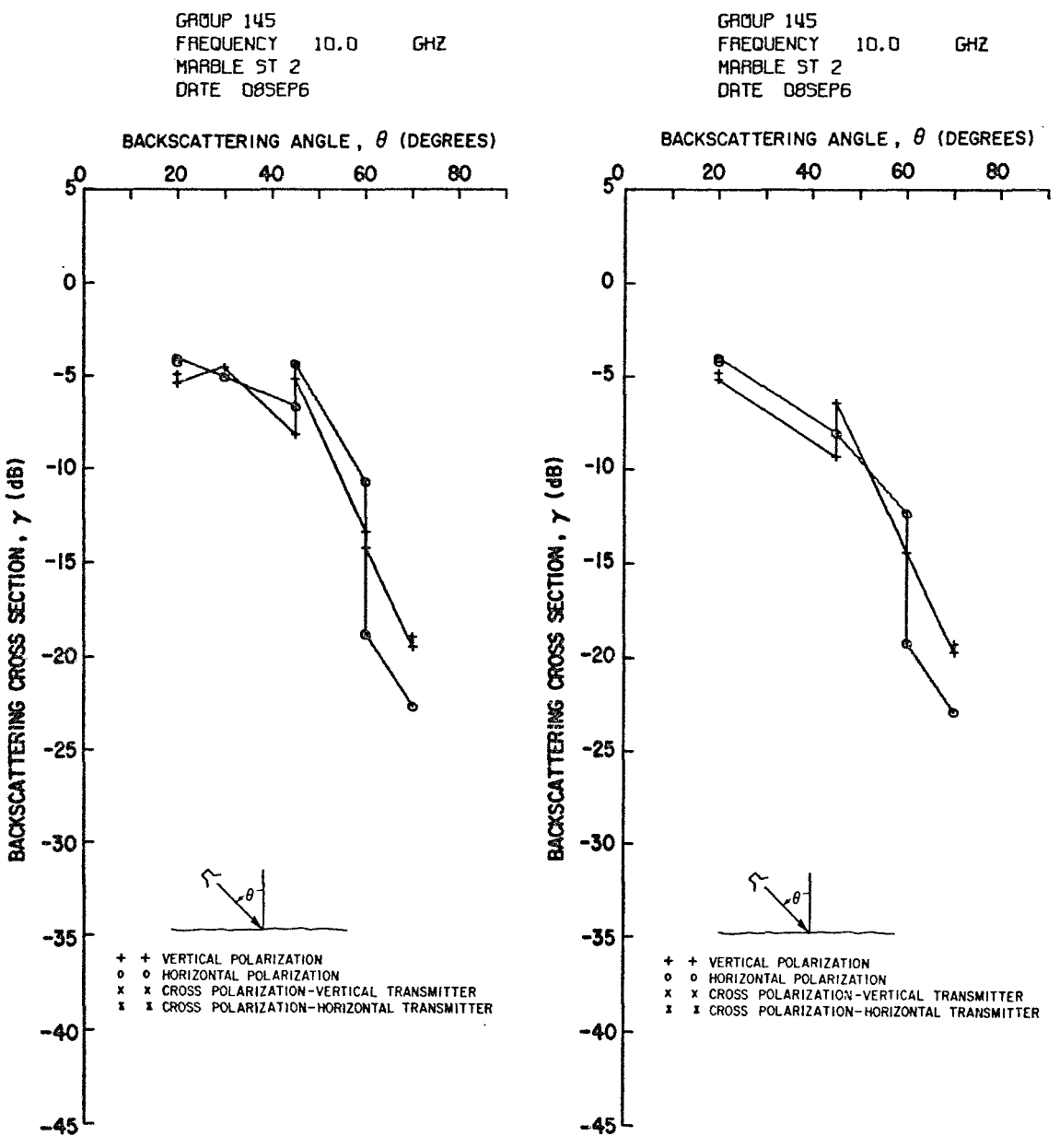

Fig. 54. Columbus limestone surface (MARBLE ST2).

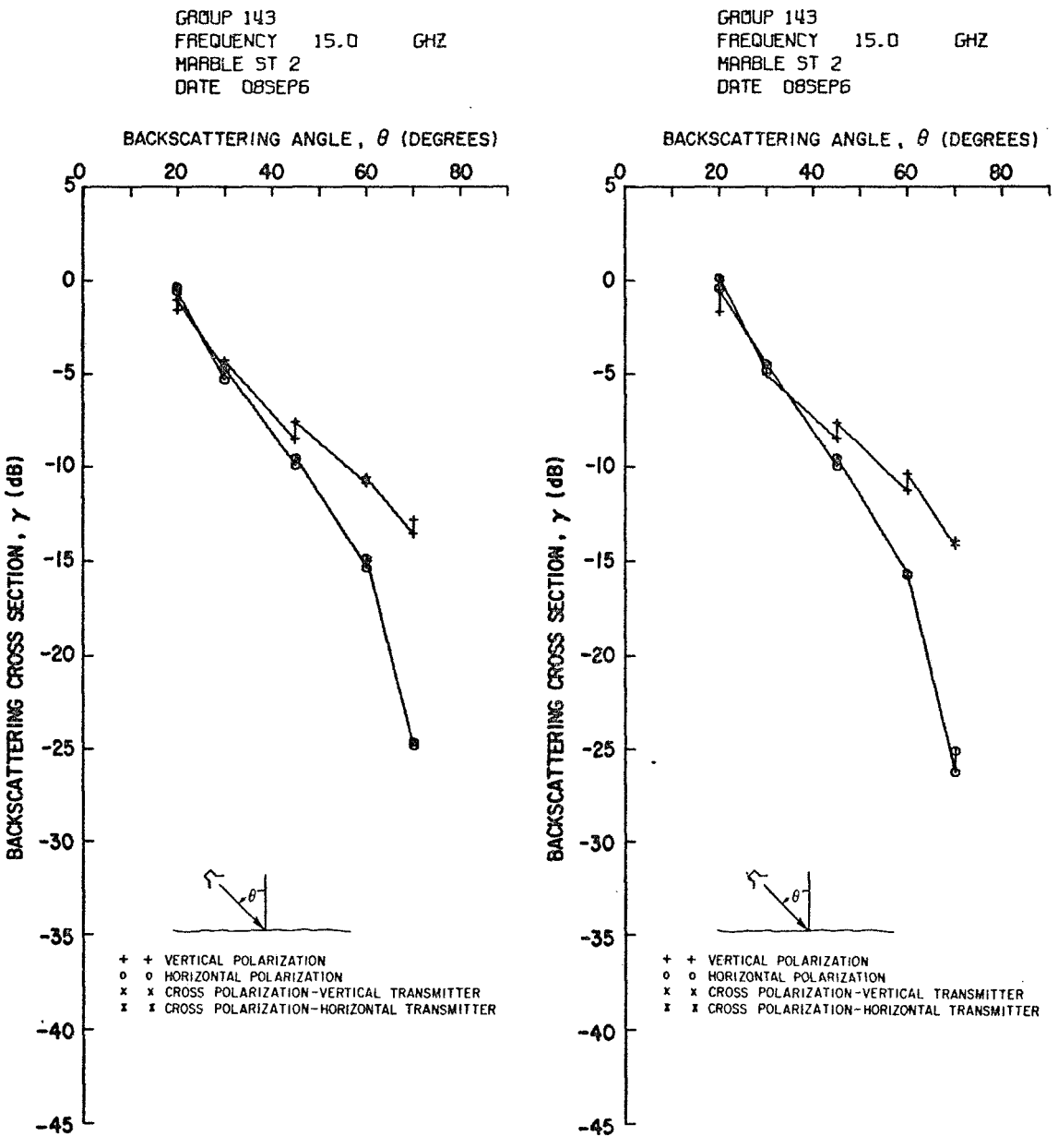

Fig. 55. Columbus limestone surface (MARBLE ST2).

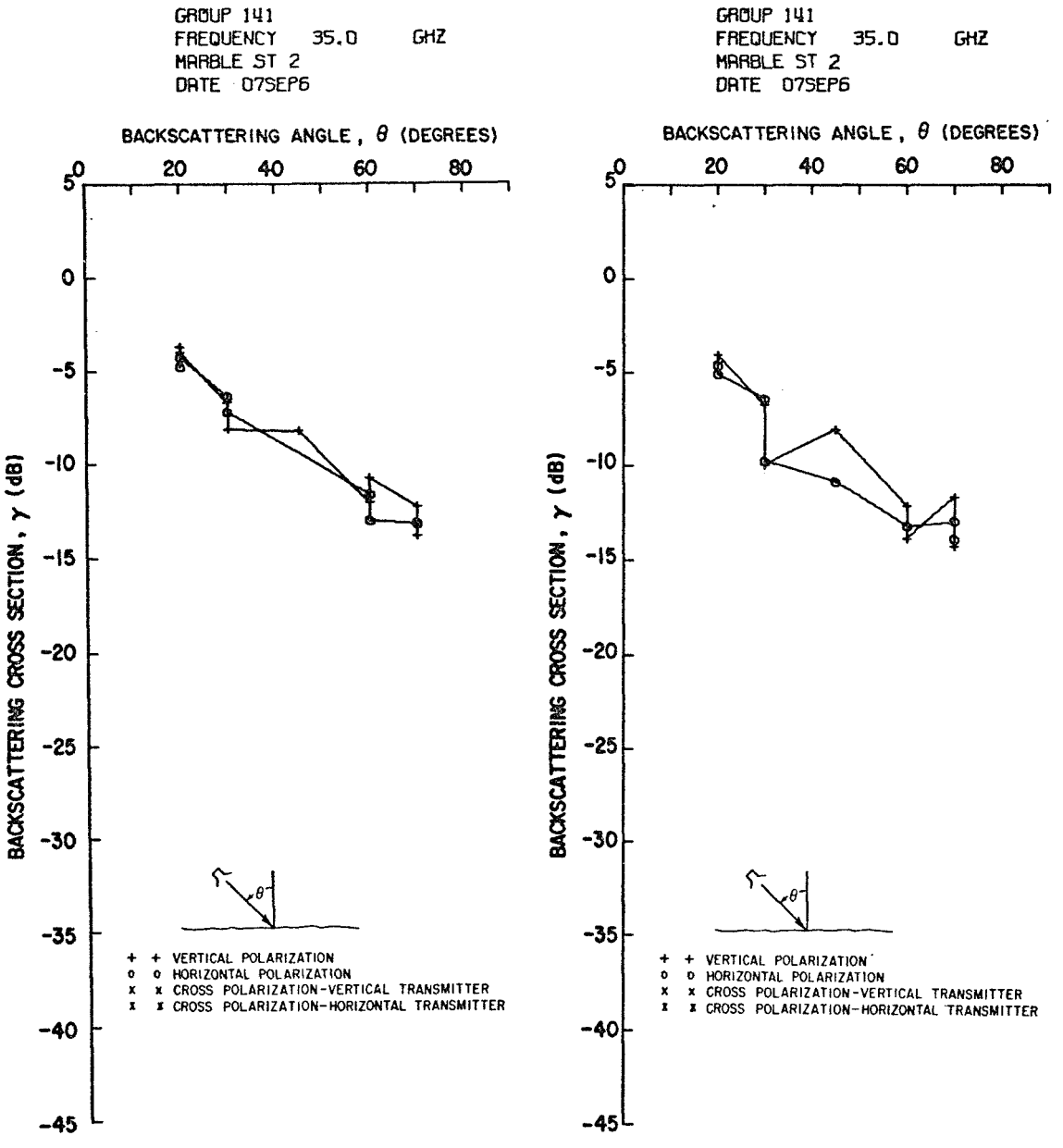

Fig. 56. Columbus limestone surface (MARBLE ST2).

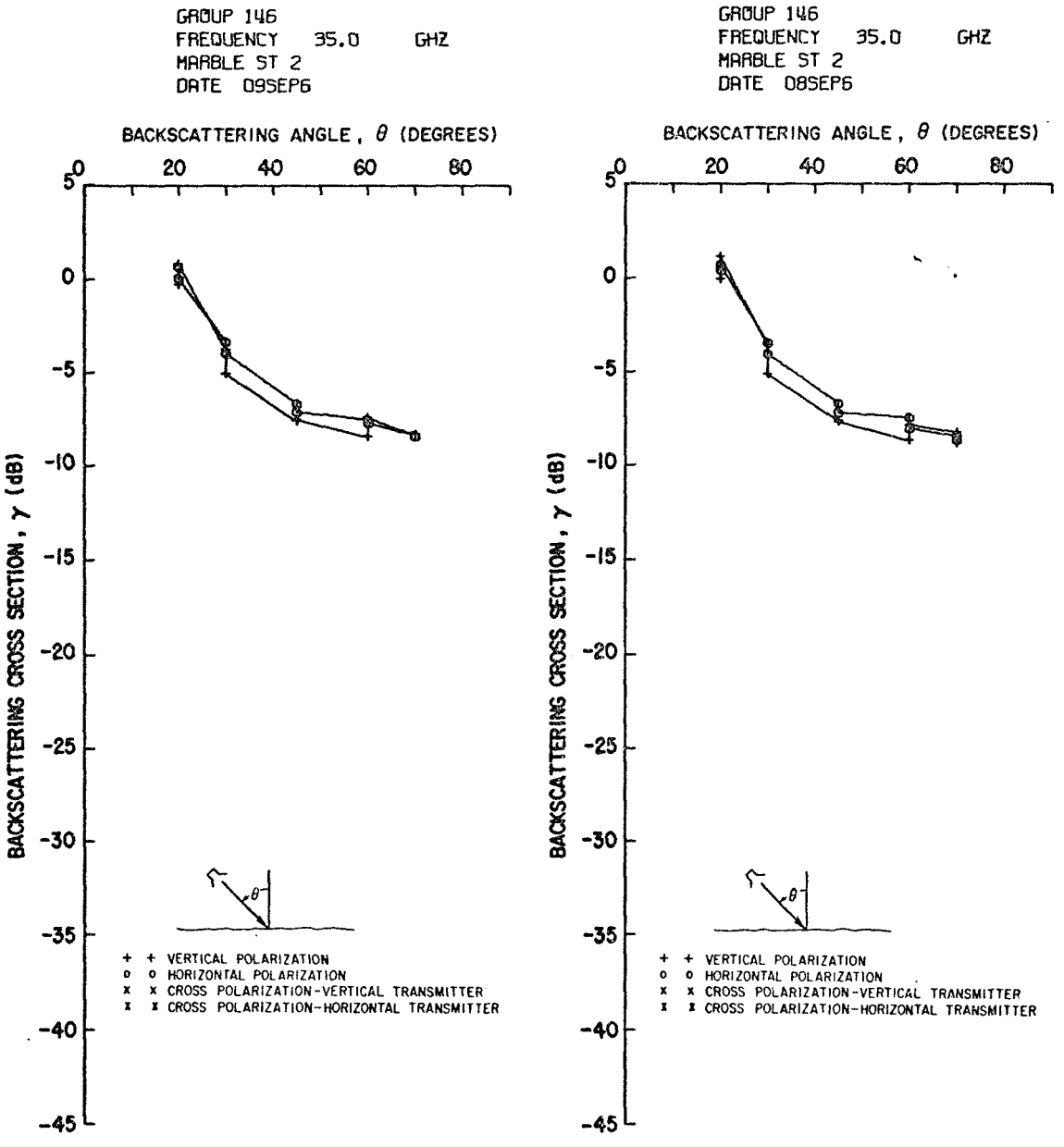

Fig. 57. Columbus limestone surface (MARBLE ST2).

E. Others

1. The asphalt surface and plowed and disced surface sites are located on The Ohio State University, Columbus, Ohio

Asphalt Surface

Group Nos. 76, 77, 78, 79

Location. In front of ElectroScience Laboratory, Columbus, Ohio

Description. Measurements were made on an asphalt surface which is located in front of The Ohio State University ElectroScience Laboratory. The surface has a r.m.s. roughness of approximately 0.3 mm; relative dielectric constant is $\varepsilon_r = 4.3 + j0.1$.

Radar data are given in Figs. 58 and 59.

Bare Soil Surface, Plowed and Disced

Group Nos. 319, 320

Location. Ohio State University Farms - West of the ElectroScience Laboratory

Description. Measurements were made on freshly plowed and disced surfaces which were located on The Ohio State University Farms. The plowed surface had 8"-12" diameter clods; the disced surface had approximately 4" diameter clods with 2"-3" ridges.

Radar data are given in Figs. 60.

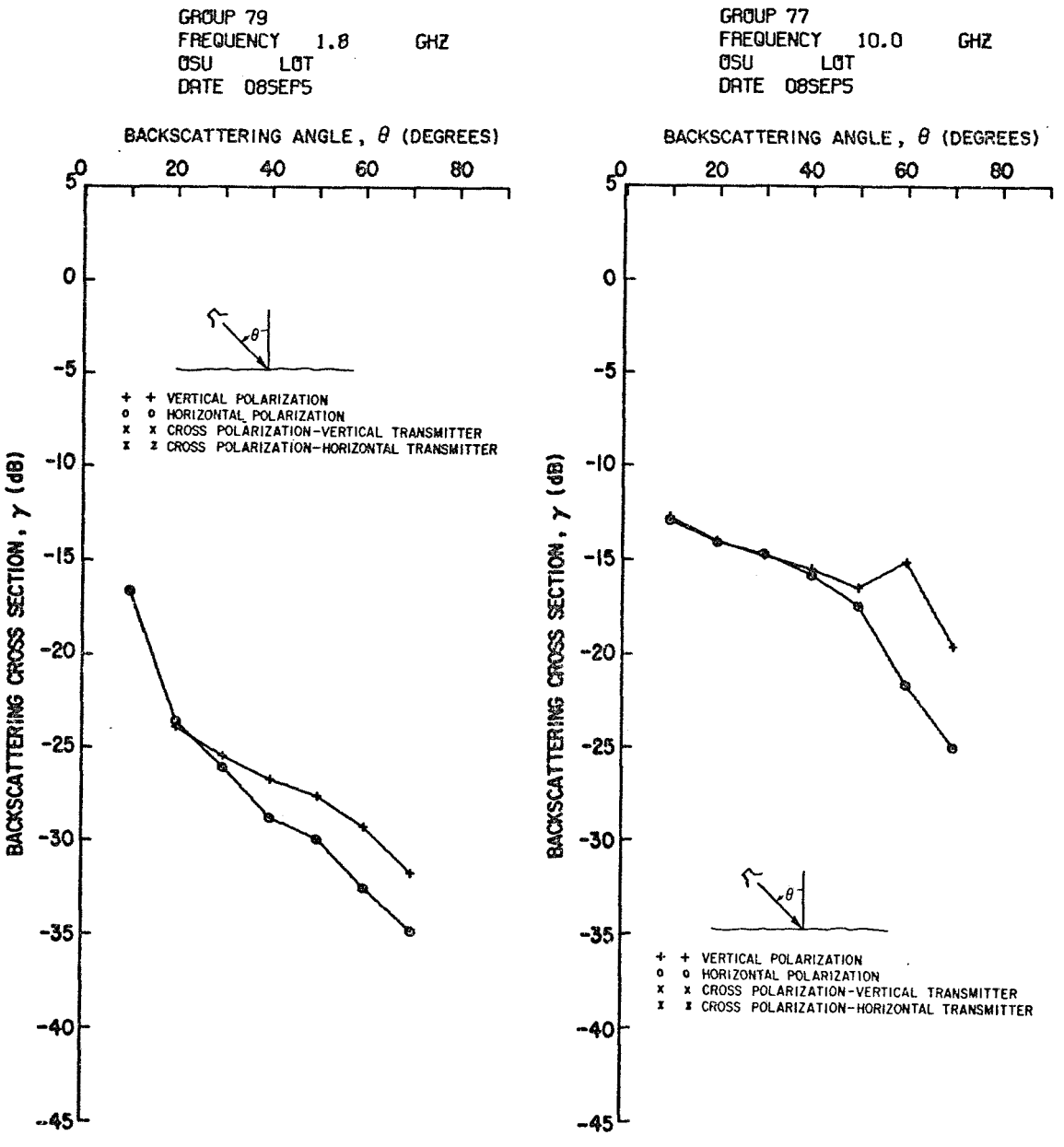

Fig. 58. Asphalt surface.

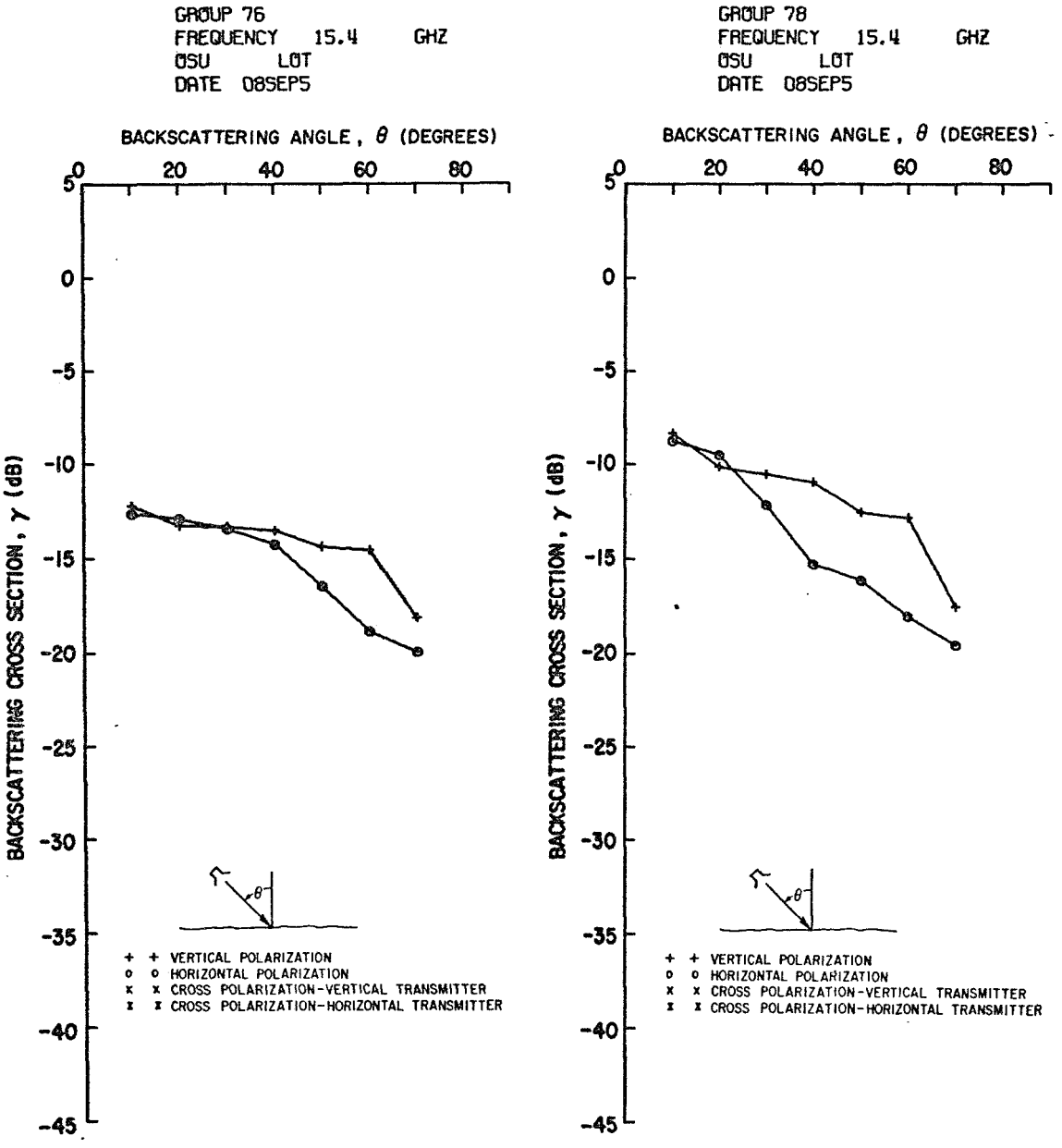

Fig. 59. Asphalt surface.

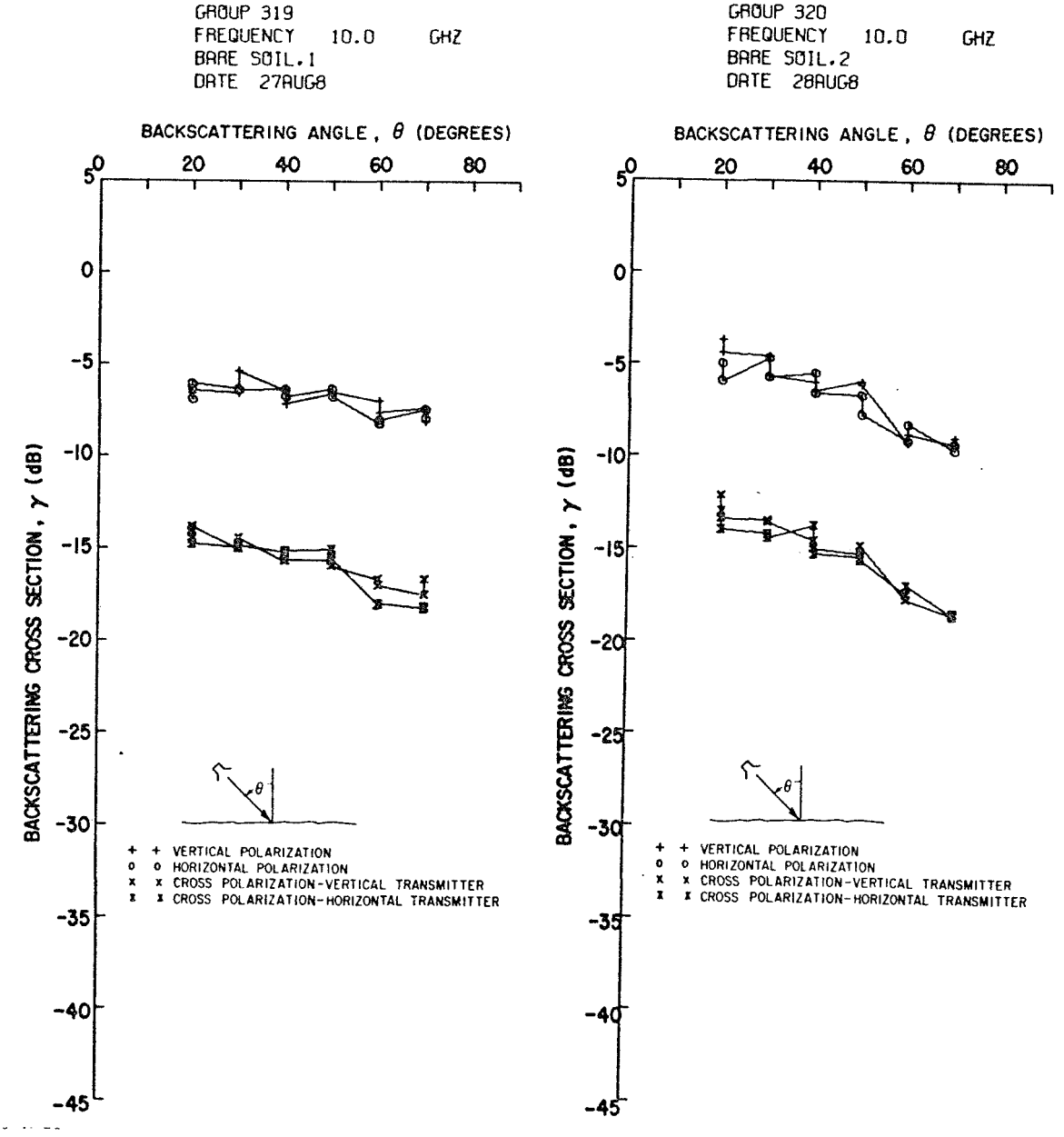

Fig. 60. Bare soil surfaces, plowed and disced.

2. The Purdue Sandfarm is located about 1 1/2 miles NE of Monterey, Indiana (see Location Map, Fig. 61). More complete descriptions of the surfaces are given on the data sheets.

Bare Soil Surface, Irrigated (SNDFM SL I) and Nonirrigated (SNDFM SL NI)

Group Nos. 127, 129, 128, 130

Location. Purdue Sandfarm

Description. Measurements were made on irrigated (SNDFM SL I) and nonirrigated (SNDFM SL NI) plots at the Purdue Sandfarm. The irrigated bare soil had 6" furrows at six-foot intervals with the surface washed to a smooth crust. The nonirrigated bare soil had some tractor tire tracks; the surface was covered with 1" clods. The soil moistures for the two surfaces are presented in Table III.

Radar data are given in Figs. 62 and 63.

TABLE III

Soil Moisture of the Irrigated and Nonirrigated Bare Soil Surfaces

Soil Depth	Irrigated	Nonirrigated
Surface	5%	<2%
6"	4%	3%
9"	25%	10%
15"	28%	16%
21"	18%	16%
27"	15%	17%
33"	16%	18%

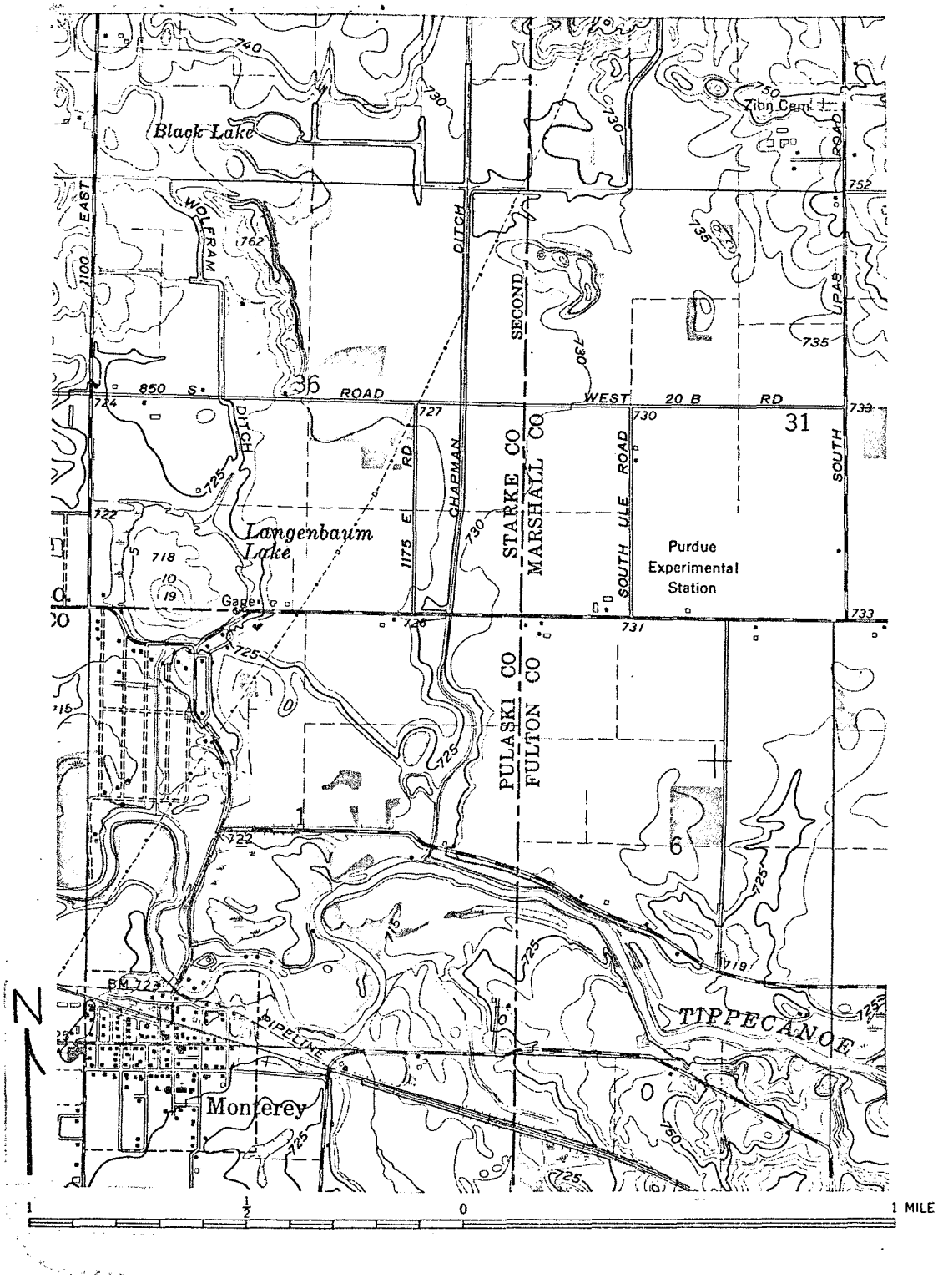

Fig. 61. (Location Map). The Purdue Sandform

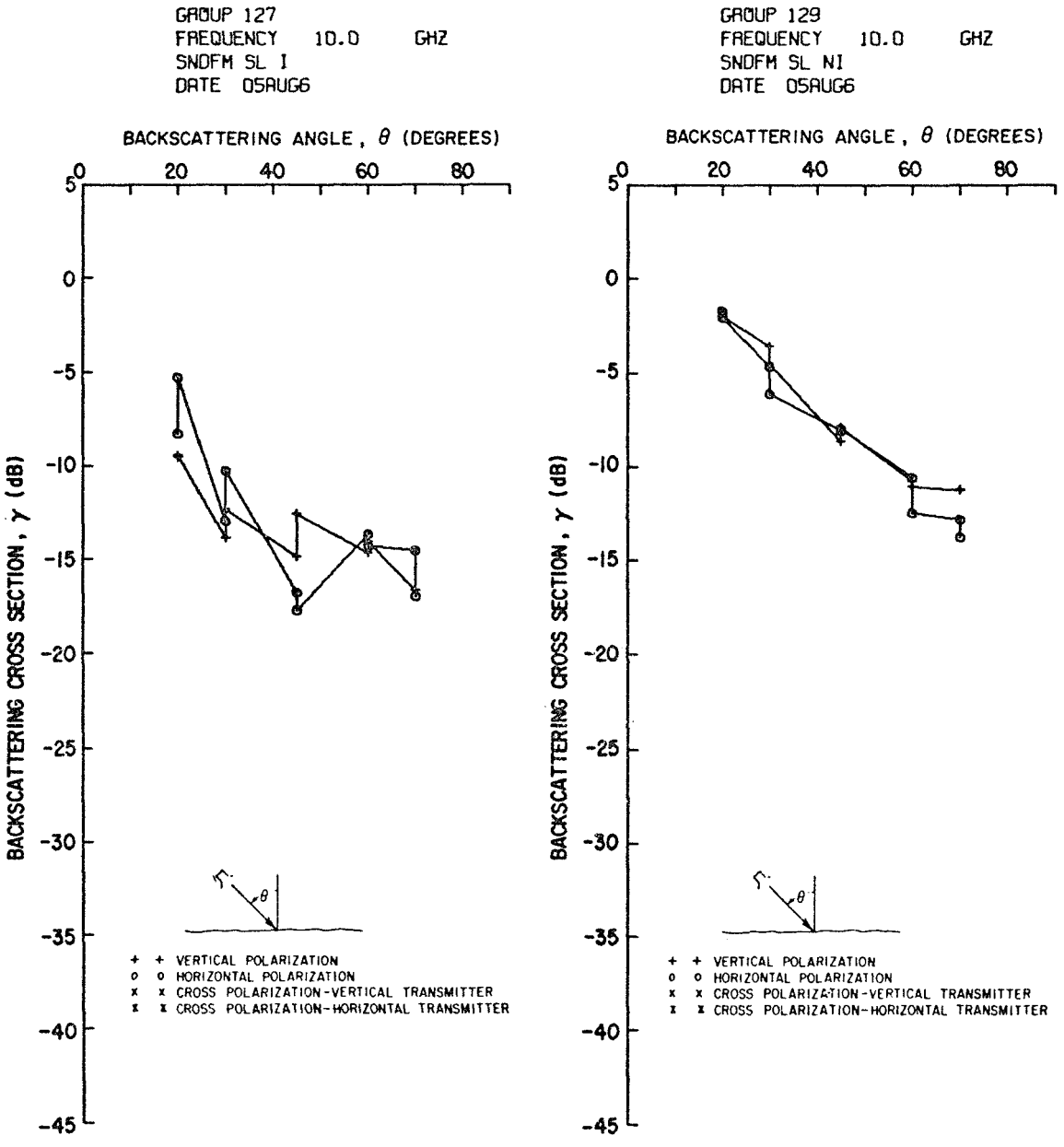

Fig. 62. Bare soil surface, irrigated (SNDFM SL I) and nonirrigated (SNDFM SL NI).

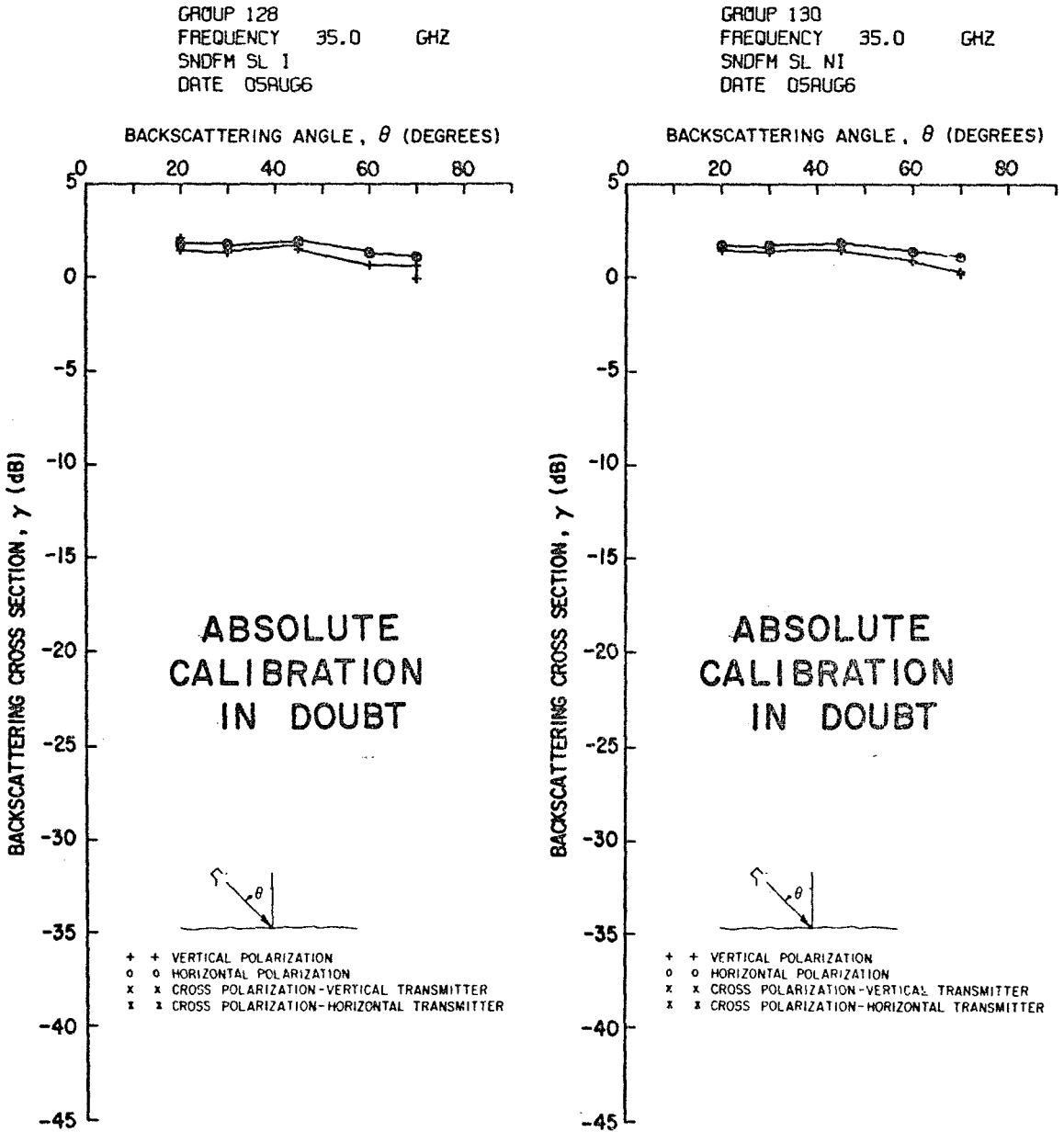

Fig. 63. Bare soil surface, irrigated (SNDFM SL I) and nonirrigated (SNDFM SL NI).

REFERENCES

1. Moore, R. K. and D. S. Simonett, "Potential Research and Earth Resource Studies with Orbiting Radars: Results of Recent Studies", AIAA 4th Annual Meeting and Technical Display, No. 67-767, October 1967.

2. Oliver, T. L. and W. H. Peake, "Radar Backscattering Data for Agricultural Surfaces", Report 1903-9, 13 Feb. 1969, Electro-Science Laboratory, The Ohio State University Research Foundation; prepared under Contract NSR-36-008-027, National Aeronautics and Space Administration, Washington, D. C., and Contract F 33615-67-C-1663, Air Force Avionics Laboratory, Wright Patterson Air Force Base, Ohio.

3. Peake, W. H., C. H. Shultz, R. L. Riegler, "The Mutual Interpretation of Active and Passive Microwave Sensor Outputs", Report 1903-3, 15 July 1966. Antenna Laboratory, The Ohio State University Research Foundation; prepared under Contract NSR-36-008-027, National Aeronautics and Space Administration, Washington, D. C.

4. Oliver, T. L. and W. H. Peake, "Microwave Brightness Temperatures of Terrain", Report 2440-4, 15 Jan. 1969, ElectroScience Laboratory, Department of Electrical Engineering, The Ohio State University, prepared under Contract F 33615-67-C-1633, Air Force Avionics Laboratory, Wright-Patterson Air Force Base, Ohio.

5. Cosgriff, R. L., W. H. Peake, R. C. Taylor, "Terrain Scattering Properties for Sensor System Design", Engineering Experiment Station Bulletin 181, May 1960, prepared in part by contracts from the Air Research and Development Command of the United States Air Force and the United States Army Signal Corps with The Ohio State University Research Foundation.

6. Oliver, T. L., "A Mobile Facility for Measuring the Backscattering and Brightness Temperature of Terrain at Microwave Frequencies", Report 1903-6, 4 October 1968, ElectroScience Laboratory, The Ohio State University Research Foundation; prepared under Contract NSR-36-008-027, National Aeronautics and Space Administration, Washington, D. C.

7. Barrick, D., "Normalization of Bistatic Radar Return", Report 1388-13, ElectroScience Laboratory, Department of Electrical Engineering, The Ohio State University, 15 January 1964; prepared under Grant No. NsG-213-61, National Aeronautics and Space Administration.

8. Kistler, Ronald E., 1966, Geologic Map of the Mono Craters Quadrangle, Mono and Tuolumne Counties, California - U. S. Geol. Surv., Geol. Quad. Map GQ-462.

9. Dibblee, T. W., Jr., 1966, Geologic Map of the Lavic Quadrangle, San Bernardino County, California - U. S. Geol. Surv., Misc. Geol. Inv. Map I-472.

10. Neal, James T. 1965, "Environmental Setting and General Surface Characteristics of Playa, in Geology, Mineralogy, and Hydrology of U. S. Playas", edited by James T. Neal, A.F.C.R.L., Environmental Research Papers, No. 96.

11. Kerr, Paul F. and Langer, Arthur M., 1965, "Mineralogical Features of Mojave Desert Playa Crusts, in Geology, Mineralogy, and Hydrology of U. S. Playas", edited by James T. Neal, A.F.C.R.L., Environmental Research Papers, No. 96.

12. Sparling, Dale Richard, 1965, "Geology of Ottawa County, Ohio", The Ohio State University, Dissertation (unpub.).